FLEXURAL BEHAVIOR OF GFRP-REINFORCED CONCRETE CONTINUOUS BEAMS

By

S. M. HASANUR RAHMAN

A Thesis submitted to the Faculty of Graduate Studies of

University of Manitoba

in partial fulfillment of the requirements for the degree of

MASTER OF SCIENCE

Department of Civil Engineering

University of Manitoba

Winnipeg, Manitoba, Canada

ABSTRACT

In this study, a total of twelve beams continuous over two spans of 2,800 mm each were constructed and tested to failure. The beams were divided into two series. Series 1 included six T-beams under symmetrical loading, while Series 2 dealt with six rectangular beams under unsymmetrical loading conditions. In Series 1, the test variables included material type, assumed percentage of moment redistribution, spacing of lateral reinforcement in flange, arrangement of shear reinforcement, and serviceability requirements. In Series 2, three different loading cases were considered, I) loading both spans equally, II) loading both spans maintaining a load ratio of 1.5 and III) loading one span only. Under the loading case II, the parameters of reinforcing material type, assumed percentage of moment redistribution and serviceability requirements were investigated.

The test results of both series showed that moment redistribution from the hogging to the sagging moment region took place in GFRP-RC beams which were designed for an assumed percentage of moment redistribution. In Series 1, the decrease of the stirrups spacing from 0.24d to 0.18d enhanced the moment redistribution percentage. Also, decreasing the spacing of lateral reinforcement in the flange from 450 to 150 mm improved the moment redistribution through enhancing the stiffness of the sagging moment region. In Series 2, the unsymmetrical loading conditions (loading case II and III) reduced the moment redistribution by reducing flexural stiffness in the heavily loaded span due to extensive cracking. Regarding serviceability in both series, the GFRP-RC beam designed for the same service moment calculated from the reference steel-RC beam, was able to meet the serviceability requirements for most types of the structural applications.

ACKNOWLEDGEMENT

I would like take this opportunity to express my sincere gratitude to Dr. Ehab El-Salakawy, Ph.D., P.Eng., Professor and Canada Research Chair in Durability and Modernization of Civil Structures, Department of Civil Engineering, University of Manitoba, for his continuous guidance and encouragement during the course of this program. Without his suggestions and support, this work would not come to a fruitful end.

I would like to thank Dr. Karam Mahmoud, Ph.D., for being with me in almost every stage of this program. I also want to acknowledge the assistance I received from my all colleagues, especially Syed Kumail Raza Naqvi, during the construction and testing of the beams. In addition, I thankfully appreciate the technical staff of W. R. McQuade Structures Laboratory at the University of Manitoba, Chad Klowak, Ph.D., Brenden Pachal, and Grant Whiteside for their helping hands. Also, the friendship I had with Syed Kumail and Puneet Anand, marked a long trail of fun and colorful moments which again and again refreshed my mind to get restarted with the research work.

I would like to gratefully acknowledge the financial support received from the Natural Science and Engineering Research Council of Canada (NSERC), through Canada Research Chairs program as well as the government of Manitoba through Manitoba Graduate Scholarship (MGS) program.

At last, but not least, no way I know to pay gratitude to my parents and three brothers who always encourage me in pursuing my dreams. From the deepest of my heart, I wish to be always with you as the way you have been in my life so far.

TABLE OF CONTENTS

LIST OF TABLES

LIST OF FIGURES

NOTATIONS

$A =$ Area of reinforcement, mm^2;

$c =$Neutral-axis depth, mm;

$d =$ Effective depth of section, mm;

$d_v =$ Effective shear depth, mm;

$E =$ Modulus of elasticity, GPa;

$f_c' =$ Concrete compressive strength, MPa;

$I =$ Moment of inertia, mm^4;

$I_{cr} =$ Cracking moment of inertia, mm^4;

$I_e =$ Effective moment of inertia, mm^4;

$I_g =$ Gross moment of inertia, mm^4;

$I_t =$ Moment of inertia of section transformed to concrete, mm^4;

$k_s =$ Coefficient regarding the effect of member size on shear strength;

$k_r =$ Coefficient regarding the effect of reinforcement rigidity on shear strength;

$L =$ Length of the span, mm;

$M_a =$ Applied moment at a certain loading level, kN.m;

$M_{cr} =$ Cracking moment, kN.m;

$n_f =$ Ratio of elastic modulus of FRP to that of concrete;

$S_{ze} =$ Equivalent crack spacing parameter;

$y_t =$ Distance from the centroid to the extreme tensile fibre, mm;

$z =$ Quantity limiting distribution of flexural reinforcement bars;

β_d= Modification factor related to the reduced tension stiffening in FRP-RC members;

$\gamma_G =$ Reduction factor of deflection in cracked phase;

$\rho_f =$ Ratio of FRP reinforcement;

$\rho_{fb} =$ Balanced reinforcement ratio;

$\lambda =$ Density factor;

μ_{φ} = Curvature ductility index;

φ_u = Curvature at ultimate condition, 1/mm;

φ_y = Curvature at yield condition, 1/mm;

μ_{θ} = Rotation ductility index;

θ_u = Rotation at ultimate condition;

θ_y = Rotation at yield condition;

μ_{Δ} = Deflection ductility index;

Δ_u= Deflection at ultimate condition, mm;

Δ_y= Deflection at yield condition, mm;

η = Percentage of moment redistribution;

$\varepsilon_x, and\ \varepsilon_l$ = Longitudinal strain at the mid-depth of the cross-section;

CHAPTER 1 - INTRODUCTION

1.1 GENERAL

Conventional steel reinforced concrete (RC) structures are continuously facing challenges to keep the structural soundness and integrity in harsh environmental conditions. Thus, the contact with sulphates, chlorides, and other corrosive environmental agents is progressively reducing the durability of these structures during their service life as a result of materials degradation, most often governed by corrosion of the steel bars (Apostolopoulos and Papadakis 2007). Though the increased alkalinity of cement provides the temporary protection for steel, the alkaline environment of concrete gets neutralised with time because of being exposed to environmental attack. So, sooner or later, the alkaline properties of concrete get reduced and it again leads to steel corrosion and concrete spalling (Holland 1997). That is why different codes of practice prescribe using thick concrete cover to reduce the crack width and permeability. Sometimes, the efficiency of solutions such as concrete surface protective coatings to stop the ingression of CO_2 and water soluble chemicals, corrosion resistant admixtures as well as epoxy coating and galvanizing of reinforcement was examined. In addition, cathodic protection that utilizes an electric current or sacrificial anode was found to be a more innovative approach to protect the reinforcing bars (Allen and Edwards 1987).

Most of these techniques are inefficient or partially succeeded (Razaqpur and Kashef 1993). Therefore, this kind of structural deterioration has led to the search for new materials and

solutions for complete substitution of steel as a reinforcing material in new construction to avoid corrosion related problems. In this context, fibre reinforced polymer (FRP) bars have emerged as a viable alternative to conventional steel reinforcement since they offer several important mechanical properties over normal steel bars. Excellent resistance against corrosion, electromagnetic neutrality, higher tensile strength, and light weight property have made civil and structural engineers to choose this material as reinforcement for concrete structures since early 1990s.

In practice, most of the civil engineering structural elements are statically indeterminate in nature. Eventually, these indeterminate reinforced concrete elements are also very common in structures such as parking garages, overpasses, and marine structures which are usually exposed to extreme and harsh weathering conditions. Due to the difference in physical and mechanical characteristics between steel and FRP bars, the design provisions developed for steel-RC structures can't be applied to FRP-RC structures. Extensive experimental and analytical studies were conducted on the applicability of FRP for the purpose of strengthening and retrofitting works. Moreover, much research investigated the prospects of FRP bars as internal reinforcement in new structures; however, the focus was mainly on the behavior of simply-supported structural elements (Benmokrane et al. 1996a, Vijay et al. 2001, Mosley et al. 2008, Rafi et al. 2009, Wang et al. 2011, Issa et al. 2011). On the contrary, limited research on the behavior of continuous beams has been done especially on the topics related to deformability and moment redistribution (Mostofinejad 1997, Grace et al. 1998, Habeeb and Ashour 2008, El-Mogy et al. 2010 and 2011, Santos et al. 2013, Mahmoud and El-Salakawy 2014 and 2016). Regarding geometrical configuration, most of the investigations were dedicated to the beams with rectangular sections. Very few studies (Grace et al. 1998, Santos et

al. 2013) investigated the behavior of continuous beams with T-sections. In addition, all previous studies on FRP-RC continuous beams were carried out under symmetrical loading arrangements. However, from the practical point of view, live loads intensity is most likely to vary from one span to another of a continuous beam depending on the type and distribution of occupancy on the floor/roof structural system. Therefore, the adjacent spans of a continuous beam can be subjected to unsymmetrical loads.

1.2 PROBLEM DEFINITION

Ductility is a very desirable and advantageous structural feature of RC structures. It is defined, for steel-RC members, as the ability to sustain inelastic deformations after yielding without loss of load carrying capacity. However, the corresponding behavior for FRP-RC members is called "deformability", which is defined by the *J*-factor (Jaeger et al. 1995, Mufti et al. 1996, Vijay et al. 1996). The deformability of FRP-RC elements allows the potential plastic hinge to form in the critical sections. Thus, the redistribution of internal stresses and moments is a logical consequence of ductility and deformability. Moment redistribution is the result of changes in the distribution of flexural stiffness along the span, particularly the ratio of stiffness of adjacent critical sections. The advantages of moment redistribution include having a favourable deformable behavior, utilizing the full capacity of adjacent sections of the span, reducing reinforcement congestion in beam-column joints, narrowing the envelope of demand moments and thus, reducing the amount of longitudinal reinforcement required.

The concept of moment redistribution in steel-RC elements is well-established (Ernst 1958; Mattock 1959; Rodriguez et al. 1959; Bryant et al. 1962; Scholz 1993; Carmo and Lopes 2008) and is recognized in many codes such as ACI 318-14 (2014) and CSA A23.3-14 (2014b). When conventional steel is used as reinforcement, the steel yielding results in most of the

moment redistribution; however, several studies (Scholz 1993 and Carmo and Lopes 2008) reported that after the formation of cracks and before yielding of the steel, at the critical sections, moment redistribution is likely to occur due to the difference in flexural stiffness along the beam. On the other hand, FRP bars do not yield rather they behave in a linear-elastic manner until failure. This property raised concerns about the ability of FRP-RC members to redistribute moments between the critical sections. However, moment redistribution in such elements was reported in many studies (Mostofinejad 1997; Habeeb and Ashour 2008; El-Mogy et al. 2010, 2011; Matos et al. 2011; Kara and Ashour 2013; Santos et al. 2013; Mahmoud and El-Salakawy 2014, 2016). In these studies, parameters such as material type, reinforcement ratio and configuration, concrete strength, stirrup spacing in the context of beams with rectangular and T-section were investigated; however, the beams were tested under symmetrical loading conditions.

From the geometrical perspective, contrary to rectangular beams, beams with T-sections have lower section modulus (*I/y* ratio, where *I* is the gross moment of inertia and *y* is the distance from the centroid to the extreme fiber in tension) at the sagging moment section than that at the hogging moment section. Since cracking moment/load is proportional to the section modulus, it is expected that flexural cracks form in the sagging moment region before the hogging moment region for beams with T-sections. This results in a reduced flexural stiffness in the sagging moment region and consequently reversed moment redistribution. On the other hand, in the post-cracking stage, the section over middle support behaves as a rectangular section while the section at mid-span region behaves as a T-section and this makes the sagging region stronger than the hogging region which results in normal moment redistribution from the hogging to the sagging moment region. These differences in behavior raise a concern about the amount and

direction of moment redistribution and the overall performance of continuous concrete beams with T-sections. In addition, for the over-reinforced sections, moment capacity doesn't increase proportionately with the amount of longitudinal reinforcement. Therefore, in case of unsymmetrical loading condition, the sagging region with higher load would be designed as highly over-reinforced, which consequently makes it a stiffer region compared to the adjacent hogging region. This implies that internal load is expected to redistribute from the hogging to the sagging region. However, due to higher elastic moment, widespread cracks produced and distributed along the higher load span can significantly reduce the effective flexural stiffness. Thus, normal moment redistribution process can get negatively affected.

This study aims at investigating the behavior and the possibility and extent of moment redistribution of large-scale GFRP-RC beams in two different series. The first series focusses on beams with T-sections under symmetrical loading whereas the second series mainly investigates the rectangular beams under different loading conditions.

1.3 RESEARCH SIGNIFICANCE

The ductility and moment redistribution of steel-RC continuous beams is well established, and many codes around the world provide the provisions of moment redistribution for designing concrete structures. On the other hand, current design codes and guidelines for FRP-RC structures such as: CSA/S806-12, ACI 440.1R-15, don't allow moment redistribution for continuous beams due to incomplete understanding and lack of test data in this regard. So far, as described earlier, some studies presented the findings such that moment redistribution in FRP-RC elements is possible. However, most of the investigations were focused on rectangular beams subjected to symmetrical loading. To date, no study was found regarding unequally-loaded FRP-RC beams. Therefore, this study is intended for better understanding of

deformability and moment redistribution in the context of T-beams along with beams subjected to unsymmetrical loading.

1.4 OBJECTIVES

The main objectives of this research are:

- Investigating the ductility and deformability of GFRP-RC continuous T-beams subjected to symmetrical loading.
- Examining the moment redistribution of GFRP-RC continuous T-beams subjected to symmetrical loading.
- Evaluating the deflection response of GFRP-RC rectangular beams under the different loading conditions.
- Examining the moment redistribution of GFRP-RC rectangular beams under different loading conditions.

The main objectives mentioned above can be obtained through the specific objectives which investigate the effect of the following parameters, well known to influence the flexural behavior of continuous beams:

- Type of reinforcing bars
- Longitudinal reinforcement configuration based on moment redistribution
- Spacing of transverse reinforcement
- Spacing of lateral bars in T-beam flange
- Serviceability of GFRP-RC beam
- Loading ratio

1.5 SCOPE OF WORK

The scope of this study was restricted to large-scale T-beams under symmetrical loading and rectangular beams subjected to unsymmetrical loading. In both cases, beams were continuous over two equal spans. All test beams, except reference beam, were longitudinally and transversely reinforced with sand-coated GFRP bars and stirrups, respectively. During testing, all beams were subjected to monotonic concentrated loads until failure occurred.

1.6 METHODOLOGY

Based on the problems, concerns and the objectives mentioned in the earlier section, the experimental scheme is divided into two series, namely Series 1 and Series 2. Series 1 includes a total of six continuous T-beams where five beams are GFRP-RC in addition to one steel-RC as control beam. The section of the beams has overall depth of 300 mm, effective flange width of 600 mm, flange thickness of 100 mm, and web width of 200 mm. The beams are subjected to symmetrical loading and tested to failure.

Series 2 also consists of six rectangular beams (200 × 300 mm) which are subjected to three loading conditions, such as I) loading both spans equally, II) loading both spans unequally (loading ratio of 1.5), and III) loading one span only. One beam in loading condition I and III, and four beams in loading condition II were investigated. The reinforcing material type, the longitudinal reinforcement ratio and the serviceability requirements were studied under the loading condition II. Mode of failure, cracking pattern, crack-width, strain variation, load-deflection, and deformability and moment redistribution are studied to have the understanding of the overall beam performances.

1.7 THESIS ORGANIZATION

This thesis consists of six chapters as follows:

Chapter 1 introduces the problem definition, the specific scope and objectives of the research, and the methodology followed to achieve these objectives.

Chapter 2 provides the information about FRP composites and their constituent materials, the theoretical background on deflection, deformability and moment redistribution, and the review and summary of the previous researches regarding these structural features.

Chapter 3 describes about the experimental program which includes the longitudinal and cross-sectional profile of the test beams, the material properties and reinforcement details. It also gives an overview on the instrumentation and test set up and the testing procedure.

The analysis and discussion of the experimental data of the test beams are presented in Chapters 4 and 5. The structural performance based on strain profile, load-crack width relationship, load-deflection response and deformability, and moment redistribution of each beam was evaluated and compared with another to understand the effect of the variables on performance.

A summary of the major findings and conclusions regarding the test results is presented in Chapter 6. In addition, the scope of future works is recommended in this chapter.

Both flexural and shear design of the test beams of Series 1 and 2 are demonstrated in Appendix A and B, respectively, using the provisions of code and guideline as applicable.

CHAPTER 2 – LITERATURE REVIEW

2.1 GENERAL

A significant number of existing infrastructures around the world are being negatively affected by corrosion of steel reinforcing bars. To increase the longevity and the protection from further deterioration by corrosion, now-a-days, FRP is increasingly being used as a viable solution. More research is needed to have better understanding of the behavior of FRP-RC continuous beams because some major issues related to deformability and moment redistribution are still not fully explored. In this chapter, material characteristics of FRP reinforcing bars are summarized, then, a brief discussion over the structural behavior of both conventional steel-RC and FRP-RC beams under symmetrical and unsymmetrical loading is presented with the main factors affecting their behavior. In addition, some experimental studies investigating the deformability and moment redistribution of FRP-RC continuous beams are described in the last sections of this chapter.

2.2 BASIC CHARACTERISTICS OF FRP REINFORCEMENT

2.2.1 Tensile Strength

Ultimate tensile strength of FRP bars exceeds that of conventional steel bars, as shown in Fig. 2.1. In addition, FRP bars show no yielding plateau, unlike steel bars, and behave linear-elastic till failure. The main factors that influence the tensile strength and tensile modulus of FRP are properties of fibre and matrix and its volume fractions, distribution of the fibres in the matrix,

physical and chemical interactions, fabrication procedure and manufacturing quality control, size, and cross-sectional area of fibres. Bond performance of matrix also affects the strength of FRP.

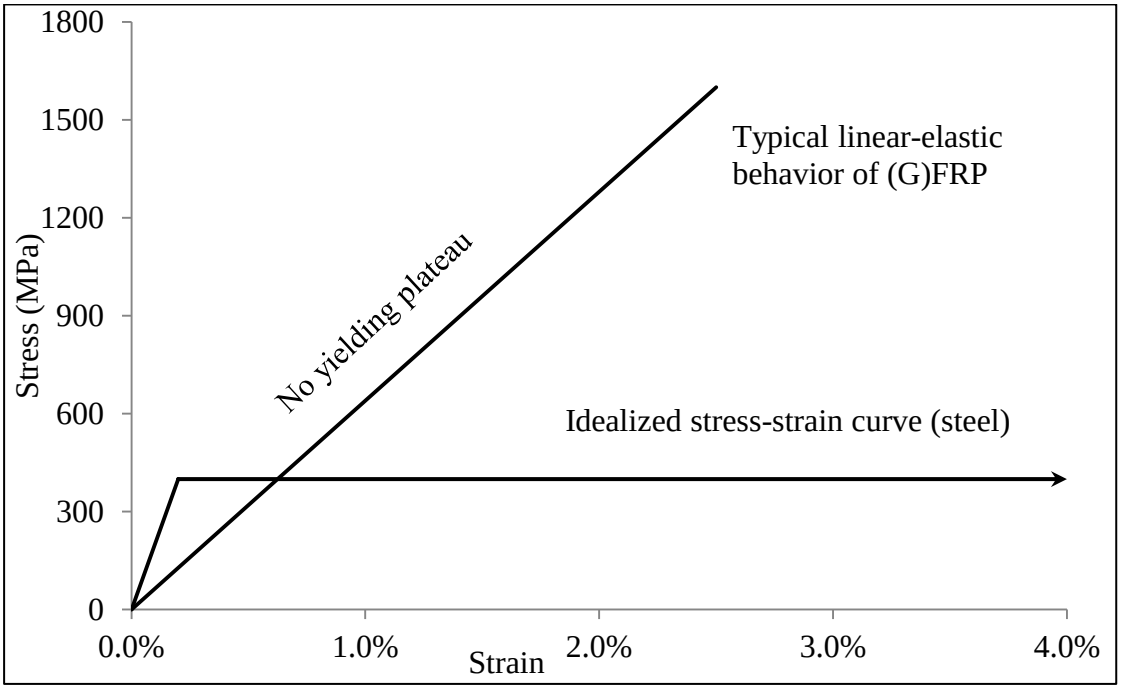

Figure 2.1: Tensile strength of typical FRP with steel bars

Malvar (1995) studied four types of GFRP bar and each type had five specimens. Each type had different deformations but identical diameters. The author concluded that bar tensile strength gets reduced because of indentations and resulted kinks in the longitudinal fibres. In a similar study, Kocaoz et al. (2005) investigated four different types of GFRP bars with the same diameter, and total 32 bars from the same manufacturer were tested. The finding of the testing program showed that splitting of the fibres was found the controlling mode of failure.

2.2.2 Compressive Strength

Generally relying on the compressive strength of FRP bar is not recommended because of its poor performance. Accurate experimental values of compressive strength of FRP are difficult to obtain as specimen geometry and testing program have high effect on the outcomes. Again, the properties of constituents and fibre volume fraction also control the modes of failure. The failure modes include micro buckling of fibres, transverse tensile fracture due to Poisson strain, and shear failure of fibres without buckling.

In other words, compressive strength increases with increasing value of tensile strength, except for Aramid FRP bars where fibres have a nonlinear behavior in compression even at low levels of stress. The compressive modulus of elasticity of FRP bar is found to be smaller than tensile modulus of elasticity and the values are above 80% for GFRP, 85% for CFRP (ACI Committee 440 2015). Lower values of the compressive modulus are attributed to the premature failures which result from the end brooming and internal fibre micro buckling. The manufacturer should provide the compressive properties of a particular bar and the method used to describe the properties as well.

2.2.3 Shear Strength

Matrix properties and local stress distribution govern the behavior of FRP bars under shear loading. In practice, the FRP reinforcing bars are subjected to transverse shear from transverse effect of loading. A significant increase in shear resistance can be gained by applying the technique of winding or braiding fibres transverse to the main reinforcing fibres. Using continuous strand mat in addition to longitudinal fibres, pultruded bars can also be strengthened (ACI Committee 440 2015). For the purpose of field application, shear properties

and details of test methods followed in characterization, should be obtained from the manufacturer.

2.2.4 Bending of FRP Bars

FRP bent bars are normally used for anchoring of longitudinal reinforcement, stirrups, and hooks. Bending of FRP bars are much more difficult compared to the steel bar. Currently, FRP reinforcing bars are fabricated using the thermosetting resin matrices and bending is carried out before the resin is fully cured because fully cured FRP bars are inflexible and rigid. At the same time, heating is not allowed to bend the bar because it would result in loss of strength due to decomposition of resin. Depending on the bending technique and type of resin, the strength varies greatly even though same fibre is used. Bent bars and hooks have to be ordered from the manufacturer.

Minimum bend radius of bent bars is generally larger to prevent the significant weakening around the tight corner and that's why, minimum allowable bend radius of FRP bars is 3.5 to 4 times the bars diameter. So, around 50% strength reduction is assumed at the bend of bars (ISIS Canada, 2007).

2.2.5 Bond Behavior of FRP Bars

Bond behavior is important to develop the required resistance against the imposed load. Not only the mechanical properties but also the environmental conditions affect the bond properties. It also depends on the surface condition of the used bar, such as: sand-coated, braided, ribbed and helically wrapped. Benmokrane et al. (1996b) studied the bond strength of FRP bars with concrete, where twenty FRP-RC beams having 1100-mm span were constructed and a total of five pull-out tests were carried out. The authors found that the bond strength of

FRP in beams was less than that in specimens used in pull-out tests by a scale of 55% to 95% depending on diameter of the reinforcing bars. It was also concluded that GFRP bars showed 60% to 90% less bond strength compared to steel bars because of having less surface interlocking with surrounding concrete. Besides, in this testing program, concrete compressive strength was not found to affect the bond strength between GFRP bars and concrete.

Achillides and Pilakoutas (2004) studied the behavior of FRP bars in concrete by testing more than 130 cube specimens under the direct pullout condition where no splitting was allowed to occur. Again, bond strength of CFRP and GFRP were found to be similar and just below the bond strength of deformed steel bar. The authors also concluded that concrete compressive strength did not control the bond strength but interlaminar shear strength appeared to affect the bond strength. The bar with smaller diameter developed higher bond strength compared to that of higher diameter.

2.3 BEHAVIOR OF STEEL-RC CONTINUOUS BEAMS

2.3.1 General

Behavior of steel-RC concrete beams at any level of load is most often characterized by moment-curvature relationship. At the lower level of loading, the moment-curvature relationship is linear and there are some changes in flexural stiffness along the beam because of cracking in the critical sections. However, after yielding at the higher level of loading, moment-curvature relationship becomes nonlinear and flexural stiffness changes significantly. Finally, it leads to redistribute the forces and moment between the critical sections.

2.3.2. Parameters Affecting the Behavior of Steel-RC Continuous Beams

Some important experimental studies were carried out to find out the factors that usually affect the behavior of continuous steel-RC beams. The behavior of continuous beams is most often characterized by moment-curvature relationship, ductility and rotational capacity. Tension and compression reinforcement ratio, transverse reinforcement ratio and spacing, concrete compressive strength, sectional geometry, and shear-span-to-depth ratio are the main parameters to affect the moment-curvature relationship, and ductility of steel reinforced beam. In this literature, effect of longitudinal reinforcement ratio and confinement are discussed as this study includes the both parameters.

2.3.2.1 Tension and Compression Reinforcement Ratio

Moment-curvature relationship for both tension and compression controlled failure mode of continuous beam were studied by Park and Pauly (1975). Compression controlled beams showed the lower curvature relative to tension controlled beams since no contribution of ductility from yielding of steel bar was available. So, increasing the amount of tension steel decreased the ductile behavior of beams. Also, increasing the compression steel increased the ductility because it counters some part of total tension reinforcement. When beam is loaded beyond the service limit, plastic rotation of the critical section due to steel yielding contributes in shifting the moment from that calculated by linear elastic analysis.

A total of twenty six continuous specimens were testes by Lin and Chen (2000). The main parameters studied were the ratio of transverse reinforcement, the tensile reinforcement ratio, the compressive reinforcement ratio and the concrete compressive strength. They found that increased compression steel with decreased tension steel improved the ductility. Increase of transverse reinforcement ratio significantly enhanced the section ductility.

2.3.2.2 Confinement

Confinement of concrete affects the structural behavior, and providing more stirrups in compression-controlled critical sections increases the ductility of beams. The effect of transverse reinforcement ratio and spacing was studied by Rodriguez et al. (1959). The effect of continuity on shear strength was also one of the variables i.e. verifying the applicability of design equations used for simply-supported beams to design the shear requirement of continuous beams. Longitudinal reinforcement ratio and span-to-effective depth ratio were found the most significant factor, and four types of failure including diagonal tension, flexural, shear-compression, and splitting failure were reported in the study. Amount of transverse reinforcement recommended by code was adequate to resist the shear failure.

Load carrying capacity of beams after diagonal tension cracks took place was influenced by the shear span length. Continuity of beam showed a clear indication of stress redistribution because yielding of steel in one of the critical sections transfer some moment to the adjacent critical section. It was also reported that shear failure even after yielding of steel is possible to occur. Lin and Chien (2000) conducted a research program in which confinement by shear reinforcement was one of the parameters. The authors concluded that increased confinement by increasing shear reinforcement resulted in higher ductility and consequently affected the moment redistribution to be higher.

2.3.3 Plastic Rotation and Ductility

The ductility of a steel-RC member is defined as the ratio of ultimate deformation to yield deformation. The deformation can be expressed as curvature or rotation or deflection. So, the definition of ductility can be any one of the followings:

$$\mu_{\varphi} = \frac{\varphi_u}{\varphi_y}$$

φ_u = Curvature at ultimate condition, φ_y = Curvature at yield condition,

$$\mu_{\theta} = \frac{\theta_u}{\theta_y}$$

θ_u = Rotation at ultimate condition, θ_y = Rotation at yield condition,

$$\mu_{\Delta} = \frac{\Delta_u}{\Delta_y}$$

Δ_u= Deflection at ultimate condition, Δ_y= Deflection at yield condition,

Rotational capacity and ductility most often governs the flexural behavior of steel-RC beam at ultimate condition. For continuous beam, flexural behavior depends on the rotational capacity and ductility of not only a particular section itself but also adjacent critical sections. Several investigations have been done to study the rotational capacity and ductility of steel-RC beams and some are described here.

Mattock (1965) conducted an investigation to find the rotational capacity of plastic hinge region of steel-RC continuous beams. The author concluded that curvature at ultimate condition was inversely proportional to neutral axis depth. It was also found that curvature was inversely proportional to the amount of tensile reinforcement and directly proportional to the amount of compression reinforcement. Since the concrete compressive strains were found to be higher than the assumed value of 0.003, inelastic rotation and curvature were greater than the expected rotation and curvature. Baker and Amarakone (1965) studied rotational capacity of steel-RC sections to have understanding regarding the moment-curvature characteristics. The parameters considered in this research work were grade of reinforcing material used, reinforcement ratio, loading pattern, axial and shear force, compression steel ratio. The

researchers found that equivalent plastic hinge length on either side of the middle support section was almost linear to the ratio of neutral axis-to-effective depth. Moreover, plastic hinge was found to get less affected by type of tension steel and grade of concrete.

Carmo and Lopes (2008) carried out an experimental investigation to study the plastic rotation capacity of continuous beams constructed with high strength concrete. The main objective of this work was to clarify the doubts whether high strength concrete can demonstrate adequate behavior to satisfy the required ductility. The authors examined the effect of tensile reinforcement ratio and transverse reinforcement ratio on rotation capacity of the plastic hinges. The beams with tensile reinforcement ratio less than 2.9% redistributed moment without losing the deformation capacity. It was found that increasing the concrete compressive strength increased the plastic behavior tendency of the beam. In addition, it was found that the longitudinal reinforcement ratio has the most influence on the beam ductility.

2.3.4 Moment Redistribution

With the initiation of cracking in the critical sections of continuous steel-RC beam, the moment redistribution can be identified by observing the theoretical moment based on elastic theory and the experimental moment. In addition, moment redistribution again occurs with the plastic deformation resulting from yielding of steel bars. The degree of moment redistribution is defined as the amount of moment that transfers from a specific section to adjacent sections of a continuous structural element, as shown in Fig. 2.2. It is represented by the coefficient,η and expressed as follows:

$$\partial = \frac{M_{reduced}}{M_{elastic}}$$

$M_{reduced}$ = Reduced moment after moment redistribution,

$M_{elastic}$ =Analysed moment based on elastic theory without moment redistribution.

Percentage of moment redistribution,$\eta = 100(1 - \partial)\%$

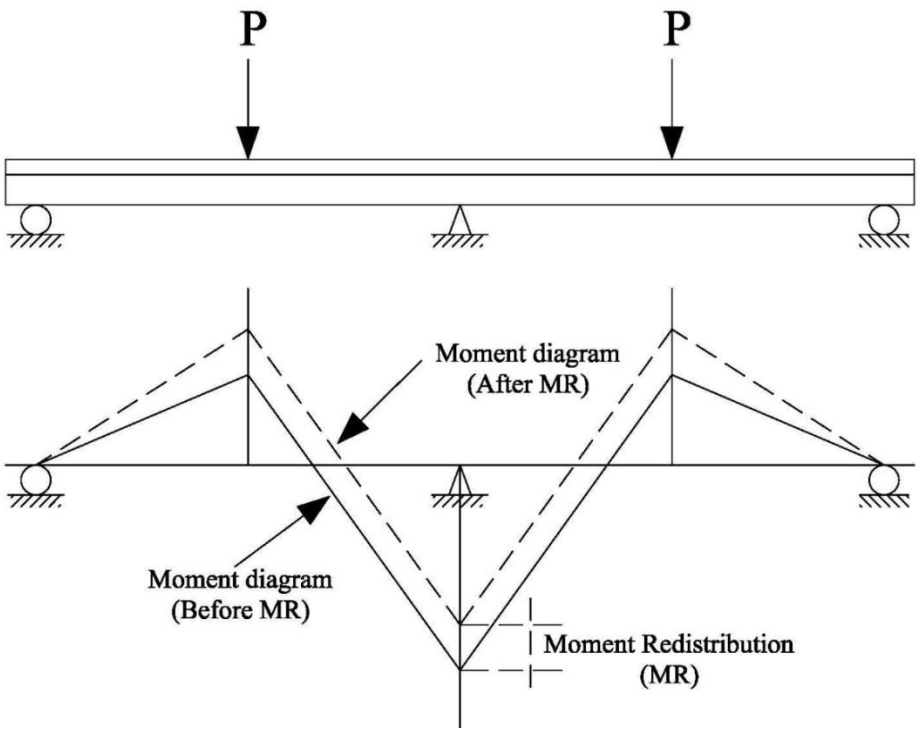

Figure 2.2: Moment redistribution from the middle support to the mid-span section

Ernst (1958) studied the moment and shear redistribution in continuous beams subjected to extreme conditions of support settlement. In this study, five different loading conditions were taken into consideration, and in two of these loading conditions, only one span was loaded. In one of the loading conditions, all supports were in contact with beam from the beginning of loading. Two beams with reinforcement ratio of 0.016 and 0.027 were tested, and moment redistribution of 16.3 and 13.02% were noticed from the mid-span to the middle support section. Also, in other loading condition where exterior support was not in contact with beam until yielding developed in the mid-span, three beams with three different reinforcement ratios

(0.008, 0.016, and 0.027) were investigated. Again, moment redistribution ranging from 6.8 to 11.9% was observed.

Mattock (1959) conducted two series of continuous beams to study the moment redistribution. One series included four two span continuous beams with cross section of 102 × 229 mm and span of 3.962 m while another series dealt with two span T-beams with a flange thickness of 89 mm, flange width of 279 mm, web width of 114 mm, and an overall height of 356 mm. In the first series, one beam was designed based on elastic analysis while the rest were designed assuming 9.4, 17.2 and 30.4% moment redistribution, respectively. The author reported that moment was redistributed at the stage of working load i.e. before the yielding stress. The amount of redistribution at service load stage was slightly more than one quarter of the assumed value of moment redistribution in design. Redistribution of moment was not found to have significant influence on the ultimate load bearing capacity of the continuous beams, and up to 25% moment redistribution, it didn't affect the performance of the specimens in both service and ultimate stages.

Scholz (1993) carried out a theoretical study to find out the effect of section stiffness and slenderness and it's variation along the span, and proposed the definition of moment redistribution. The author derived a relation that accounts for the percentage of moment redistribution and neutral-axis-to-effective depth ratio $(\frac{c}{d})$ at ultimate. It was concluded that assumption of uniform stiffness after cracking no longer exists. The variation of stiffness along the span might change the elastic moment diagram and affects the moment-curvature relationship.

Scott (1997) investigated the moment redistribution of 5.2 m long continuous beam with 300 mm width, and variable depth (400 mm, 250 mm, and 150 mm). Maximum concrete compressive strength of the specimens was 110 MPa and he showed that moment redistribution in continuous beams can be identified in four stages. First stage is up to the first cracking, it showed small percentage of redistribution due to stiffness variations resulting from different amount of reinforcement in the critical sections. Second stage is formation of first flexural cracking; this crack reduced the stiffness of support section considerably, relative to that of the uncracked sections, which caused sudden increase in the magnitude of redistribution percentage. Third stage is up to the formation of all major cracks, a zone of fairly constant redistribution was observed once all major cracks had formed, and a stable distribution of flexural stiffness established. Fourth stage is reinforcement yielding that lead to a local reduction in flexural stiffness which, together with plastic rotation and more slip, resulted in further changes in relative stiffness and increased levels of moment redistribution.

To have better understanding of moment redistribution, Carmo and Lopes (2006) studied the factors affecting the moment redistribution. The authors argued that the required plastic rotation to ensure moment redistribution should be smaller or equal to available plastic rotations. The required plastic rotation is determined based on deformation compatibility conditions. Therefore, moment redistribution should be calculated based on overall member behavior instead of section behavior. The authors addressed some factors affecting the plastic rotation such as concrete compressive strength, size and shape of cross-section, shear reinforcement ratio, slenderness of member, and longitudinal reinforcement. The authors concluded that higher compressive strength would require higher rotation, and the continuous

beams with concentrated load at mid span would require less plastic rotation compared to that required by uniformly loaded continuous beams.

2.4. BEHAVIOR OF FRP-RC CONTINUOUS BEAMS

2.4.1 General

The behavior of fiber reinforced polymer (FRP)-reinforced concrete (RC) beams depends on the mechanical properties of FRP as well as concrete used in the structural element. The FRP bars show linear stress-strain relationship up to failure. This is the main reason for the different behavior of FRP-RC sections compared to that of conventional steel-RC sections. Furthermore, the behavior of continuous beam is significantly depends on the behavior of adjacent critical sections of the element.

In this chapter, a brief discussion on the flexural and the shear behavior of FRP-RC continuous beam is presented with the main factors affecting the behavior. In addition, the available experimental studies investigating the ductility and moment redistribution of FRP-RC continuous beams are described in the last sections of this chapter.

2.4.2 Deflection Behavior

One of the major serviceability concerns for GFRP-RC beams is deflection. The GFRP-RC elements with similar reinforcement ratios to steel-RC counterparts show higher deflection because of the lower modulus of elasticity of GFRP bars compared to that of conventional steel. There are two different approaches for calculating the deflection; one is based on effective moment of inertia while the other one is curvature integration approach. There are several models available for calculating the effective/equivalent moment of inertia of the element and some of them are described here.

The model of ISIS Canada (2007) assumes a uniform moment of inertia instead of actual variable moment of inertia along the beam span to calculate the deflection. Large number of formulations for effective moment of inertia were examined by Mota et al. (2006) and the following expression gave the most consistent and conservative result over the entire range of specimens.

The effective moment of inertia,

$$I_e = {I_t I_{cr}}\Big/{(I_{cr} + (1 - 0.5(M_{cr}/M_a)^2)(I_t - I_{cr}))}$$

Where,

I_t= Moment of inertia of uncracked section transformed to equivalent concrete,

I_{cr}= Moment of inertia of cracked section,

M_{cr}= Cracking moment,

M_a= Moment at any load level,

Load-deflection response of continuous GFRP-RC beams was investigated by Habeeb and Ashour (2008). The widely acknowledged Branson`s equation of effective moment inertia which was derived for steel-RC beams subjected to service loads, was modified with a factor (β_d) to take into consideration the less tension stiffening effect of FRP-RC beams. The authors introduced a reduction factor (γ_G) to the second term which represents the post-cracking phase. For the deflections of continuous beams, γ_G of 0.6 was found to be very effective to predict the deflections of tested beams.

The effective moment of inertia,

$$I_e = (M_{cr}/M_a)^3 \beta_d I_g + (1 - (M_{cr}/M_a)^3 I_{cr} \gamma_G \leq I_g$$

$$\text{Where, } \beta_d = 0.2 * (\rho_f/\rho_{fb}) \leq 1$$

β_d= Reduction coefficient related to the reduced tension stiffening in FRP-RC members.

Moreover, ACI 440.1R-15 (ACI Committee 440 2015) suggests an expression for the effective moment of inertia with a different γ factor, which depends on load and boundary conditions and accounts for the uncracked regions and stiffness variation in the cracked regions. The γ factor in the expression corresponds to the uniformly distributed loading condition.

$$I_e' = {I_{cr}}\Big/{(1-\gamma(M_{cr}/M_a)^2(1-I_{cr}/I_g))} \leq I_g$$

Where $M_a \geq M_{cr}$ and $\gamma = 1.72 - 0.72 * (M_{cr}/M_a)$

2.4.3 Ductility and Deformability

Ductility of steel-RC members is defined as the ratio of deflection or curvature at ultimate loading to that at yielding of steel. The yielding plateau of steel is the key to quantify the ductility of steel-RC beams. Since FRP doesn't yield, the definition of ductility for steel-RC beams is not directly applicable to FRP-RC beams. However; there are two main approaches available to quantify the deformability of FRP-RC elements. The first one is deformation based approach which was introduced by Jaeger et al. (1995) under the name of *J*-factor (sometimes referred to DFs). This factor is a means of comparison of safety level at ultimate and that at service level, and accounts for the increase in moment as well as in curvature or deflection. The Canadian Highway Bridge Design Code (CHBDC) (CSA S6-14) defined the service state corresponding to maximum compressive concrete strain of 0.001. CHBDC requires the deformability factors to be greater than 4 for rectangular beams and 6 for beams with T-sections.

By definition,

J-factor = Strength factor × Deformation factor (curvature/deflection)

$$Strength\ factor = \frac{Moment\ at\ ultimate}{Moment\ at\ concrete\ compressive\ strain\ of\ 0.001}$$

$$Curvature\ factor = \frac{Curvature\ at\ ultimate}{Curvature\ at\ concrete\ compressive\ strain\ of\ 0.001}$$

$$Deflection\ factor = \frac{Deflection\ at\ ultimate}{Deflection\ at\ concrete\ compressive\ strain\ of\ 0.001}$$

The second approach is energy based and was modified by Grace et al. (1998) and defines the deformability as a ratio of inelastic energy to total energy. In this approach, area under the load-deformation curve is referred to total energy, as described in Fig. 2.3. To separate the elastic energy from the total energy, the weight of load was considered in the loading stage of pre-cracking, post-cracking, and concrete softening. This approach also accounts for the effect of type, modulus of elasticity, and tensile strength of the reinforcing bar as well as the type of stirrups, the failure mode, and the concrete softening in case of failure by concrete crushing.

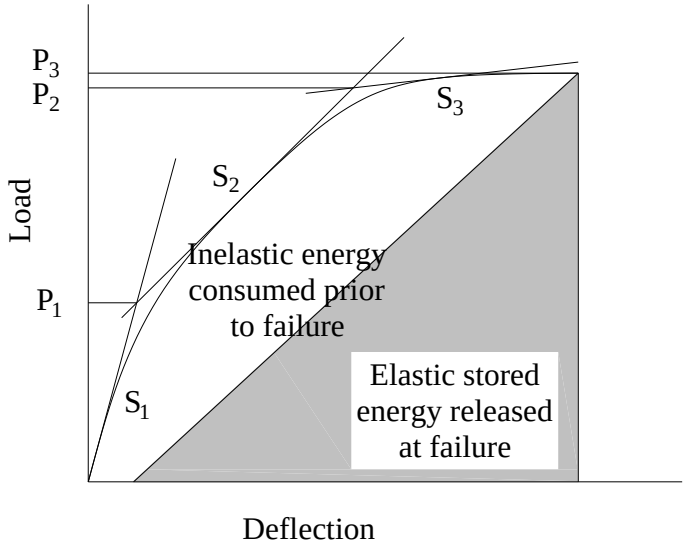

Figure 2.3: Total, elastic and inelastic energy at failure (reproduced from Grace et al. 1998)

The slope of elastic energy line can be written in the form of following expression,

$$S = \alpha\beta\gamma \frac{E_f}{E_s} \times \frac{f_y}{f_{ds}} \frac{P_1 S_1 + (P_2 - P_1)S_2 + (P_3 - P_2)S_3}{P_3}$$

Where,

α =factor for stirrup type (1.0, 0.95, and 0.98 for steel, GFRP, and CFRP, respectively); β =factor for failure mode (1.0, 0.95, and 0.98 for compressive flexure, flexure shear, and shear, respectively); γ =factor for reinforcement type (1.0, 4.0, and 2.1 for steel, GFRP, and CFRP, respectively); E_f =modulus of elasticity of FRP; E_s =modulus of elasticity of steel; f_y = yield strength of steel; f_{ds} =design strength of FRP;

S_1 =Slope of pre-cracking stage of loading;

S_2 =Slope of post-cracking stage of loading;

S_3 =Slope of concrete softening stage of loading;

P_1 =Load corresponding to intersecting point of slope S_1 and S_2;

P_2 =Load corresponding to intersecting point of slope S_2 and S_3;

P_3 =Ultimate load;

Based on the ratio of the inelastic-to-total energy, the beam deformability can be classified as ductile, semi-ductile, and brittle according to energy ratio which is greater than 75%, 70 to 74%, and less than 69%, respectively.

In the same study, the authors conducted a research work to investigate the behavior and ductility of simple rectangular, and continuous T-beam reinforced with FRP. Three types of reinforcing bars, conventional steel, GFRP and CFRP, were used as longitudinal and transverse reinforcement. The overall span of continuous beams was 7600 mm including end projection of 150 mm, and the bottom and top width of the tapered section were 76 mm and 101 mm, respectively. The flange width was 388 mm and overall section depth was 338 mm including the flange thickness of 50 mm. The specimens were cast with concrete compressive strength of

48.26 MPa. The loading scheme for continuous beams includes applying the load until impending failure followed by unloading to have the record of residual deformation. Increased shear deformation, and mid-span deflection were reported as a result of using GFRP stirrups. Furthermore, the continuous T-beams were found to experience higher energy ratio presenting more ductile behavior compared to their simply supported counterparts.

Vijay and GangaRao (2001) studied the factors affecting bending behavior of GFRP-RC members and introduced energy absorption concept that is based on curvature limit state with an attempt to unify deflection limit and crack width limit, and to represent deformability factors (DFs) as well. According to the study, the factors affecting the deformability were found as following:

- uniform elongation of FRP bars compared to localized yielding of steel bars,
- effect of confinement,
- bond between concrete and bars,
- uniform crack distribution and spacing in FRP-RC concrete,

They also concluded that compression controlled failure is better than tension controlled failure and listed the advantages as higher moment capacity, better deformability, relatively gradual failure, and lower crack width and deflection. They also reported that DFs were in the range of 6.7 to 13.9 in case of compression failure, and higher percent of tension reinforcement resulted in higher DF.

2.4.4 Moment Redistribution

Continuous beams usually have potential to redistribute the moment between the critical sections. The advantages of moment redistribution includes favourable deformable behavior, utilizing the full capacity of more cross-sections of span, ease of concrete placement, reducing

reinforcement congestion in column-beam joint when negative moment gets reduced, and economies associated with narrow envelope of maximum negative and positive moment after moment redistribution.

The structural behavior of FRP-RC beams is significantly different from that of steel-RC beams because stress-strain relationship of FRP is elastic up to failure. So, FRP-RC beams don't undergo significant plastic deformation unless beams are adequately confined by stirrups. However, moment redistribution in FRP-reinforced concrete sections is possible, like steel-RC beams, due to cracking, inelasticity in concrete, and difference of stiffness between the critical sections of member.

Mostofinejad (1997) studied the behavior of ten continuous reinforced concrete beams giving special attention to ductility and moment redistribution. All beams were 6500 mm long with end projection of 250 mm, and width and overall depth of beams were 250 mm and 350 mm, respectively. Two of the beams were reinforced with conventional steel, and other eight specimens were designed with CFRP. Two of these eight specimens were under-reinforced while others were over-reinforced. To study the confinement, CFRP grid which is known as NEFMAC was used. Based on the analytical and experimental results, "curvature pseudo-ductility factor" and "deflection pseudo-ductility factor" were proposed for FRP-RC beams. The conventional steel reinforced concrete beams experienced the full plastic redistribution and high ductility. FRP over-reinforced beams showed moment redistribution of almost 50%. It was also reported that confinement applied at compression zone by NEFMAC did not significantly contribute to either ductility or moment redistribution.

Habeeb and Ashour (2008) studied the flexural behavior of two simply and three continuously supported beams which were longitudinally reinforced with GFRP bars and transversely reinforced with steel stirrups. Continuously supported beams had two spans, each having a span of 2750 mm. All the specimens were 200 mm in width and 300 mm in depth. Only parameter studied here was longitudinal reinforcement ratio. Four types of failure mode were reported. One of the four failures was bar rupture which was observed in bottom layer of the mid-span of under-reinforced beams. Concrete crushing failure occurred in the over-reinforced beams. Concrete crushing combined with shear failure was observed when diagonal shear crack emerged at the late stage of loading and propagated at the time of concrete crushing failure on the top. This failure was found in the beam with both top and bottom sections having designed as over-reinforced. Conventional ductile flexural failure mode occurred in the steel reinforced concrete beam because of yielding of tensile steel reinforcement followed by concrete crushing at both critical sections. The authors concluded that earlier and wider cracks developed in GFRP reinforced beams compared to steel reinforced beams due to lower modulus of elasticity of GFRP bars. The GFRP reinforced continuous beams did not show any remarkable load redistribution. Over-reinforcing the bottom layer of both simply and continuously supported beams showed higher load carrying capacity and enhanced the ability to reduce deflection and delay crack propagation.

Ten large scale continuous concrete beams were tested by El-Mogy et al. (2010 and 2011) to study the parameters that include the flexural reinforcement ratio, material of longitudinal and transverse reinforcement, spacing and ratio of transverse reinforcement. There were two series; series-I was related to investigating the effect of material type and ratio of longitudinal reinforcement while series-II dealt with material type, spacing, and ratio of transverse

reinforcement. The beams with cross section of 200× 300 mm were continuous over two equal spans of 2,800 mm each. GFRP, CFRP, and conventional steel were used in the testing program. The experimental results of series-I showed that moment redistribution is possible in FRP-RC beams due to a number of factors. The high elastic deformation provided by FRP and the material nonlinearity resulted from concrete crushing, cracking, and bond slippage were found as two main factors contributing to moment redistribution. In the stage of linear stress distribution in concrete, the moment redistribution was mainly caused by cracking due to high elastic deformations of FRP bars. But the nonlinearity of concrete along with the FRP slippage contributed to the moment redistribution at the loading close to ultimate failure.

All the beams of series-II were found to fail by the concrete crushing in both middle support and mid span sections, with wide cracks at the middle support section. The number of cracks at the middle support section in beams with smaller stirrup spacing (*d/3*) was found more than the beams with wider spacing (*d/2*). These beams were capable to redistribute more than 20% of the connecting bending moment from the middle support section to mid span section, and also achieved the expected failure load. Decreasing the stirrup spacing keeping the same transverse reinforcement ratio affected the moment redistribution significantly. The authors concluded that the GFRP-RC beams designed assuming 20% moment redistribution were able to redistribute the elastic moment from negative moment section to positive moment section without any adverse effect on ultimate load carrying capacity. Reinforcement configuration that was chosen in the program played a positive role on deflection reduction while maintaining same load carrying capacity by elastic analysis.

Matos et al. (2011) studied the service and failure response, and confinement effect in the critical cross-sections of three small scale GFRP-RC and one steel-RC continuous beams. A

procedure to calculate the confinement effect due to decreasing the stirrup spacing was also presented. The rectangular beams were 100 mm wide and 120 mm deep, and were cast with concrete compressive strength of around 30 MPa. GFRP-RC specimens showed wide cracks and low stiffness, owing to the low modulus of elasticity of GFRP bars. Reducing the spacing of stirrups in the critical sections increased both strength and deformability. Overall, reduced cracking in service condition, and higher load carrying capacity at failure due to higher force redistribution were observed. In this way, the development of a crack hinge over the middle support highlighted the better performance. Moreover, significant increase in strength and deformability was observed as a result of confinement applied at the critical zones.

Santos et al. (2013) carried out an experimental program over seven small-scale continuous T-beams reinforced with GFRP bars and stirrups. The parameters studied in this investigation were GFRP reinforcement ratio and confinement level in the critical sections of potential plastic hinge formation. Higher confinement level was designed to be achieved by decreasing the spacing of transverse reinforcement as well as placing additional half-depth stirrups in the compression side of the critical sections. The beams were 2,200 mm long with flange width of 300 mm; flange thickness of 40 mm; web width and overall depth were 100 mm and 120 mm, respectively. These specimens were cast with a 28-day concrete strength of approximately 30 MPa, and were subjected to one concentrated load applied at the mid-span. The authors concluded that structural performances i.e. deflection recovery after unloading, more moment redistribution from the middle support section to mid-span section, and higher failure load were observed as the mid-span section had increased reinforcement ratio. They also found that increasing concrete confinement with higher percentage of transverse reinforcement enabled

the middle support section to exhibit more moment redistribution, and also promoted plastic hinge formation.

Mahmoud and El-Salakawy (2014 and 2016) investigated the moment redistribution in shear-critical continuous beams. All test beams had 200 × 300 mm cross section and were continuous over two spans of 2,800 mm each. Three main variables namely, concrete strength, longitudinal reinforcement ratio, and transverse reinforcement ratio were investigated. All test beams were designed to satisfy an assumed 20% moment redistribution. During testing, the beams were subjected to a two-point loading system in each span where the shear span-to-depth ratio was kept constant at 3. It was observed that all test beams failed in shear near the interior support after moment redistribution of approximately 20% or higher took place from the hogging moment region to sagging moment region. The authors also concluded that increasing the shear reinforcement ratio by increasing the stirrup diameter while maintaining the same stirrup spacing did not result in significant increase in shear strength. However, increasing the shear reinforcement ratio by using stirrups with small spacing was found to be efficient in increasing shear strength of the test beams.

CHAPTER 3 – EXPERIMENTAL PROGRAM

3.1 GENERAL

The current study aimed at investigating the behavior of T-beams under symmetrical loading in Series 1, and the behavior of rectangular beams under unsymmetrical loading in Series 2. The main objective of this program was to investigate the behavior of continuous beams paying special attention to evaluating moment redistribution. The program was designed to carry out testing of a total of twelve specimens with six specimens in each series. The following sections of this chapter describe the properties of materials used, loading condition and geometry, description and design of the specimens, test instrumentation and set up, and testing procedure.

3.2 MATERIAL PROPERTIES

In this project, conventional steel and sand-coated GFRP bars with different sizes were used for longitudinal and transverse reinforcement of the test beams. During the course of experimental investigation, the properties of concrete and steel were obtained from the ancillary tests conducted in the laboratory. In the following sections, different properties of the reinforcement and concrete, which were used in the construction of all test beams, are given in details.

3.2.1 Reinforcing Bars

The mechanical properties of the used steel bars were obtained through tensile tests carried out in the laboratory. In case of GFRP bars, the characteristic design values including strength and strain, defined by CSA/S806-12 (CSA 2012), were determined from the material certificate that

was provided by the manufacturer. The reinforcing materials were from two different lots which were ordered for each series of beams separately. The material properties of the steel bars and GFRP bars are summarized in Tables 3.1 and 3.2, respectively.

Table 3.1 - Properties of steel bars

Material type	Bar size	Nominal Diameter (mm)	Area (mm^2)	Yield strength (MPa)	Elastic modulus (GPa)	Yield strain (%)
Steel	8	8.0	50.3	400	200	0.20
	10M	11.3	100.0	410	200	0.21
	15M	15.9	200.0	460	200	0.23
	20M	19.9	300.0	430	195	0.22
	25M	25.2	500.0	460	200	0.23

Table 3.2 - Properties of GFRP bars

Series	Bar size	Nominal Diameter (mm)	Area (mm^2)		Tensile strength (MPa)	Elastic modulus (GPa)	Ultimate strain (%)
			Nominal	Annex A[a]			
Series 1	No.10	9.5	71.3	83	1,770	65	2.7
	No.10 (bent)	9.5	71.3	83	1,350[b]	52[b]	2.6[b]
	No.13 (bent)	12.7	126.7	152	1,330[b]	53[b]	2.5[b]
	No.16	15.9	197.9	235	1,680	65	2.6
	No.22	22.23	388.0	443	1,600	67	2.3
Series 2	No.10 (bent)	9.5	71.3	79	1,350[b]	52[b]	2.6[b]
	No.13 (bent)	12.7	126.7	149	1,280[b]	52[b]	2.5[b]
	No.13	12.7	126.7	147	1,680	65	2.6
	No.16	15.9	197.9	232	1,610	65	2.5
	No.22	22.2	387.9	439	1,430	68	2.1
	No.25	25.4	506.9	582	1,400	68	2.1

[a] Average cross-sectional area calculated according to CSA/S806-12, Annex A
[b] Straight portion property
The properties of the GFRP bars are calculated based on the nominal area.

3.2.2 Concrete

Normal weight, ready-mixed concrete with a target 28-day compressive strength of 40 MPa was used to cast all beams. The maximum size of aggregate used in the concrete mix was 20 mm in Series 1 while that was 10 mm in Series 2. On the day of testing, at least five cylinders of standard size (100 × 200 mm) were tested to determine the average concrete compressive strength for each beam according to CSA A23.1/A23.2-14 (CSA 2014c). Table 3.3 and 3.4 enlist the concrete compressive strength of all test beams of Series 1 and Series 2, respectively.

3.3 LOADING CONDITION AND GEOMETRY

All test specimens were 6,000-mm long and were continuous over two equal spans of 2,800 mm each. Each specimen was provided with extra 200 mm overhang at both ends to provide adequate anchorage. In addition, in Series 1, special requirement regarding the geometry of isolated T-beam specified only in ACI 318-11 (ACI Committee 318 2011) was also considered. The ACI 318-11 requires the flange thickness not to be less than one-half the web width and an effective flange width not to be more than four times the web width. Considering these requirements, an overall beam depth of 300 mm along with 200-mm web width was selected. Also, flange width and thickness of 600 and 100 mm, respectively were selected, as shown in Fig. 3.1. Series 2 was dedicated to the rectangular beams with cross-section of 200 × 300 mm and tested under three different loading cases: I) equal load *P* (symmetrical) on both spans, II) load *P* on one span and 1.5*P* on the other, and III) load *P* on one span only, as demonstrated in Fig. 3.2.

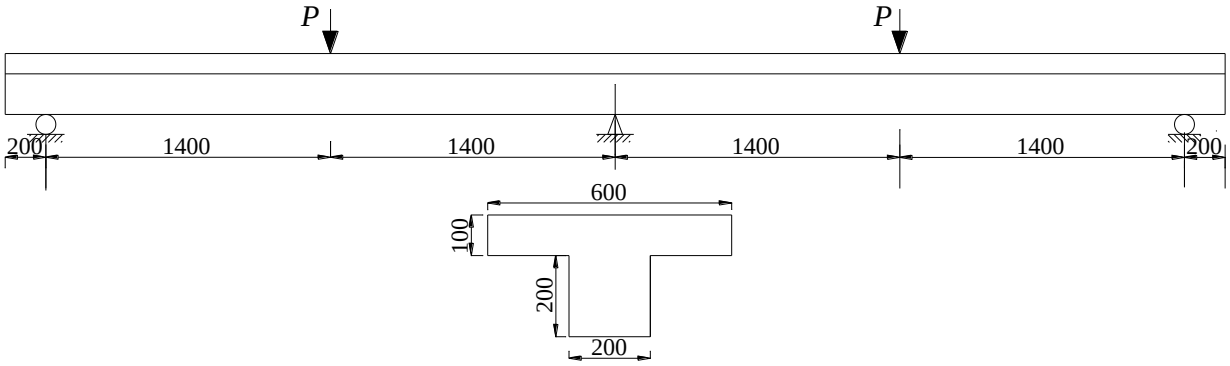

Figure 3.1: Loading condition with longitudinal and sectional profile of the test beams of Series 1 (dimensions in mm)

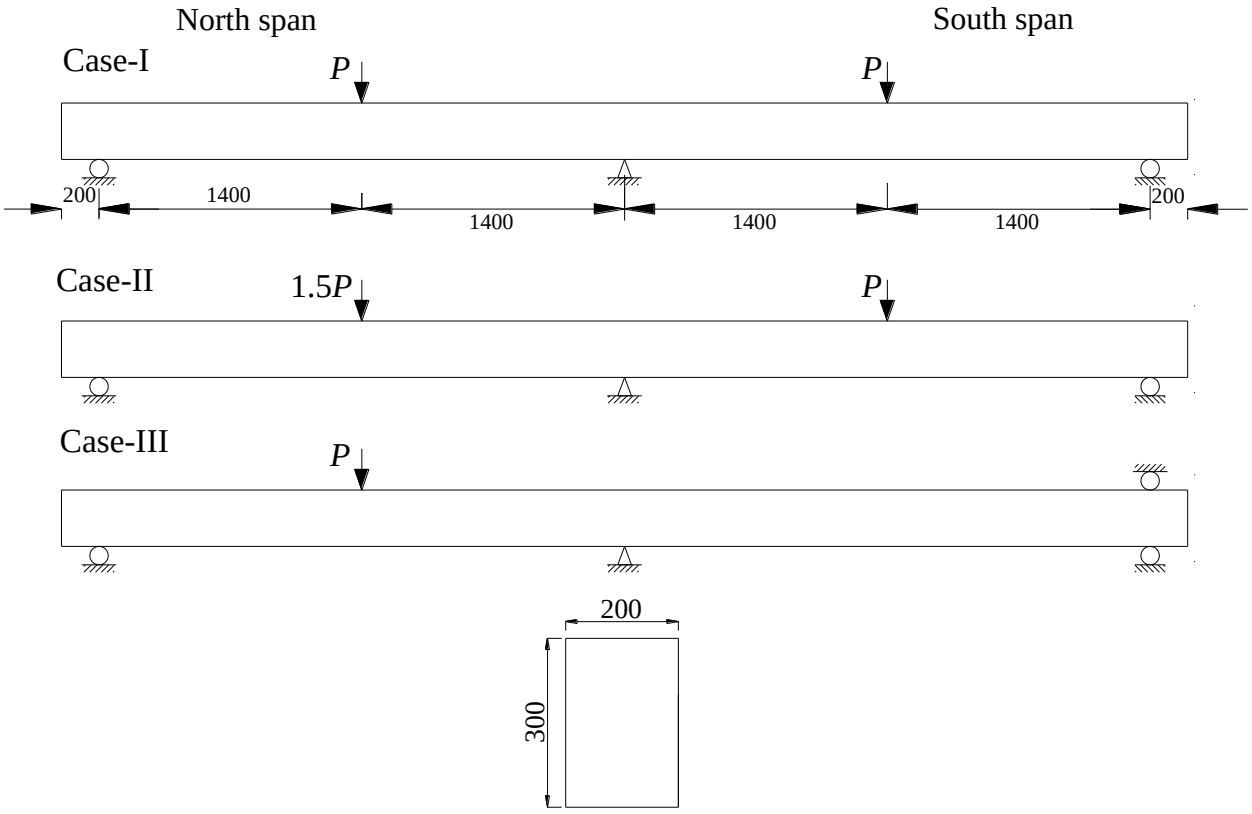

Figure 3.2: Loading conditions with longitudinal and sectional profile of the test beams of Series 2 (dimensions in mm)

3.4 DESCRIPTION OF SPECIMENS

The experimental program consisted of two series of beams, each of which includes six beams. The following sections describe the designation of each beam from both series.

3.4.1 Series 1

One beam was reinforced with steel to serve as a reference, while the other five were reinforced with GFRP bars and stirrups. The test parameters included the type of reinforcing material (steel or GFRP), the assumed percentage of moment redistribution (either no moment redistribution or 15%), the spacing of lateral reinforcement in flange (450 or 150 mm), the arrangement of

stirrups (No. 13 spaced at 75 mm or No. 10 spaced at 45 mm), and the design criteria (serviceability or ultimate strength requirements). The nomenclature of the test beams can be explained as following. The first letter stands for the type of reinforcing material used ("S" for steel and "G" for GFRP). The second letter refers to the design criteria where "u" for ultimate limit states (ULS), and "s" for service limit states (SLS). The third letter represents the moment redistribution percentage ("E" and "R" for no and 15% moment redistribution, respectively). The fourth character illustrates the spacing of stirrups, expressed as percentage of the effective depth of the beam, while the last character denotes the spacing of the lateral bars in the flange, which is expressed as multiples the flange thickness. For example, GuR-30-4.5 is reinforced with GFRP bars designed based on ULS with 15% moment redistribution from the hogging to the sagging moment region. The spacing of stirrups was 30% of the effective depth (75 mm c/c) and the lateral bars in the flange were spaced at 4.5 times the flange thickness (450 mm c/c). All these details are given in Fig. 3.3.

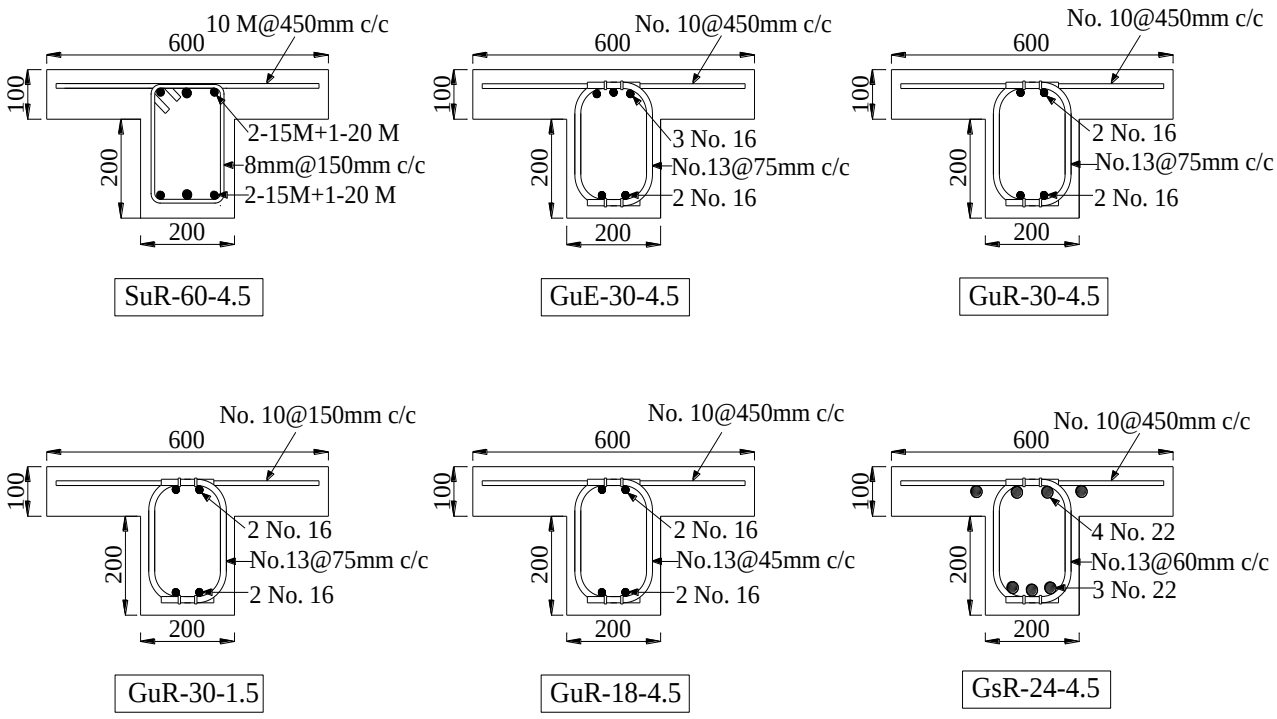

Figure 3.3: Details of the test beams in Series 1

3.4.2 Series 2

The test beams were subjected to three different loading cases: I) equal load *P* (symmetrical) on both spans, II) load *P* on one span and 1.5*P* on the other, and III) load *P* on one span only, as demonstrated in Fig. 3.2. One beam was tested for each of loading cases I and III; whereas, four beams were tested under loading case II. The four beams investigated three parameters; the type of reinforcing material (steel or GFRP), the assumed percentage of moment redistribution (0% or 20%), and the design criteria (ultimate or serviceability limit state). The nomenclature of the beams can be described as follows. The first letter represents the type of reinforcing material ("S" for steel and "G" for GFRP). The second letter stands for the type of "limit state design" where "u" and "s" refers to ultimate limit state (ULS), and serviceability limit state (SLS), respectively. The third letter (E or R) denotes whether the beam was designed for elastic moment

(E) or considering 20% redistributed moment from hogging to sagging region (R). Finally, the last character refers to the loading case. For example, GuR-II can be described as GFRP-RC beam designed based on ULS with an assumed moment redistribution of 20% and tested under loading case II. Fig. 3.4 shows all these details of both spans in Series 2.

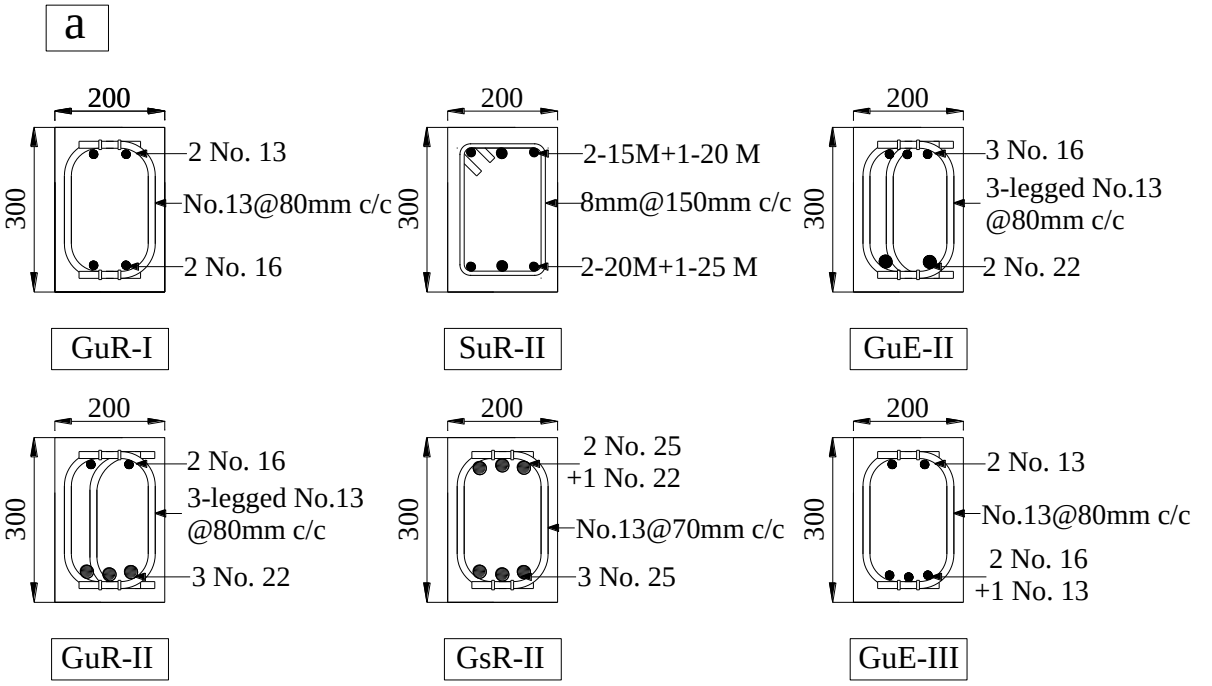

Figure 3.4: Details of the test beams of (a) north span and (b) south span in Series 2

3.5 DESIGN OF SPECIMENS

In this test program, the Canadian standard CSA/S806-12 (CSA 2012) was followed to design all test specimens to satisfy both flexural and shear strength requirements.

3.5.1 Series 1

The reference beam SuR-60-4.5 was first designed, as given in Appendix A, for flexure and shear following the Canadian standard CSA/A23.3 (CSA 2014b) to meet a target design load of 155 kN in each span assuming 15% moment redistribution. The service load of beam SuR-60-4.5 was calculated based on satisfying a crack control parameter, z = 25,000 N/mm (assuming exterior exposure). Afterwards, beam GsR-24-4.5 was designed to satisfy the requirements for that service load using z = 38,000 N/mm for exterior exposure according to the CSA/S806-12 (CSA 2012). It is worth mentioning that these values for crack control limits are equivalent to a crack width of 0.3 and 0.5 mm in steel- and FRP-RC structures, respectively. The other GFRP-RC beams were designed for the same target load (155 kN). Beam GuE-30-4.5 was designed according to CSA/S806-12 (CSA 2012) that does not allow moment redistribution whereas, the remaining beams were provided with the longitudinal reinforcements to satisfy an assumed percentage of 15% moment redistribution. In all GFRP-RC beams, both the hogging and the sagging moment critical sections were over-reinforced to ensure failure by concrete crushing. Regarding the transverse reinforcement (stirrups), El-Mogy et al. (2011) concluded that decreasing the spacing of stirrups enhanced the moment redistribution while Mahmoud and El-Salakawy (2016) reported that the stirrup diameter had little effect on the moment redistribution. As such, 10 mm-diameter stirrups spaced at 45 mm, while maintaining approximately the same ratio of transverse reinforcement, were chosen for beam GuR-18-4.5 to study the effect of stirrup

spacing. In addition, GuR-30-1.5 was constructed to study the effect of the spacing of lateral bars in flange. Table 3.3 shows the reinforcement details of all test beams.

Table 3.3 - Concrete compressive strength and reinforcement details of Series 1 test beams

Beam	Concrete strength, f_c' (MPa)	Longitudinal reinforcement				Transverse reinforcement		Spacing of lateral bars in flange (mm)
		Hogging region		Sagging region		Bar size	Spacing (mm)	
		Bars	ρ/ρ_b	Bars	ρ/ρ_b			
SuR-60-4.5	43	2-15M+1-20M	0.33	2-15M+1-20M	0.11	8.0	150	450
GuE-30-4.5	44	3 No. 16	4.72	2 No. 16	1.05	No.13	75	450
GuR-30-4.5	42	2 No. 16	3.27	2 No. 16	1.10	No.13	75	450
GuR-30-1.5	45	2 No. 16	3.09	2 No. 16	1.04	No.13	75	150
GuR-18-4.5	45	2 No. 16	3.09	2 No. 16	1.04	No.10	45	450
GsR-24-4.5	44	4 No. 22	11.9	3 No. 22	2.97	No.13	60	450

ρ = provided longitudinal reinforcement ratio

ρ_b = balanced reinforcement ratio

3.5.2 Series 2

The details of flexural and transverse reinforcement of the test beams are enlisted in Table 3.4. The steel-RC beam SuR-II (reference beam for loading case II) was designed according to CSA/A23.3 standards (CSA 2014b) to carry a target load of P = 125 kN on one span and 1.5 P (187.5 kN) on the other, as described in Appendix B. Then, beams GuE-II and GuE-III were designed for the elastic moments and corresponding shear force according to CSA/S806-12 standards (CSA 2012) to have the same load carrying capacity (P) under the specified loading case. Beams GuR-I and GuR-II were also provided with the longitudinal reinforcement to satisfy an assumed MR of 20% from the hogging to the sagging moment region. Lastly, beam GsR-II was designed to have the same service moment as that of the steel-RC beam SuR-II. It is worth mentioning that a crack control parameter, z which equals to 25,000 N/mm, and 38,000 N/mm (assuming exterior exposure) in steel- and GFRP-RC members, respectively, governed the SLS based design of the hogging moment region.

Table 3.4 - Concrete compressive strength and reinforcement details of the Series 2 test beams

Beam	Concrete strength, f_c', (MPa)	Longitudinal reinforcement			Transverse reinforcement			
		North mid-span	Central support section	South mid-span	North span		South span	
					Bar size	Spacing (mm)	Bar size	Spacing (mm)
GuR-I	39	2 No. 16	2 No. 13	2 No. 16	No. 13	80	No. 13	80
SuR-II	43	2-20 M+1-25 M	2-15 M+1-20 M	2-20 M	8.0	150	8.0	150
GuE-II	43	2 No. 22	3 No. 16	2 No. 13	No. 13[a]	80	No. 13	80
GuR-II	43	3 No. 22	2 No. 16	2 No. 13	No. 13[a]	80	No. 13	80
GsR-II	39	3 No. 25	2 No. 25 +1 No. 22	2 No. 25	No. 13	70	No. 13	120
GuE-III	41	2 No. 16+1 No. 13	2 No. 13	2 No. 13	No. 13	80	No. 10	80

[a] 3-legged stirrup placed in staggered arrangement

ρ = provided longitudinal reinforcement ratio

ρ_b = balanced reinforcement ratio

3.6 BEAM CONSTRUCTION

Some preliminary works were accomplished before the construction of test beams such as: building the formworks, and preparing the reinforcement cages. Afterwards, surface of the reinforcing bars was prepared and cleaned for the strain gauges to be attached on the designated points of interest. Reinforcement cages were carefully assembled (Fig. 3.5) and placed on plastic chairs in the plywood formworks, as shown in Fig. 3.6. Oiling the formworks was done to facilitate the removal of the specimens once they were cast and cured. During concrete pouring in the formworks, electrical vibrator was used to ensure better compaction, and care was taken to avoid the concrete segregation and prevent the strain gauges from being damaged in this process. At the time of concrete casting, at least thirty cylinders of standard size (100 mm × 200 mm) were cast to determine the average concrete compressive strength at 3^{rd}, 7^{th}, 14^{th}, and the day of testing. The constructed beams as well as the concrete cylinders were properly wet cured with help of burlaps and plastic sheet to gain the full design concrete compressive.

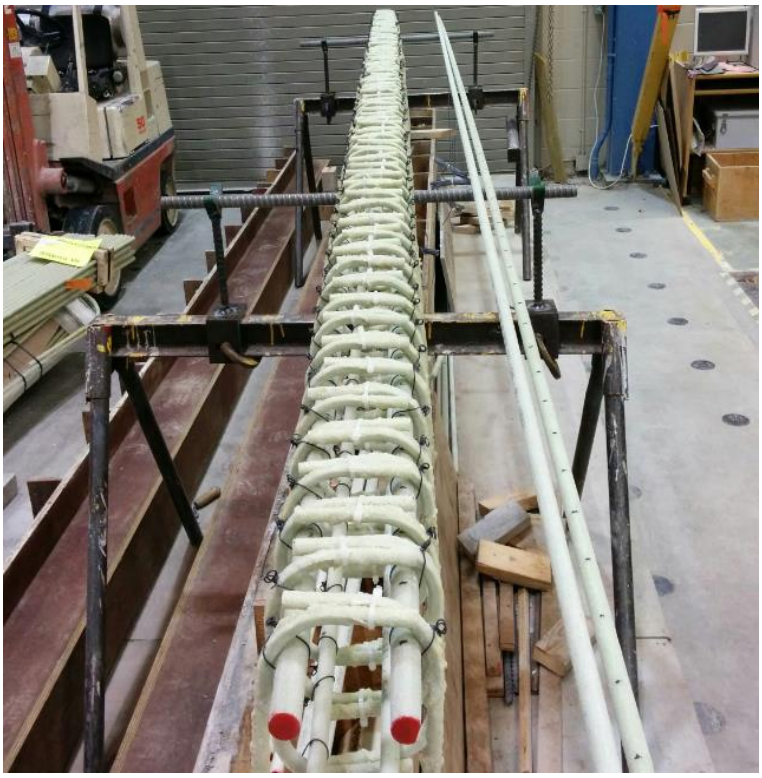

Fig. 3.5: Assembling of reinforcement cage of the test beams

Fig. 3.6: Reinforcement cage in the formworks before casting of concrete

3.7 INSTRUMENTATION AND TEST SET UP

To conduct an experimental work, it is an essential part to have a sound equipment and instrumentation system to record load value, deflection, crack-width, strains of concrete and reinforcement in the critical sections. In this program, all instruments were connected to the computerized data acquisition system for the purpose of continuous and automatic data collection. The used equipment and instrumentations are given below:

1) One MTS electro-hydraulic jack with a capacity of 1000 kN
2) Three force transducers (load cells)
3) Rigid steel frame and a spreader beam
4) Smooth bearing plates with roller supports
5) Automatic data acquisition system (DAQ) with 64 channels
6) Six linear variable differential transducers (LVDTs)
7) Three PI gauges
8) Nine electrical strain gauges for reinforcing bars
9) Three concrete strain gauges

In this program, as moment redistribution was one of the primary focuses of this study, the support reactions were measured with help of highly précised load cells. To measure the deflections along the beam, LVDTs were placed at every quarter and at mid-point of either span. To have strain values of reinforcing bars at the critical locations, total nine electrical strain gauges were attached to the prepared surface of reinforcement. Each of the three critical sections had total of three strain gauges; one was placed exactly at the loading point while other two were placed at a point equal to effective depth away from the middle one on either side. Moreover, measuring the crack widths in the critical sections was accomplished by installing 200-mm PI

gauge on the extreme tensile fibre of concrete. During the test, data acquisition system monitored by a computer recorded the magnitude of applied load, deflections along beam length, crack widths, and strain readings at the points of interest. Figure 3.7 and 3.8 show the details of the instrumentation and test setup.

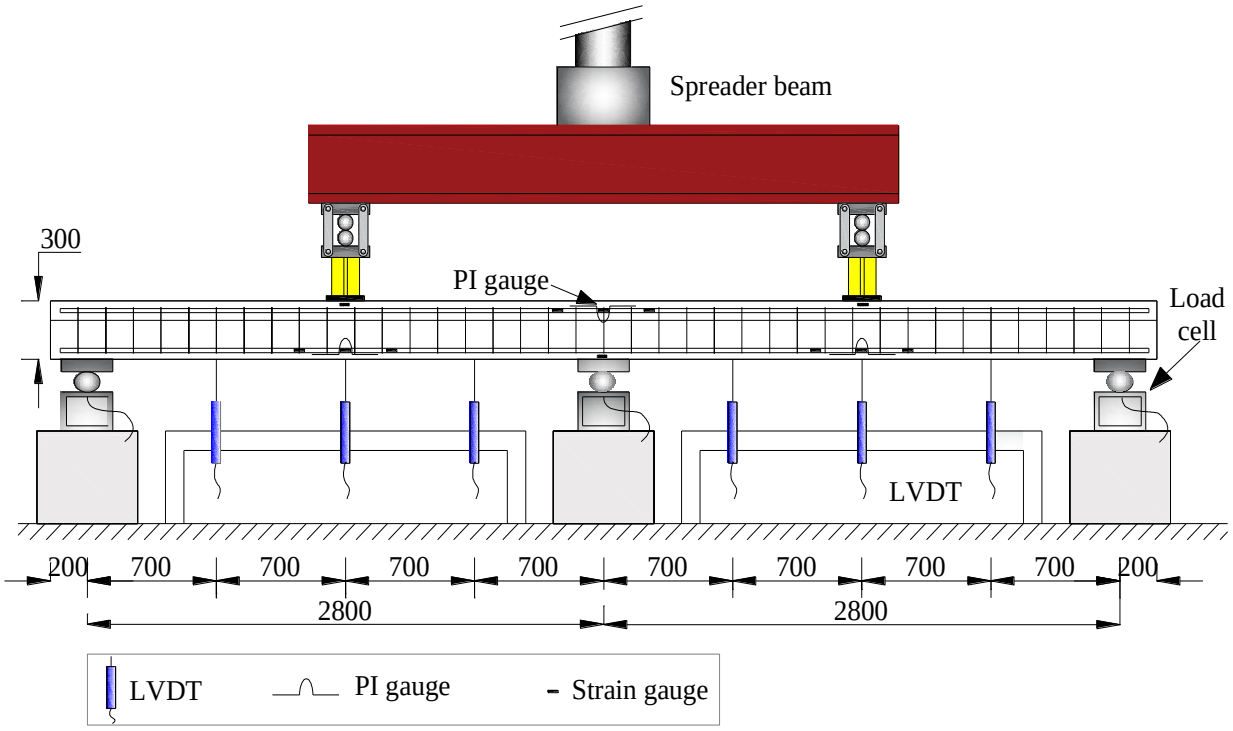

Figure 3.7: Test set up and instrumentations of the test beams of Series 1 (all dimensions in mm)

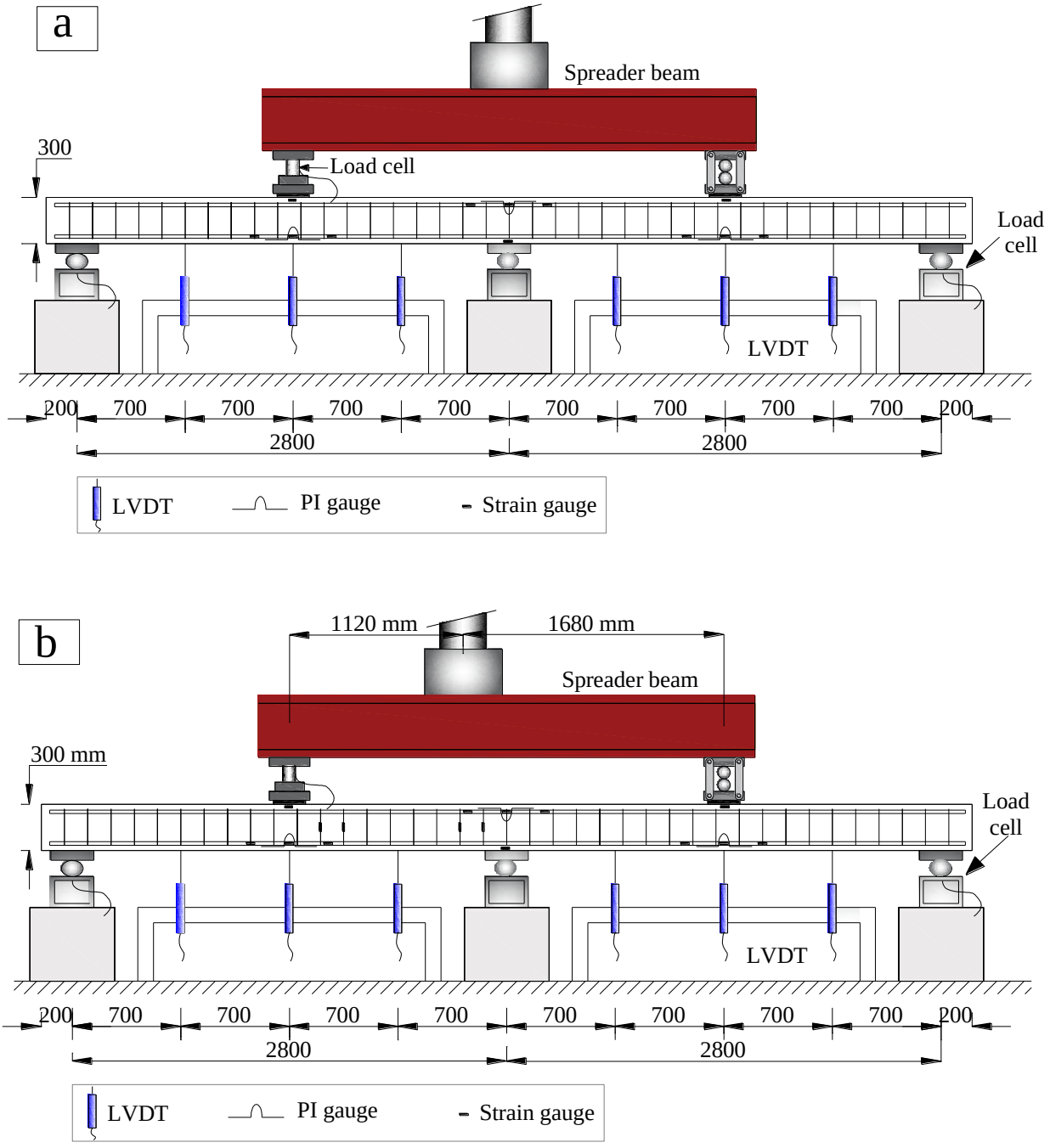

Figure 3.8: Test set up and instrumentations of the test beams in loading (a) case I, (b) case II and (c) case III in Series 2 (Continued)

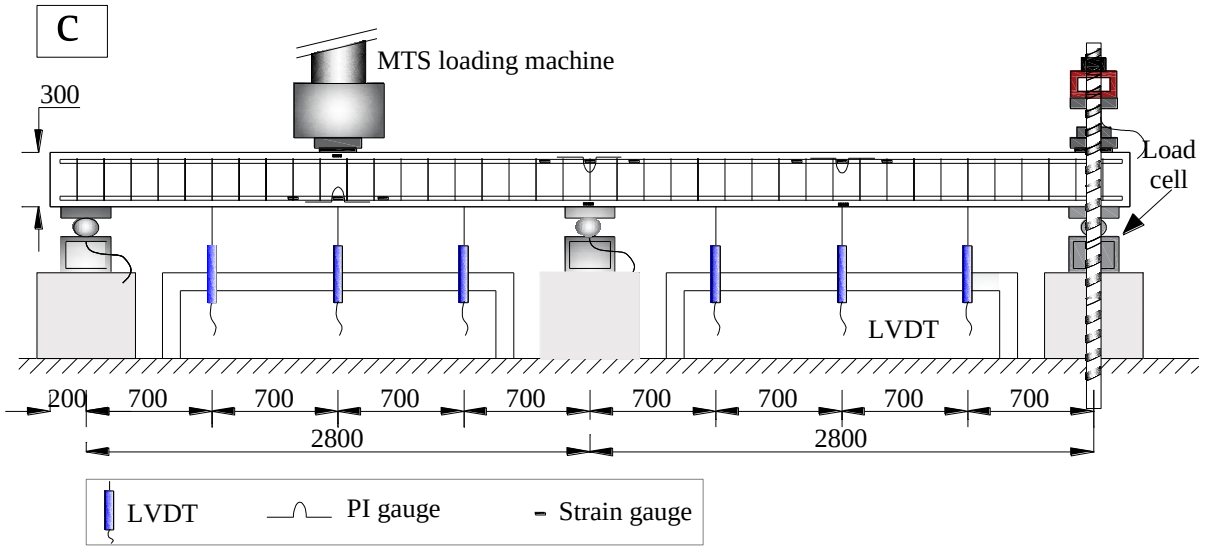

Figure 3.8: Test set up and instrumentations of the test beams in loading (a) case I, (b) case II and (c) case III in Series 2 (all dimensions in mm)

3.8 TESTING PROCEDURE

After the test beams have gained the design compressive strength of around 40 MPa, the beams were placed in the experimental set up. Then the beams were painted and marked with grid in order to trace the cracking pattern during testing. A hydraulic actuator having capacity of 1000 kN was operated to apply concentrated load. As a means of transmitting load to beam, the steel plates provided were thick and wide enough to avoid the premature crushing failure. In addition, a thin layer of neoprene strip beneath the steel plate was used to provide a uniform and smooth contact between the loading plates and the concrete surface of the test beams. Before commencing for the load application, leveling of the supports was checked out by observing the readings of load cell and then matching it with the elastic reactions.

All beams except GuE-III were subjected to monotonic loading where a loading rate of 10 kN/min was maintained until the failure took place. In case of GuE-III under Series 2, loading rate was 5 kN/min. After each interval of 20 kN, loading was stopped, and crack propagation with increasing loads was carefully followed and simultaneously marked. Fig. 3.9 and 3.10 shows the test beam of Series 1 and Series 2, respectively, during testing.

Figure 3.9: Photo of test beam of Series 1 during testing

Figure 3.10: Photo of test beam (case II) of Series 2 during testing

CHAPTER 4– RESULTS AND DISCUSSIONS OF SERIES 1

4.1 GENERAL

This chapter presents the test results of Series 1 which includes a total of six beams with T-section. All beams, as mentioned earlier, were 6,000-mm long and continuous over two spans of 2,800 mm each. Each beam was subjected to monotonic loading till failure occurs. While testing the beams, the crack initiation and growth with loading were traced with marks, and finally, the modes of failure were carefully observed. Also, the support reactions, the strains of both concrete and longitudinal bars, the crack widths in the critical regions, and the deflections along the span were closely monitored and recorded.

Based on the observations and analyses of the recorded data, the beam performances addressing the variation of crack widths, strains, and mid-span deflections with increasing load were explored. The deformability and the moment redistribution of all beams were also evaluated based on the response of load-deflection/moment-curvature and the experimental support reactions, respectively. Furthermore, the effect of each test variable on beam performances is importantly focussed in the discussions presented in this chapter.

4.2 GENERAL BEHAVIOR AND CRACKING PATTERN

Fig. 4.1 shows the cracking pattern of the test beams at failure. All tested beams showed similar cracking behavior in terms of initiation, propagation, number and spacing of cracks until failure. The first flexural crack in all beams formed simultaneously in the sagging moment region of

both spans followed by vertical flexural crack at the section over middle support. The cracking in the sagging moment region occurred at approximately 14, 9, 12, 12, 10 and 9% of the failure load for beams SuR-60-4.5, GuE-30-4.5, GuR-30-4.5, GuR-30-1.5, GuR-18-4.5 and GsR-24-4.5, respectively. However, these percentages were 24, 16, 19, 14, 17 and 14% of the failure load, respectively, in the hogging moment region. More cracks formed in the hogging and sagging moment regions with increasing the applied load while the existing cracks grew wider and deeper. The majority of the flexural cracks developed at a load up to 50-60% of failure load.

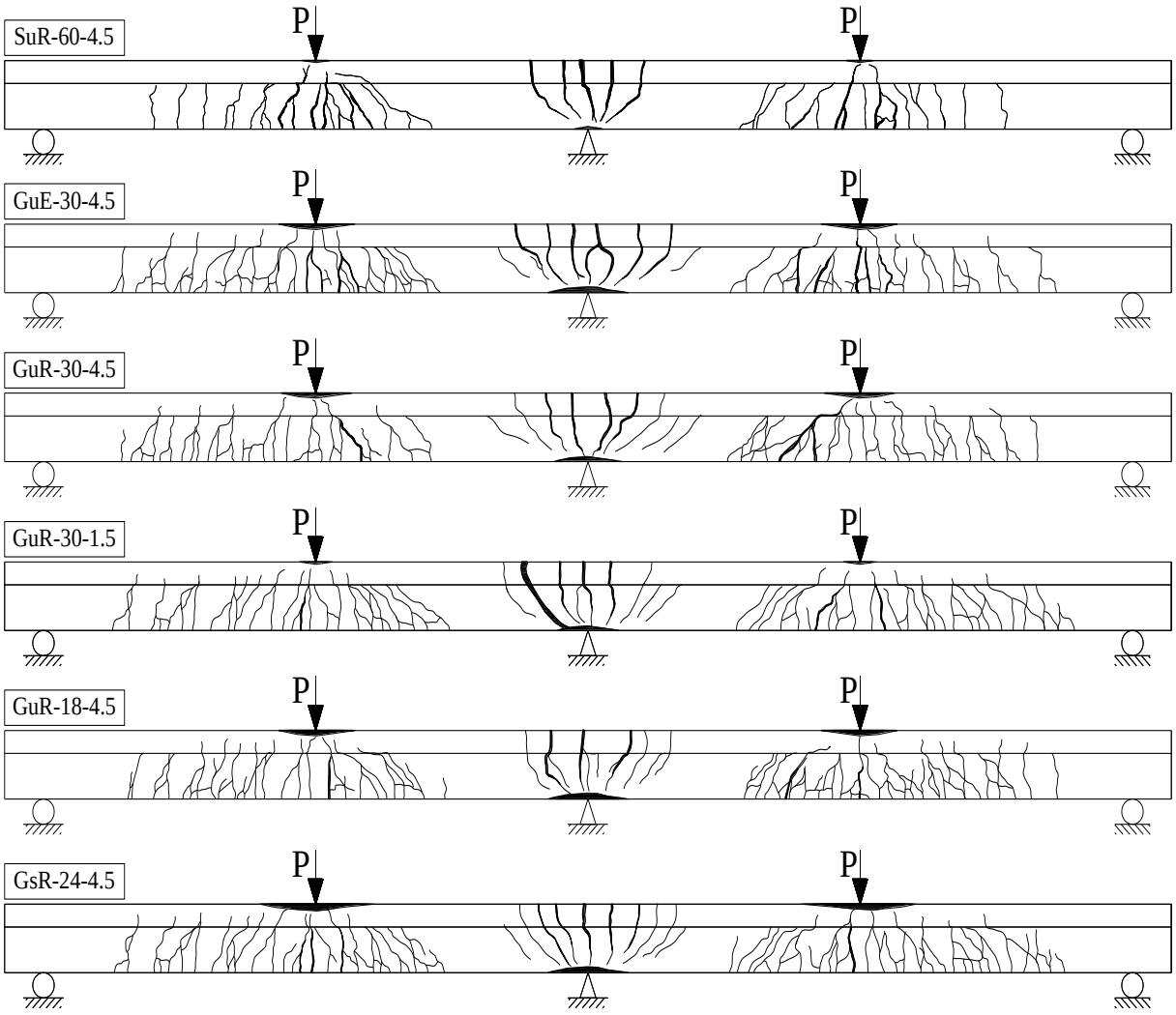

Figure 4.1: Cracking pattern of test beams at failure

Two cracks along the overhanging flange-web interface were observed in both spans in all test beams, except beam GuR-30-1.5, at a load of 45-55% of their failure load (Fig. 4.2). In beam GuR-30-1.5, one longitudinal crack in the centerline of flange at mid-span was noticed at 64% of failure load. The effect of these cracks on the behavior of the beams will be discussed later. Approaching failure, diagonal cracks developed near the middle support and in the sagging moment regions. Also, it was noted that the hogging moment region in each beam had small number of wide cracks in contrast to large number of narrow cracks in the sagging moment region. Moreover, it can be seen that the GFRP-RC beams exhibited more cracks in the hogging and sagging moment regions compared to the reference steel-RC beam SuR-60-4.5. Furthermore, the arrangement of longitudinal GFRP reinforcement was found to have no effect on the cracking pattern.

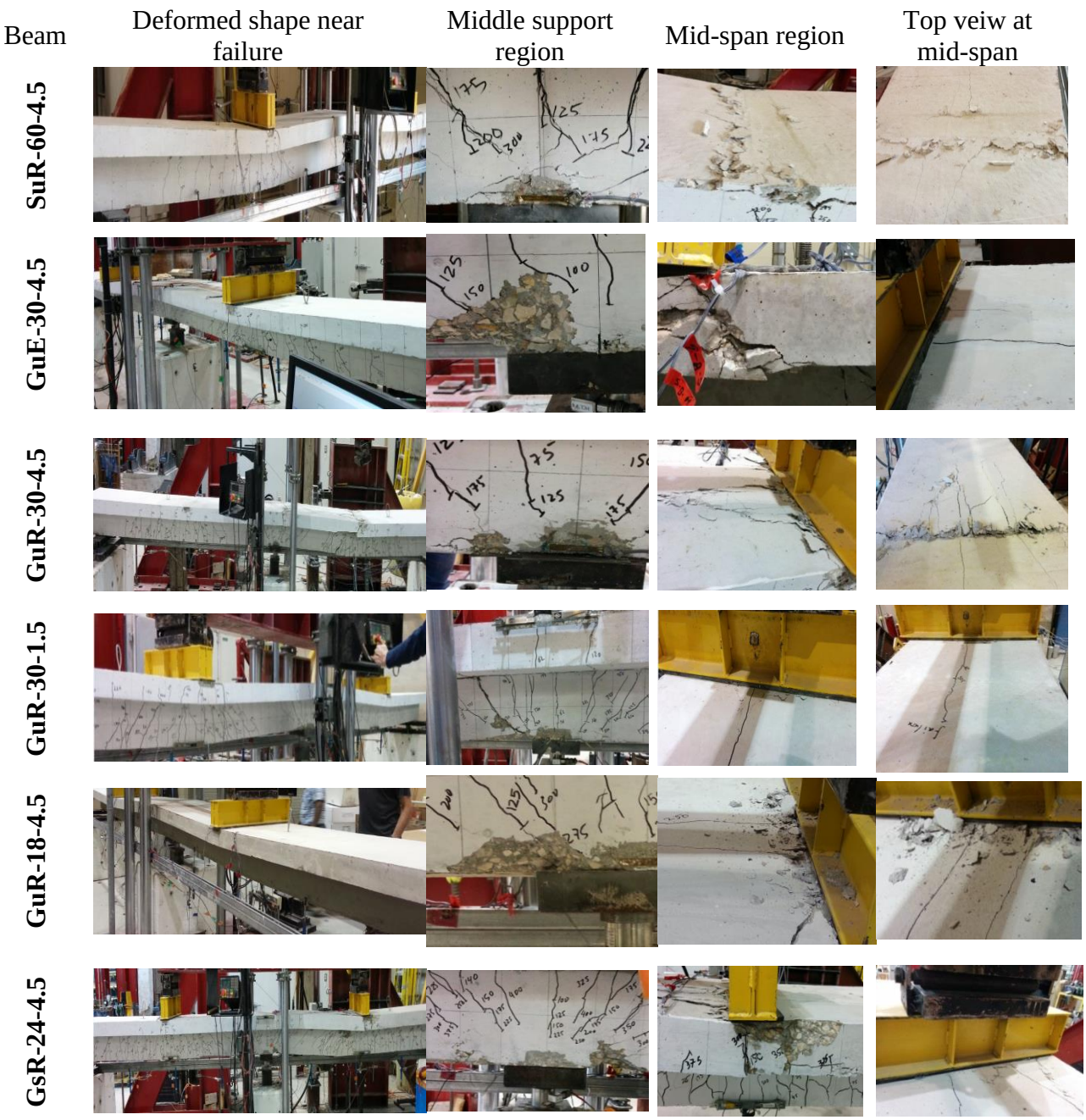

Figure 4.2: Mode of failure and longitudinal cracks at the web-flange interface of test beams

4.3 MODE OF FAILURE

Figure 4.2 shows the mode of failure in both the hogging and sagging moment regions and the longitudinal overhanging flange-web interface crack in the sagging moment region for all beams. It is worth mentioning that the mode of failure of beams GuE-30-4.5 and GuR-18-4.5 was

similar to that observed in beam GuR-30-4.5. Beam SuR-60-4.5 demonstrated tension-controlled failure with ample warning in form of wide cracks and large mid-span deflection. The yielding of steel took place at the middle support section followed by yielding of the steel reinforcement at mid-span section. Finally crushing of concrete took place in both regions. In all GFRP-RC beams except GuR-30-1.5, concrete crushing, as expected, was the mode of failure. Spalling of concrete was observed in the hogging moment region; however, the beams continued to resist more load until crushing of concrete under the spreader beam took place. At ultimate condition, GuR-30-1.5 experienced crushing of the concrete in the middle support region and continued to carry additional load until it failed due to diagonal shear crack near the middle support.

As it was mentioned previously, two longitudinal cracks at the overhanging flange-web interface were observed in all test beams except GuR-30-1.5. These cracks resulted in a change in the behavior of the sagging region from a full T-section behavior to a partial T-section behavior. This partial separation of the flange resulted in the failure of the sagging moment section at a moment lower than the calculated capacity of the T-section but higher than the calculated capacity of the rectangular section assuming no contribution from of the flange. In case of beam GuR-30-1.5, the closer spacing of the lateral reinforcement in the flange improved the composite behavior of the T-section; however, the beam failed in shear before reaching the full capacity of the T-section.

4.4 CRACK WIDTH

Fig. 4.3 shows the load-average crack width relationship in the hogging and the sagging moment regions. In general, cracks in the hogging moment region were significantly wider than those in the sagging moment region. Considering beams SuR-60-4.5 and GsR-24-4.5, the crack widths were similar at both critical sections until the yielding of steel reinforcement occurred.

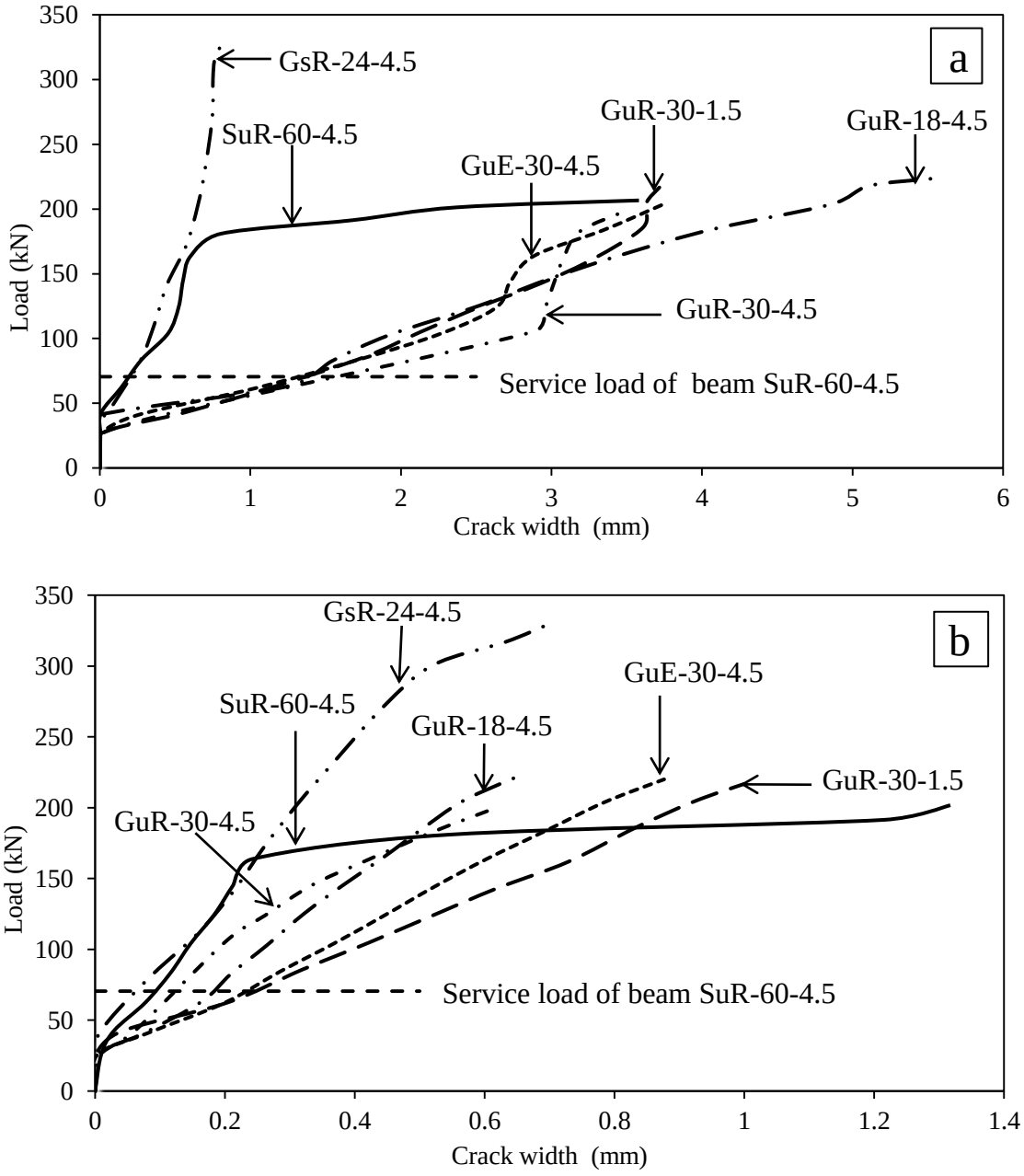

Figure 4.3: Load-crack width relationship at (a) the hogging moment section and (b) the sagging moment section

After yielding, beam SuR-60-4.5 exhibited significant increase in crack width until failure. On the other hand, the GFRP reinforcement in beam GsR-24-4.5 continued to control the crack width until failure. At the service load level (71 kN) of these two beams, the crack width in the

hogging moment region was 0.24 and 0.28 mm in beam SuR-60-4.5 and GsR-24-4.5, respectively. The beams designed for the ULS, showed wide crack widths in both the hogging and the sagging moment regions. At the same service load level calculated for the steel-RC beam, the crack width, in beams designed for the ULS, in the hogging moment region was greater than the limit of 0.5 mm specified in the CSA/S806-12 (CSA 2012). The crack width ranged from 1.28 to 1.46 mm. On the other hand, at the same service load level, the crack width measured in the sagging moment region ranged between 0.24 to 0.29 mm, which is approximately 48 and 54% of the limit of 0.5 mm. The crack width for all test beams at different load levels are listed in Table 4.1.

Table 4.1- Crack width and deflection of test beams

Beam	**Crack width (mm)**						**Deflection (mm)**		
	at service load[a]		at design load[b]		at failure load		at service load[a]	at design load[b]	at failure load
	Middle support	Mid-span	Middle support	Mid-span	Middle support	Mid-span			
SuR-60-4.5	0.24	0.23	0.56	0.30	3.56	1.78	1.0	5.9	52.0
GsR-24-4.5	0.28	0.19	0.50	0.36	0.82	1.04	1.8	8.0	34.9
GuE-30-4.5	1.39	0.24	2.69	0.56	3.78	0.88	6.7	24.4	47.8
GuR-30-4.5	1.28	0.24	3.05	0.38	3.50	0.61	6.2	24.7	42.9
GuR-30-1.5	1.46	0.25	3.18	0.81	3.72	1.17	5.5	27.6	50.8
GuR-18-4.5	1.34	0.29	3.21	0.48	5.52	0.77	7.2	26.9	58.1

[a] Service load calculated for the steel-RC beam (71 kN)

[b]Design load calculated for the steel-RC beam (155 kN)

Based on the crack width limit specified in the CSA/S806-12 (CSA 2012), the service load was approximately 50 kN for beam GuE-30-4.5 and 40 kN for beams GuR-30-4.5, GuR-18-4.5, GuR-30-1.5. At this load level, the crack width in the hogging and sagging moment regions was within the limit of 0.5 mm where the crack width at the hogging moment region was 0.4, 0.44, 0.49 and 0.43 mm in beams GuE-30-4.5, GuR-30-4.5, GuR-30-1.5, and GuR-18-4.5, respectively. The crack width in the sagging moment region was in the range of 0.12 to 0.22 mm.

4.5 STRAINS IN REINFORCEMENT AND CONCRETE

The variation of strain in concrete and longitudinal reinforcement with the applied load in the hogging and the sagging moment regions is shown in Fig. 4.4. The maximum measured strains in concrete over the middle support of all tested beams reached to or exceeded the crushing strain of 3,500 micro-strains, as specified in the CSA/S806-12 (CSA 2012). However, it started to decrease at higher load levels because the developed cracks were very close to the strain gauge location. On the other hand, the strains in concrete in the sagging moment region were less than those in the hogging moment region especially at higher load levels. This could be attributed to the formation of longitudinal cracks along the interface of web and overhanging flange in the sagging moment region that resulted in a partial separation of the overhanging flange. Since the spreader beam was placed across the entire width of the beam in the mid-span region, the flange was stressed laterally due to slab action. These lateral stresses reduce the longitudinal compressive strains (Nilson et al. 2010).

The tensile strains in longitudinal reinforcement were very small in the pre-cracking stage. Once cracks formed, a sudden increase of strain in the reinforcing bars was noticed at both critical sections. The GFRP-RC beams designed for ULS showed similar strains until failure while the GFRP-RC beam designed for SLS (GsR-24-4.5) exhibited significantly lower strains because of

the high longitudinal reinforcement ratio. At service load level, the measured strain in steel reinforcement was approximately 900 micro-strains, while the maximum measured strain in beam GsR-24-4.5 was 1680 micro-strain, which is approximately 7% of the characteristic tensile strain of the used GFRP bars. This percentage is less than the specified service limit of 25% in the CSA/S806-12 (CSA 2012). At the same service load level of 71 kN, the strain in beams designed for ULS was lower than that limit. The strain in the hogging moment region was approximately 3,330, 4,180, 4,560 and 4,530 micro-strains in beams GuE-30-4.5, GuR-30-4.5, GuR-30-1.5 and GuR-18-4.5, respectively. At failure, the strains in steel reinforcement of beam SuR-60-4.5 in the hogging and sagging moment regions was approximately 25,000 and 33,000 micro-strain, respectively. In beam GsR-24-4.5, the strain was 7,300 and 9,300 micro-strain in the hogging and sagging moment region, respectively. In case of the other GFRP-RC beams designed for the ULS, the strain values lied between 11,250 and 17,500 micro-strains that are well below the ultimate strain of the used GFRP bars. At failure, the strain in reinforcement in the sagging moment region was higher than that in the hogging moment region by 43, 33, 33 and 12% in beams GuE-30-4.5, GuR-30-4.5, GuR-30-1.5, and GuR-18-4.5, respectively. This could be attributed to the early formation of cracks in the sagging moment region, the excessive cracking observed in that region and the moment redistribution that resulted in a higher value of the bending moment in the sagging moment region compared to that in the hogging moment region. In beam GuE-30-4.5 only, the bending moment in the sagging moment region was lower than that in the hogging moment region; however, the high strain can be attributed to the lower reinforcement ratio in that region.

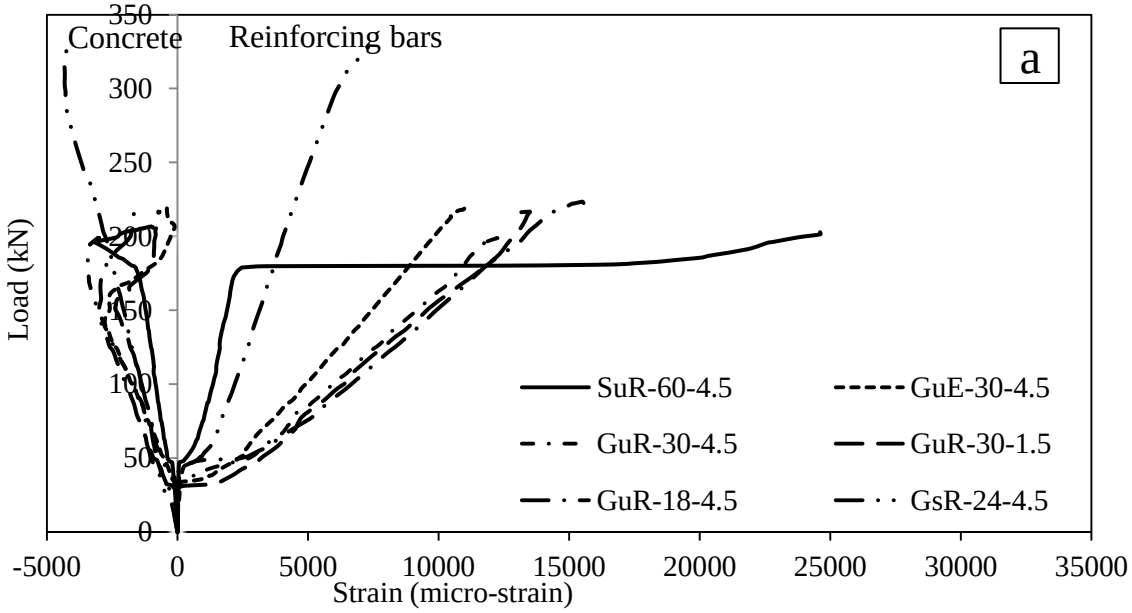

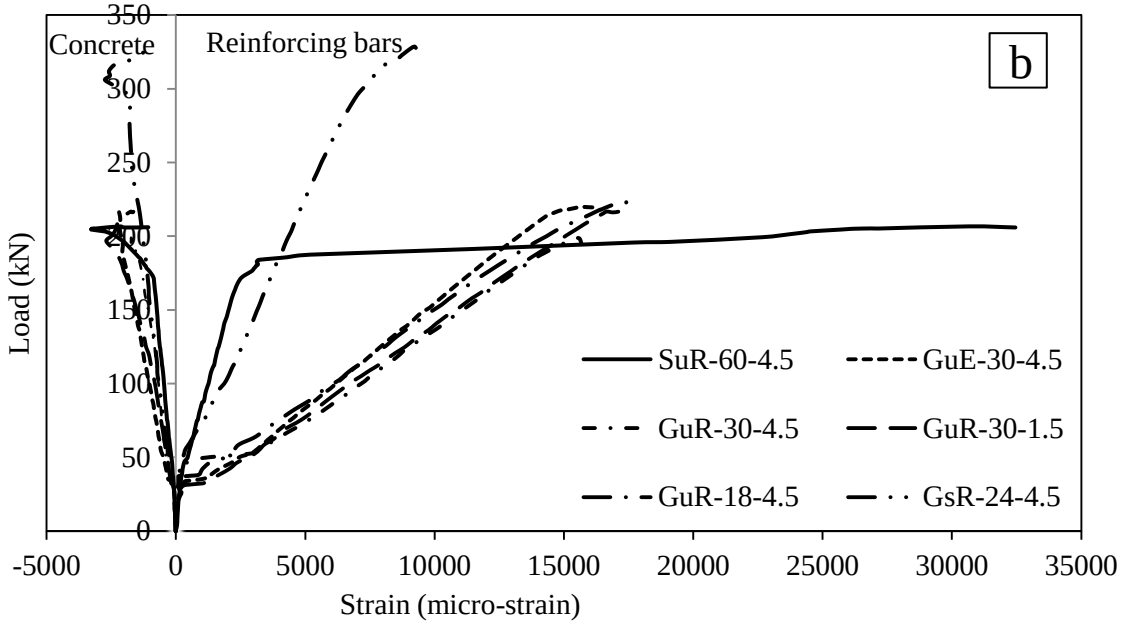

Figure 4.4: Strain variation in concrete and reinforcing bars at (a) the hogging moment section and (b) the sagging moment section

4.6 LOAD-DEFLECTION RESPONSE

The load-deflection behavior at mid-span of all test beams is depicted in Fig. 4.5. As mentioned earlier, cracks first formed in the sagging moment regions followed by cracking in the hogging

moment region. However, formation of cracks at mid-span did not cause any significant change in the flexural stiffness of the beam. Once cracks formed at the section over middle support, the deflection increased rapidly due to the significant rotation over the middle support. In general, the load-deflection behavior of all beams is characterized by linear pre-cracking and post-cracking stages; however, a third stage that started either after yielding in steel-RC beam or concrete softening due to crushing in GFRP-RC beams was also observed.

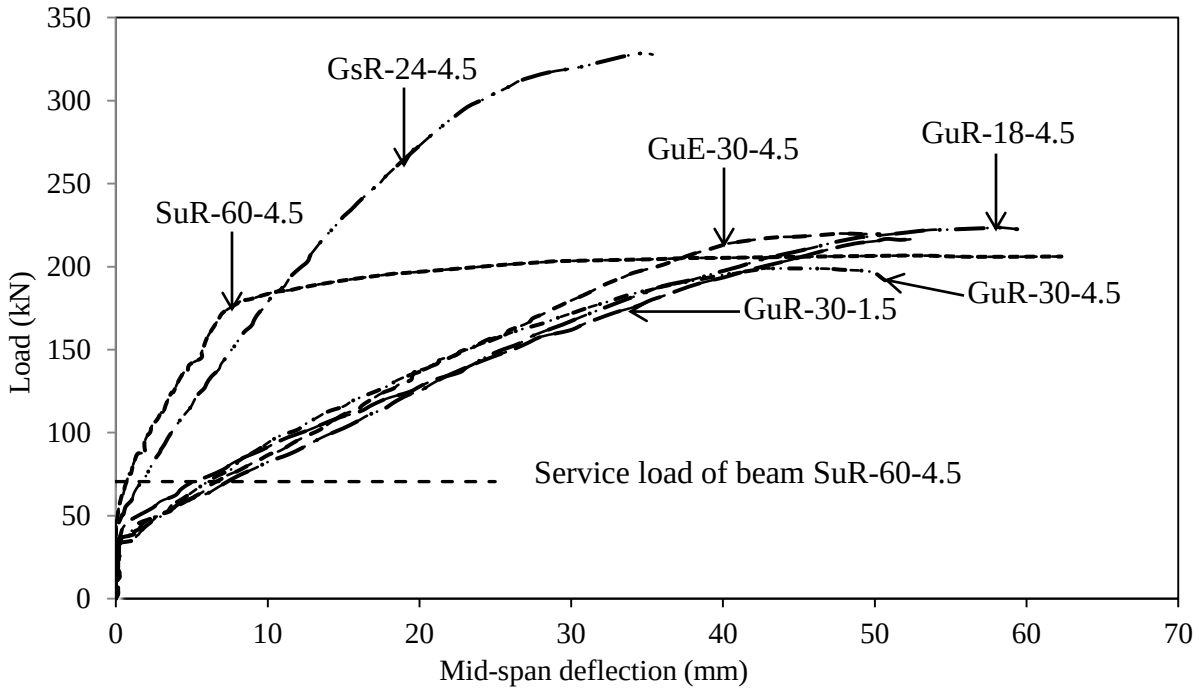

Figure 4.5: Load-deflection relationship of test beams

In the case of beams SuR-60-4.5 and GsR-24-4.5, the deflection at the service load (71 kN) was 1.0 and 2.1 mm, respectively, which is less than the allowable deflection specified in the CSA/S806-12 (span/480 = 5.6 mm to span/180 = 14.8 mm) depending on the supporting elements and structural function. Also, for beams, designed for the ULS, the deflection at the same service load (71 kN) was 6.7, 6.2, 5.5, and 7.2 mm for GuE-30-4.5, GuR-30-4.5, GuR-30-1.5, and GuR-18-4.5, respectively. These deflections do not satisfy the serviceability requirement

for certain applications. At the service load calculated based on the crack width limit (50 kN for beam GuE-30-4.5 and 40 kN for beams GuR-30-4.5, GuR-18-4.5, GuR-30-1.5) the measured deflections satisfied the serviceability requirement and were in the range of 0.9 to 2.5 mm.

4.7 DEFORMABILITY AND DUCTILITY

Fig. 4.6 shows the moment-curvature relationship of all test beams at the hogging moment section. The conventional steel-RC beam, SuR-60-4.5, showed typical moment-curvature behavior due to yielding of steel at the hogging moment section. In GFRP-RC beams, a tri-linear moment-curvature relationship was observed in all beams. However, beams GuE-30-4.5 and GsR-24-4.5, at the post-cracking stage, demonstrated steeper moment-curvature curve compared to the other GFRP-RC beams. This behavior was anticipated due to the higher longitudinal reinforcement ratio that enabled the section to control the crack width and consequently limit the rotation in the middle support region.

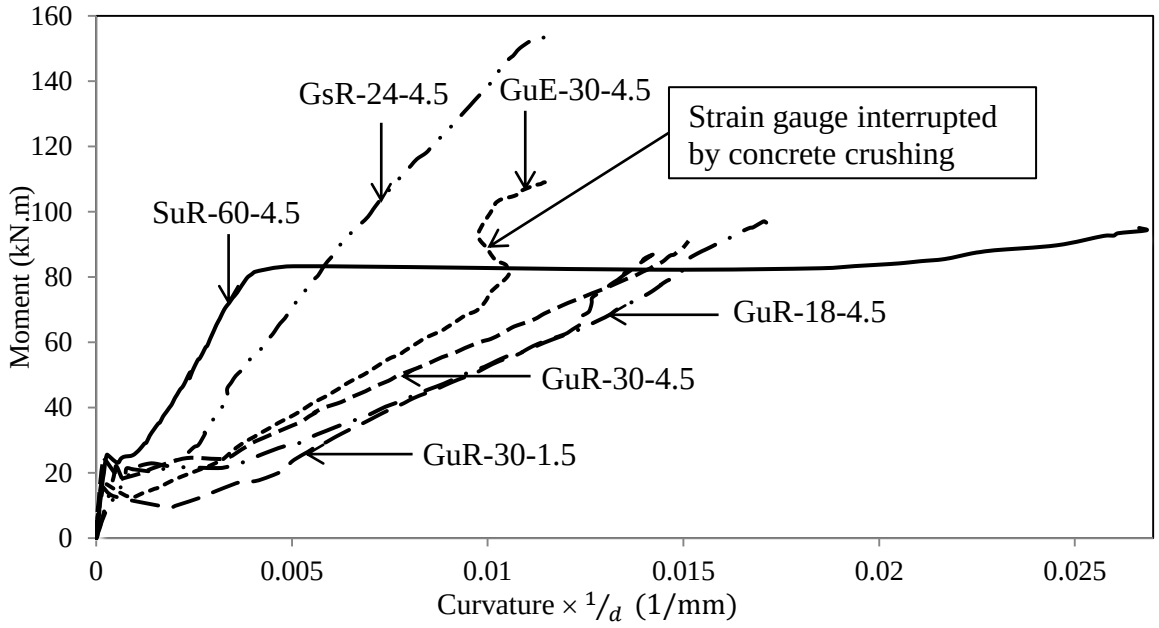

Figure 4.6: Moment-curvature relationship at the hogging moment section of test beams

The ductility index (DI) of beam SuR-60-4.5 that was calculated as the ratio of the deflection at ultimate to the deflection at yielding was 6.97. The concept of ductility for conventional steel-RC beams is not applicable to FRP-RC beams; rather two main approaches can be taken into account in this regard. The first one is "deformation-based approach" in which "deformability factor" is calculated to quantify the deformability of FRP-RC elements. Deformability of FRP-RC beams is represented by the deformability "*J*-factor" that was proposed by Jaeger et al. (1995). The *J*-factor equals to the strength factor multiplied by the deformation factor (curvature/deflection).

Where,

$$\text{Strength Factor} = \frac{\text{Moment at ultimate}}{\text{Moment at concrete compressive strain of } 0.001}$$

$$\text{Curvature/Deflection Factor} = \frac{\text{Curvature/Deflection at ultimate}}{\text{Curvature/Deflection at concrete compressive strain of } 0.001}$$

The second approach is "energy-based" that defines the ductility as a ratio of the inelastic energy-to-the total energy (Grace et al. 1998) where the total energy is the area under the load-deformation curve. This approach accounts for the effect of type, modulus of elasticity, and tensile strength of the reinforcing material as well as the type of stirrups, the failure mode, and the concrete softening in case of compression-controlled failure. Based on the ratio of the inelastic-to-total energy, the mode of failure can be classified as ductile, semi-ductile, and brittle according to the range of energy ratio that is "greater than 75%", "70% to 74%", and "less than 69%", respectively. The *J*-factor and energy ratio were calculated for the GFRP-RC beams and listed in Table 4.2. All GFRP-RC beams showed very consistent results according to both deformation-based and energy-based approaches.

The strength and the deflection factors were calculated using the experimental moments and deflections at a measured compressive strain of 1000 micro-strain in the concrete in the sagging moment region. It can be seen that all test beams demonstrated adequate deformability when compared to the minimum deformability factor of 6.0 specified by the CHBDC code (CSA-S6-14) for T-beams. Among the GFRP-RC beams, beam GuR-18-4.5 had the highest *J*-factor of 14.97. This is due to the higher deflection factor compared to that in the other beams which was a result of using a small spacing of stirrups that, in turn, enhanced the confinement of concrete.

Table 4.2- Deformability factor and energy ductility of test beams.

Beams	Deformability factor (DF)			Energy Ductility[a]		
	Strength factor	deflection factor	*J*-factor	Total energy (kN.mm)	Inelastic energy (kN.mm)	Inelastic/Total (%)
SuR-60-4.5	-	-	-	9794	8464	86%
GuE-30-4.5	2.2	3.9	8.57	6959	4600	66%
GuR-30-4.5	1.64	4.98	8.16	5781	3722	64%
GuR-30-1.5	3.02	3.10	9.36	7243	4795	66%
GuR-18-4.5	2.38	6.28	14.97	8807	6222	71%
GsR-24-4.5	2.27	4.5	10.22	8063	5176	64%

[a] Energy ductility according to Grace et al. (1998)

In addition, from the perspective of "energy-based approach", all the GFRP-RC beams showed a ratio of inelastic-to-total energy lower than that of the steel-RC beam, as shown in Table 4.2. Again, beam GuR-18-4.5 had superior performance in absorbing the energy compared to the other ULS-based GFRP-RC beams due to the enhanced concrete confinement. Considering the classification proposed by Grace et al. (1998), beam SuR-60-4.5 exhibited ductile failure while

beam GuR-18-4.5 exhibited semi-ductile failure. On the other hand, the failure was brittle in beams GuE-30-4.5, GuR-30-4.5, GuR-30-1.5 and GsR-24-4.5. Grace et al. (1998) reported similar failure modes for FRP-RC beams with T-sections.

4.8 MOMENT REDISTRIBUTION AND LOAD CARRYING CAPACITY

The relationship between the applied load on each span (*P*) and the end reaction for all test beams is presented in Fig. 4.7. It can be seen that, before cracking, the measured end reaction followed the reaction calculated according to the elastic theory. The formation of first flexural crack in the sagging moment region did not noticeably affect the measured end reaction; however, cracking of the section over middle support caused the section to undergo a substantial amount of rotation and thus, resulted in higher end reaction than the elastic reaction. This means that a redistribution of the internal forces from the hogging to the sagging moment region occurred. This behavior continued until the failure of the beam.

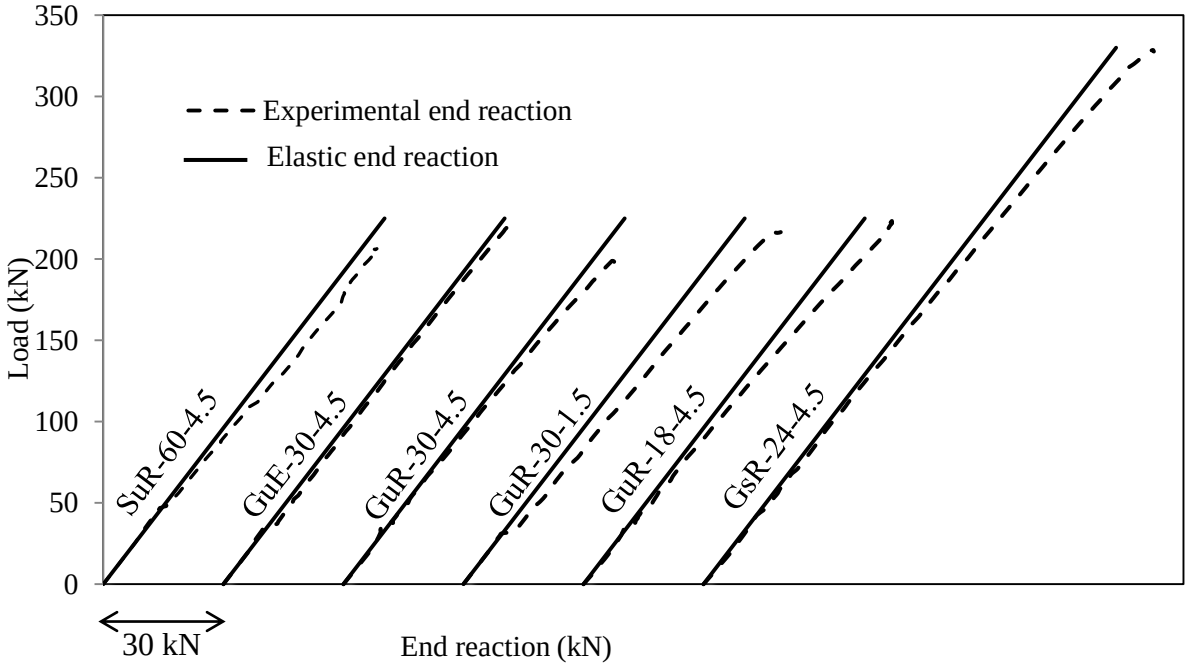

Figure 4.7: Load-end reaction relationship of test beams

Table 4.3 shows the change of the bending moment in the sagging and hogging moment sections, as a result of change in end reaction, at different loading levels. The experimental moment was calculated using the measured end reaction and then compared to the elastic moment to evaluate the percentage of moment redistribution. It can be seen that the bending moments were very similar to those calculated according to the elastic theory until cracks formed in the sagging moment region. When the cracks formed in the hogging moment region, the moment in the sagging moment region was higher than that calculated based on the elastic theory while the hogging moment was less than that obtained by the elastic theory. At any loading stage, the difference between the experimental and theoretical moments was dependent on the moment redistribution percentage exhibited by the beam.

The steel-RC beam, SuR-60-4.5, redistributed 15.9% of the hogging moments at design load (155 kN) level and reached a maximum of 17.1% at approximately 83% of ultimate load. After yielding of the reinforcement in the sagging region, the moment redistribution percentage decreased and reached 10.1% at failure. The GFRP-RC beam GuE-30-4.5, designed for no moment redistribution, showed approximately 4.8 and 5.7% moment redistribution at design and failure load, respectively. In addition, beams GuR-30-4.5, GuR-30-1.5, GuR-18-4.5 and GsR-24-4.5 designed assuming 15% moment redistribution, exhibited 8.1, 20.7, 15.2 and 7.2% moment redistribution, respectively, at the design load level (155 kN). At failure, the percentage of the moment redistribution of these beams reached 14.8, 23.3, 17.8 and 15.9%, respectively.

Table 4.3- Moments at hogging and sagging moment sections at different load levels

Loading stage			SuR-60-4.5	GuE-30-4.5	GuR-30-4.5	GuR-30-1.5	GuR-18-4.5	GsR-24-4.5
Cracking at sagging zone	Load (kN)		29	20	25	25	21	30
	Moments (kN.m)	Hogg.	15.2	10.5	13.1	13.3	11.1	15.8
		Sagg.	12.7	8.8	10.9	10.6	9.2	13.1
	MR (%)		No moment redistribution occurred in this stage					
Cracking at hogging zone	Load (kN)		50	35	38	31	38	45
	Moments (kN.m)	Hogg.	25.6	18.0	19.8	16.2	19.7	23.3
		Sagg.	22.2	15.5	16.7	13.6	16.8	19.8
	MR (%)		2.6	2.0	0.8	0.6	1.4	1.3
At service load[a]	Load (kN)		71					
	Moments (kN.m)	Hogg.	35.2	35.9	36.2	33.0	35.1	35.4
		Sagg.	32.1	31.7	31.6	33.2	32.2	32.0
	MR (%)		5.6	3.6	2.9	11.6	5.9	5.1
At design load	Load (kN)		155					
	Moments (kN.m)	Hogg.	68.4	77.5	74.8	64.5	69.0	75.5
		Sagg.	74.3	69.8	71.1	76.2	74.0	70.7
	MR (%)		15.9	4.8	8.1	20.7	15.2	7.2
At failure	Load (kN)		207	220	199	217	223	329
	Moments (kN.m)	Hogg.	97.7	108.9	89.0	87.4	96.3	145.3
		Sagg.	96.0	99.5	94.8	108.2	107.9	157.6
	MR (%)		10.1	5.7	14.8	23.3	17.8	15.9

[a] Service load is calculated for the steel-RC (SuR-60-4.5) beam

The high moment redistribution in beam GuR-30-1.5 can be attributed to the high flexural stiffness of the sagging moment region as a result of the improved composite action (T-section) due to providing more lateral reinforcement in the flange. Also, in case of beam GuR-18-4.5, the small spacing of stirrups enhanced the confinement that enabled the beam to undergo large rotation and consequently high moment redistribution. In general, it can be concluded that the beams that were designed for an assumed percentage of MR, could successfully reach the target, and their redistribution capability was enhanced by providing either the transverse reinforcement with small spacing in the flange or the stirrups with small spacing.

Regarding the load carrying capacity of beams designed for the ULS, it can be seen that, all test beams failed at a load greater than the target load (155 kN). The failure load was approximately 34, 42, 28, 40, and 44% higher than the design load for beams SuR-60-4.5, GuE-30-4.5, GuR-30-4.5, GuR-30-1.5, and GuR-18-4.5, respectively. These higher capacities may be due to the ability of the beams to redistribute the bending moment between the critical sections, the ability of the beams to resist additional load after crushing of the concrete in the hogging moment region and the high reserve of the flexural capacity of the hogging section. Also, at failure, the bending moment at the hogging moment section in the steel-RC beam was higher than the calculated capacity, according to the CSA/A23.3-14 (CSA 2014b), by only 7%. Similarly, in all GFRP-RC beams, the bending moment at the middle support section exceeded the flexural capacity calculated according to CSA/S806-12 (CSA 2012). The average experimental-to-predicted ratio of bending moment at the middle support section was 1.25. This high reserve in flexural capacity could be attributed to the confinement of concrete provided by the transverse reinforcement which increased the confined concrete strength and hence the flexural capacity of the section.

On the other hand, the bending moment at mid-span section did not reach the calculated flexural capacity of the T-section in all beams. In beam SuR-60-4.5, the bending moment at failure was 96% of the calculated capacity. In the GFRP-RC beams, the average ratio of the experimental-to-predicted moment capacity was 0.74. This can be attributed to the partial separation of the flange due to the longitudinal cracks at the overhanging flange-web interface in beams GuE-30-4.5, GuR-30-4.5, GuR-18-4.5 and GsR-24-4.5 or the shear failure in beam GuR-30-1.5. The ratio of experimental-to-predicted moment capacity of beams GuR-30-1.5 and GuR-18-4.5 was slightly higher than that of the other three GFRP-RC beams (Table 4.4). This may be due to the improvement in the T-section behavior in the sagging moment region, and the enhancement in deformability as a result of decreasing the spacing of the lateral bars in the flange in beam GuR-30-1.5 and the small spacing of stirrups in beam GuR-18-4.5, respectively. It is worth mentioning that the experimental bending moment at the sagging moment section was greater than the calculated flexural capacity neglecting the presence of the flange at the mid-span section (considering 200×300 mm rectangular section), as shown in Table 4.4.

Table 4.4- Failure load, experimental and predicted failure moments and moment redistribution of test beams

Beams	Failure load (kN)	Experimental moment (kN.m)		Predicted moment[a] (kN.m)			Experimental /Predicted			Moment redistribution (%)
		Hogging section	Sagging section	Hogging section	Sagging section		Hogging section	Sagging section		
					T-Sec	R-Sec		T-Sec	R-Sec	
SuR-60-4.5	207	97.7	96.0	91.3	99.6	91.3	1.07	0.96	1.05	10.1
GuE-30-4.5	220	108.9	99.5	85.1	138.3	72.9	1.28	0.72	1.36	5.7
GuR-30-4.5	199	89.0	94.8	71.2	135.4	71.2	1.25	0.70	1.33	14.8
GuR-30-1.5	217	87.4	108.2	73.7	139.7	73.7	1.19	0.78	1.47	23.3
GuR-18-4.5	223	96.3	107.9	73.7	139.7	73.7	1.31	0.77	1.46	17.8
GsR-24-4.5	329	145.3	157.6	118.1	218.7	107.6	1.23	0.72	1.46	15.9

[a] Calculated according to CSA/A23.3 (CSA 2014) or CSA/S806-12 (CSA 2012) as appropriate.

CHAPTER 5– RESULTS AND DISCUSSIONS OF SERIES 2

5.1 GENERAL

The test results of Series 2 which includes a total of six beams subjected to different loading conditions are presented in this chapter. All test beams were 6,000-mm long and continuous over two spans of 2,800 mm each. Each beam was subjected to monotonic loading till failure occurs. The crack initiation and propagation during testing were traced with marks, and finally, the modes of failure were carefully observed. Also, the support reactions, the strains of both concrete and longitudinal bars, the crack widths in the critical regions, and the deflections along the span were closely monitored and recorded.

Based on the observations and analyses of recorded data, the beam performances including the variation of crack widths, strains, and mid-span deflections with moment were investigated. The moment redistribution of all beams was also evaluated by comparing the elastic moment with the experimental moment calculated based on the experimental support reactions. Furthermore, the effect of each test variable on beam performances is presented in this chapter.

5.2 GENERAL BEHAVIOR AND MODE OF FAILURE

In case of beam GuR-I, subjected to symmetrical loading, cracks initiated in the hogging moment region at approximately 17 kN (12% of failure load P =144 kN) followed by cracking in the sagging moment region at 23 kN (16% of failure load). Under the loading cases II and III, the maximum bending moment is at the north mid-span section of the test beams. Therefore, the first

flexural crack in these beams initiated in the north sagging moment region followed by similar cracks in the hogging and the south sagging moment region, respectively. In loading case II, beams GuE-II, GuR-II, GsR-II and SuR-II had the first flexural crack at approximately 22, 23, 27 and 30 kN which represents 9, 10, 8 and 14% of their respective failure load (1.5P= 243, 224, 322 and 218 kN, respectively). In the hogging moment region of the same beams, the flexural cracks formed when the load reached 12, 14, 10 and 18% of the 1.5P, respectively. In these beams, cracks formed in the less loaded span at a load of 23, 25, 20 and 30%, respectively, of the failure load (1.5P). In loading case III, the cracking load in beam GuE-III was approximately 10 and 18% of the failure load (P = 172 kN) at the north mid-span and middle support sections, respectively. As the applied load increased, new cracks formed while the existing ones grew wider and deeper until the applied load reached 50-60% of the ultimate load. Afterwards, diagonal cracks near the loading points and the middle support along with minor flexural cracks were observed before failure.

Fig. 5.1 shows the location and mode of failure of the test beams under different loading conditions. All the GFRP-RC beams experienced concrete crushing at either the hogging moment section, the higher load sagging section or both and thus showed “compression-controlled” mode of failure. In beam GuR-I, concrete crushing was visible at the hogging moment section; however, it continued to carry more load until failure took place due to excessive concrete crushing in the same region associated with widening of formed diagonal cracks near the middle support. Beams GuE-II, GuR-II and GsR-II experienced concrete crushing at the hogging moment section followed by concrete crushing at the north sagging moment section. However, no sign of concrete crushing in the south mid-span region was observed. It is worth mentioning that the north mid-span section of beam GsR-II had significant

concrete crushing compared to that observed in other beams of case II. Also, beam GuE-III failed due to concrete crushing that took place at the north sagging moment section, as shown in Fig. 5.1. In contrary, beam SuR-II experienced yielding of the longitudinal reinforcement; however, it failed in shear due to a sudden diagonal crack in the higher load span. Therefore, this beam did not show the expected ductile behavior.

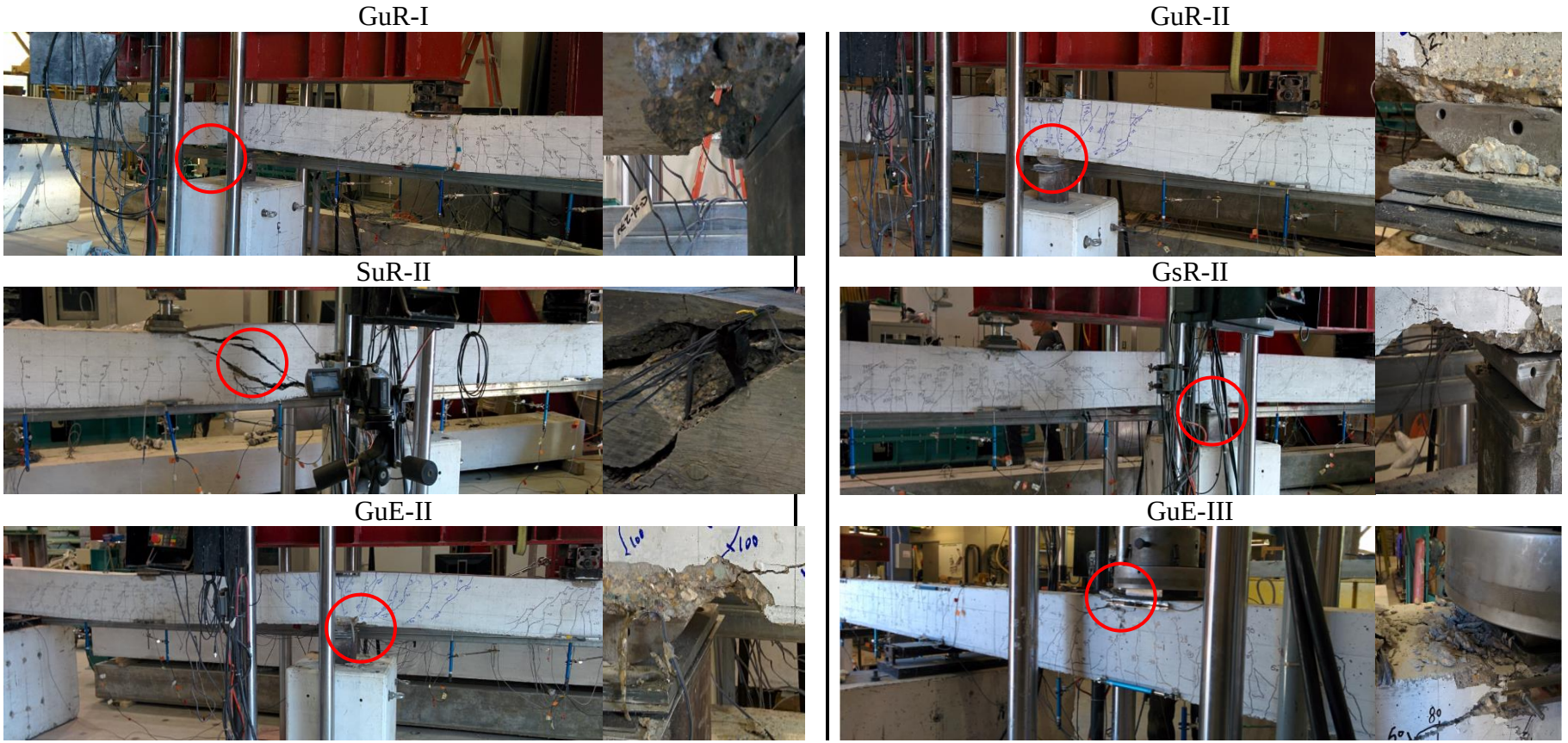

Figure 5.1: Mode of failure of test beams

5.3 CRACKING PATTERN AND CRACK WIDTH

The pattern and distribution of cracks in all test beams, at failure, are depicted in Fig. 5.2. In beam GuR-I, similar cracking pattern on both sagging moment regions was observed. In loading case II, all test beams showed similar cracking behavior in terms of crack initiation and propagation, and intensity and distribution of cracks. Higher intensity of cracks in the higher load span compared to that in the less loaded span was observed in each beam. When the load was applied on only one span, beam GuE-III, extensive cracks with small spacing in the north sagging moment region were observed. In the unloaded span, the cracks started at the top and propagated straight towards the bottom of the beam. All the cracks in this span were vertical and within a distance of 1,400 mm (half the span) from the middle support. The steel-RC beam, SuR-II, showed less cracks with larger spacing in comparison with that of GFRP-RC beam GuR-II. This can be attributed to the different bond behavior characterized by surface condition of the reinforcing bars. Similar findings were reported by Kassem et al. (2011). Also, beams GuE-II and GuR-II designed to meet the requirements of an assumed moment redistribution of 0 and 20%, respectively, showed similar cracking pattern in the hogging and sagging moment regions.

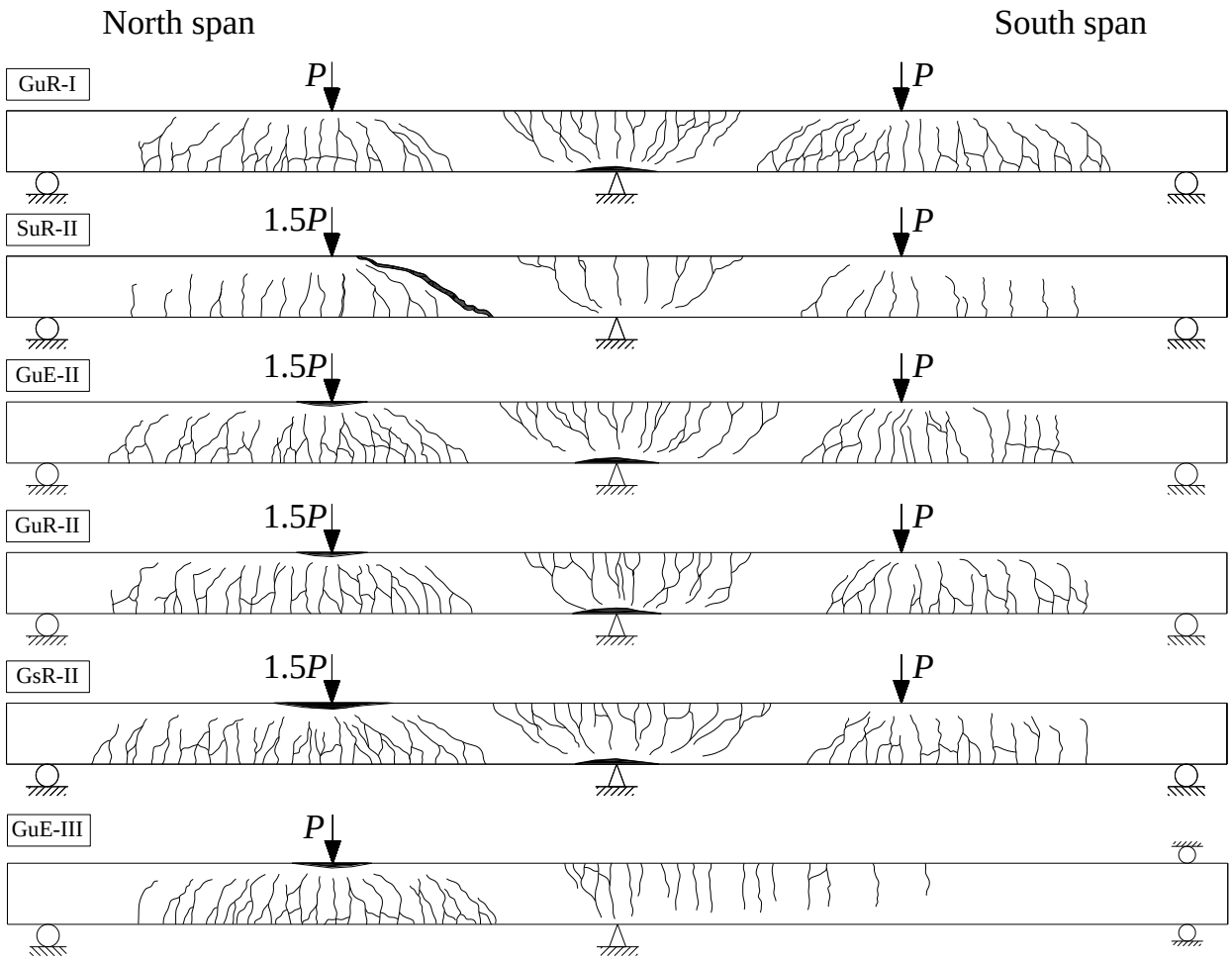

Figure 5.2: Cracking pattern and concrete crushing of test beams at failure load

Fig. 5.3 shows the moment-average crack width relationship in the sagging and hogging moment regions for all test beams. In beam GuR-I, tested under symmetrical loading, the sagging moment sections showed slightly smaller crack widths compared to that of the hogging moment section. In general, in loading case II and III, the crack widths observed in the north mid-span were the least among the three critical sections. This is due to the large longitudinal reinforcement ratio provided at the higher load sagging region compared to those at other regions. As a result of the high modulus of elasticity of the steel bars, beam SuR-II showed narrower cracks at the three different regions compared to its counterpart reinforced with GFRP

bars (beam GuR-II). Regarding the effect of reinforcement ratio on the crack width, the cracks in the north sagging region in beam GuR-II were approximately 40% smaller than that of GuE-II whereas no significant difference was found in the hogging moment region. Moreover, both beams SuR-II and GsR-II, designed for the same service moment, had similar moment-crack width relationship at all critical sections, as shown in Fig. 5.3. The crack width in beams SuR-II and GsR-II at service load level was 0.18 and 0.16 mm in the hogging moment region, 0.15 and 0.13 mm in the north sagging moment region, and 0.17 and 0.16 mm in the south sagging moment region, respectively. As the crack width criterion governed the serviceability based design of beam GsR-II, it satisfied the crack width limitation which is 0.5 mm for FRP-RC elements for exterior exposure, specified in CSA/S806-12 (CSA 2012).

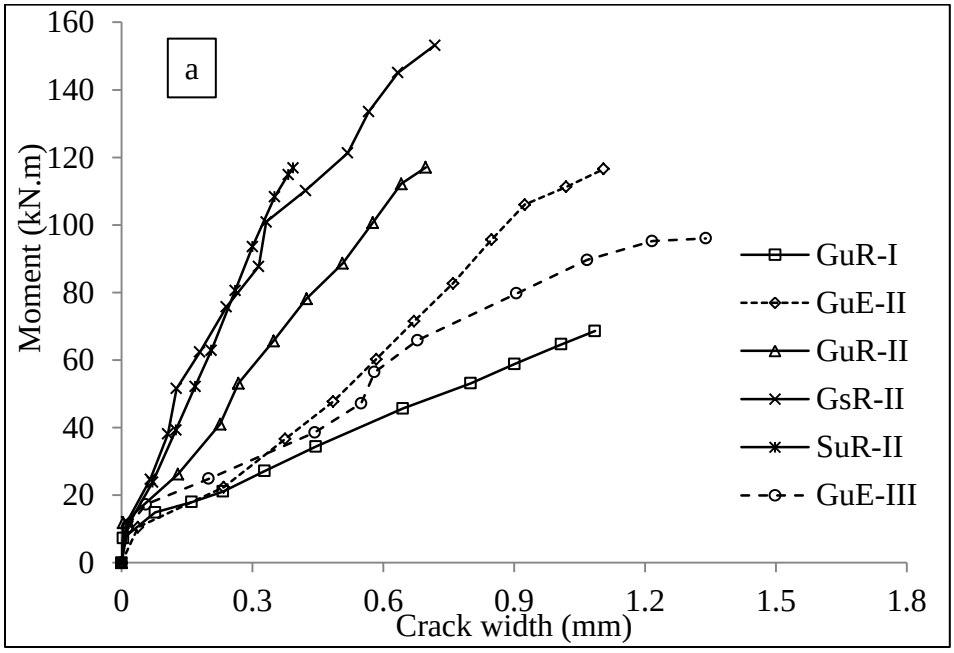

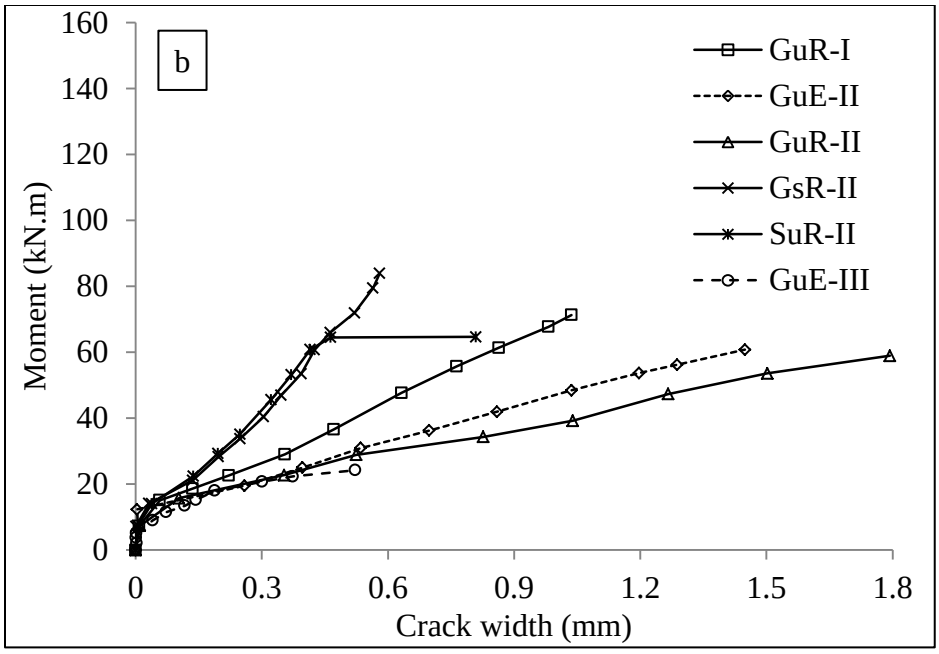

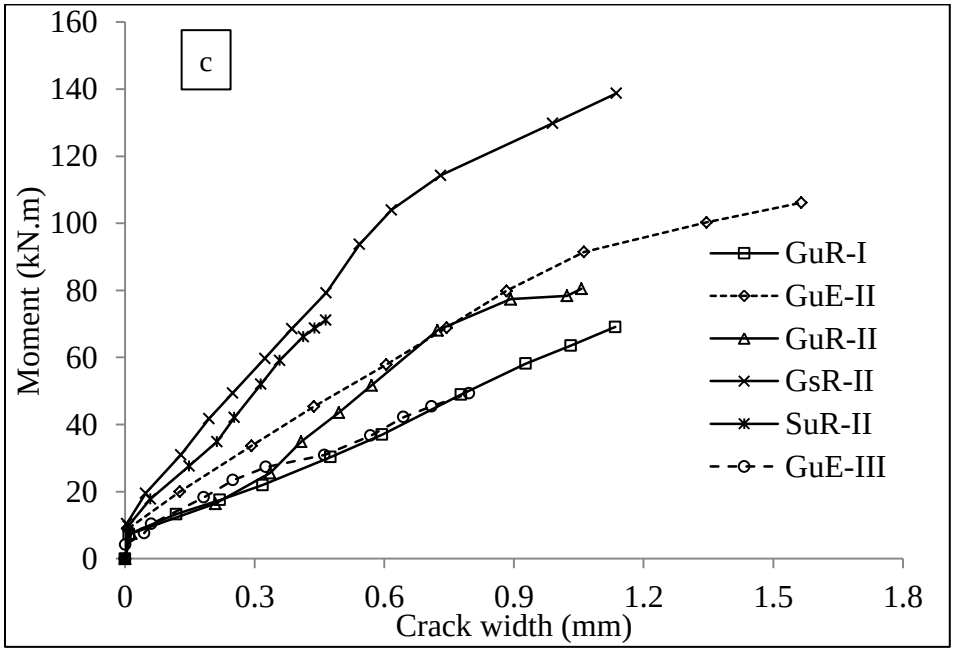

Figure 5.3: Moment-crack width relationship at (a) the north mid-span section, (b) the south mid-span section and (c) the middle support section

5.4 STRAINS IN CONCRETE AND REINFORCEMENT

The strain variation in both concrete and longitudinal reinforcement with the applied moment at the middle support and mid-span sections is plotted in Fig. 5.4. The concrete strains in all critical sections increased linearly up to 50% of the failure moment. Afterwards, at higher loads, the strains increased non-linearly with the applied moments. As the cracks propagated towards the strain gauge location, the compressive strains decreased and this continued until failure occurred. At the same moment level in all critical sections, a rapid increase in strains in concrete was observed in beams which were reinforced with relatively low amount of reinforcement. As expected, in all GFRP-RC beams, the concrete compressive stains were very close to or exceeded the crushing strain of 3,500 micro-strains, specified in the CSA/S806-12 (CSA 2012). In contrary, the concrete strains were less than 3,500 micro-strains in beam SuR-II which failed in shear right after yielding of the longitudinal reinforcement.

At the pre-cracking stage, strains in the longitudinal reinforcement were very small in all test beams; however, they increased rapidly with the formation of cracks. The strains at failure in beam GuR-I reached 49, 42 and 43% of their ultimate strains at the section of middle support, north mid-span and south mid-span, respectively. In the north mid-span section of beams GuE-II and GuR-II, the strains measured at failure were 52 and 31% of the ultimate strain, respectively. However, they had the same strain level, approximately 42% at the middle support and 55% at the south mid-span sections. In loading case-III, the strains at failure were 34 and 53% in the middle support and north mid-span, respectively.

The material type of reinforcing bar had significant effect on the measured strains. At the middle support and north mid-span sections, the strain in beam GuR-II was approximately 2.7 times those in beam SuR-II, at the design load level. Also, at the south mid-span section, the strain in

GuR-II was approximately 6 times that in beam SuR-II. This could be attributed to the high axial stiffness of the steel reinforcement compared to that of the GFRP reinforcement. Regarding the effect of longitudinal reinforcement ratio on the measured strains, beam GuR-II had 17% more strain at the hogging moment region compared to that of beam GuE-II at the design moment level. However, the strain at the north sagging moment region was less than that in beam GuE-II by 67% at the design load. This could be attributed to the increased and reduced amount of reinforcement in the sagging and hogging moment region, respectively, which is result of considering the moment redistribution in the design process.

The strains in beams SuR-II and GsR-II were similar at both middle support and south mid-span sections since the provided reinforcement in both beams had similar axial stiffness. However, at the north mid-span section, the measured strain in beam GsR-II was approximately 2.15 times that in beam SuR-II. Regarding the measured strains at the service load level (P = 58 kN), beam SuR-II experienced 1,170, 820 and 720 micro-strains at the middle support, north mid-span, and south mid-span sections, respectively. At these critical sections, on the other hand, the strains in beam GsR-II were 1,320, 1,790 and 1,140 micro-strains which represent only 6.3, 8.5 and 5.4% of the characteristic design strain, respectively. Thus, beam GsR-II satisfied the strain limit of 25% of the bar rupture strain as specified in the CSA/S806-12 standard (CSA 2012).

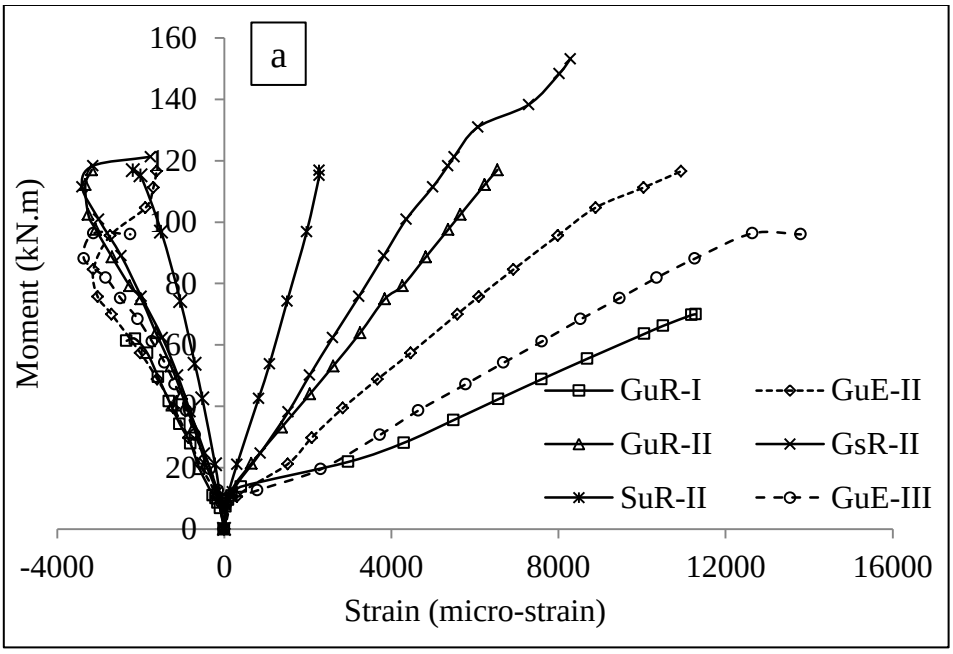
a
160
140
120
100
80
60
40
20
0
Moment (kN.m)
-4000
0
4000
8000
12000
16000
Strain (micro-strain)
GuR-I
GuE-II
GuR-II
GsR-II
SuR-II
GuE-III

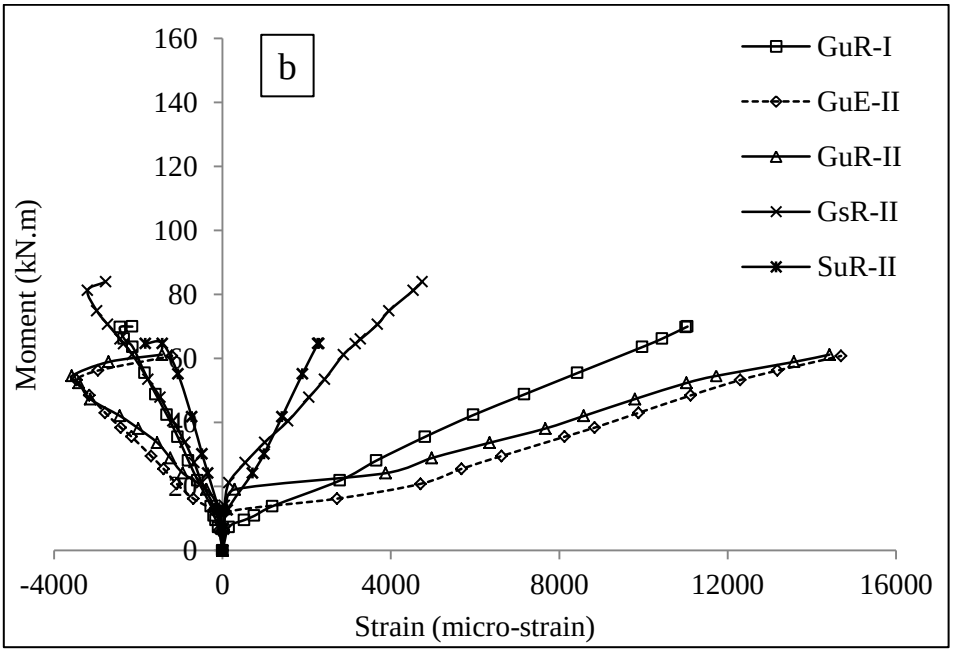
b
160
140
120
100
80
60
40
20
0
Moment (kN.m)
-4000
0
4000
8000
12000
16000
Strain (micro-strain)
GuR-I
GuE-II
GuR-II
GsR-II
SuR-II

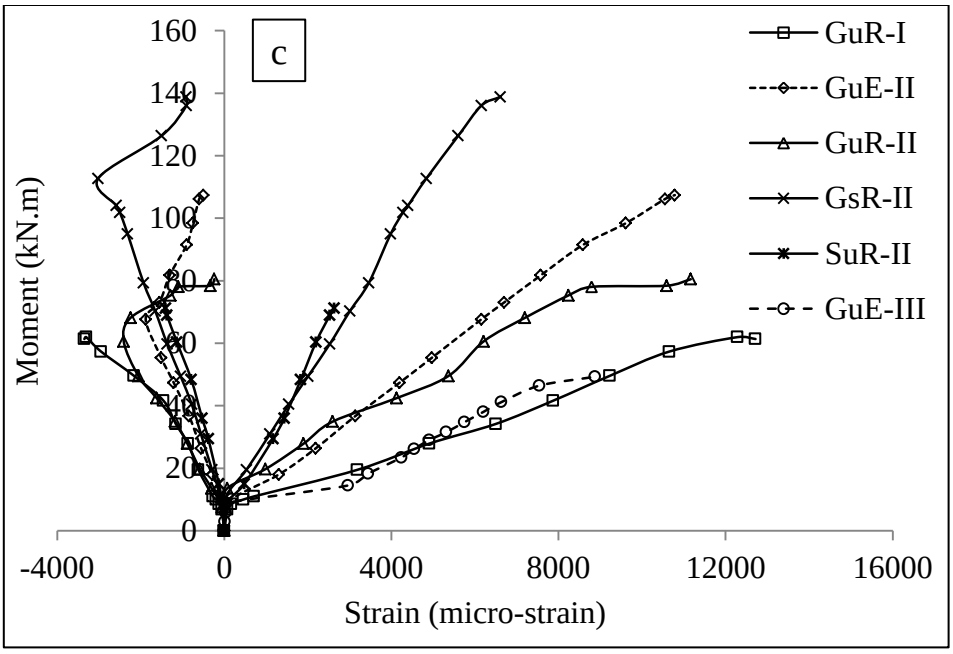

Figure 5.4: Strain variation in concrete and reinforcing bars at (a) the north mid-span section, (b) the south mid-span section and (c) the middle support section

5.5 MOMENT REDISTRIBUTION

As the cracks formed in the maximum moment regions, the flexural stiffness changed and consequently, the internal forces redistributed among the critical sections. This resulted in deviation of the measured experimental reactions from the elastic (theoretical) ones. These measured reactions were used to calculate the experimental moments and then the percentage of the moment redistribution. The experimental and theoretical moments at failure, at the three critical sections are documented in Table 5.1. Also, Fig. 5.5 shows the calculated moment redistribution versus the applied load for all test beams. The symmetrically loaded beam, GuR-I, exhibited moment redistribution of 19.3 and 22.3% at the design load of P = 125 kN and at failure load, respectively. In loading case II and III, beams GuE-II and GuE-III, designed for elastic moment, exhibited negative moment redistribution which was approximately 4.0 and

9.9%, respectively, at failure load. This could be attributed to the reduced flexural stiffness due to the extensive cracking observed in the higher load span. Regarding the effect of the material type, both beams SuR-II and GuR-II redistributed moments in a similar manner up to failure. The moment redistribution in these two beams, at failure, was approximately 25.4 and 19.7%, respectively. It should be noted that although beam SuR-II experienced shear failure it was able to redistribute the bending moment.

Similar results were reported in shear-critical beams where more than 20% moment redistribution occurred in beams having similar dimensions and spans (Mahmoud and El-Salakawy 2014 and 2015).

Beam GuE-II, designed for the elastic moments, showed reversed moment redistribution. On the other hand, beam GuR-II, designed for 20% moment redistribution, showed normal moment redistribution. This behavior may be attributed to the reinforcement arrangement/ratio at the different critical sections. The relatively larger amount of reinforcement at the hogging moment region in beam GuE-II was able to control the crack widths which, in turn, made the middle support region stiffer than the sagging moment region and therefore, the internal forces redistributed from the sagging to the hogging moment region. The opposite occurred for beam GuR-II where the north mid-span section was stiffer than the middle support section. Also, it was noted that beam GuR-I, tested under symmetrical loading condition, exhibited higher percentage of moment redistribution compared to that in beam GuR-II. The moment redistribution at failure was 22.3 and 19.7% in beams GuR-I and GuR-II, respectively. This is due to the higher intensity of cracks in the middle support section under symmetrical loading conditions, as opposite to the unsymmetrical loading case. It is worth mentioning that in a study conducted by El-Mogy et al.

(2011) on continuous FRP-RC beams tested under symmetrical loading, the percentage of moment redistribution was reported in the range of 23-37%.

Beam GsR-II could achieve a maximum of 13.5% moment redistribution at 64% of the failure load, however, the percentage then reduced to 9.1% at failure load. The low moment redistribution is a result of the high reinforcement ratio at the hogging moment region which, in turn, resulted in a reduced rotational capacity of the middle support section. Again, in a beam designed for serviceability tested under symmetrical loading (El-Mogy et al. 2011), the moment redistribution was approximately 33%. Therefore, it can be concluded that the unsymmetrical loading on continuous beams could negatively affect the moment redistribution between the critical sections. Furthermore, beam GsR-II had less moment redistribution than beam SuR-II. This is due to the extensive cracking in GsR-II which reduced the stiffness in the sagging moment region. The opposite could be seen in SuR-II where the sagging moment region seemed to be stronger than the hogging moment region due to the high axial stiffness of the steel which controlled the crack widths in that region. In general, it can be summarized that moment redistribution was possible in ULS based beams that could successfully achieve the assumed percentage of moment redistribution of 20% under different loading patterns.

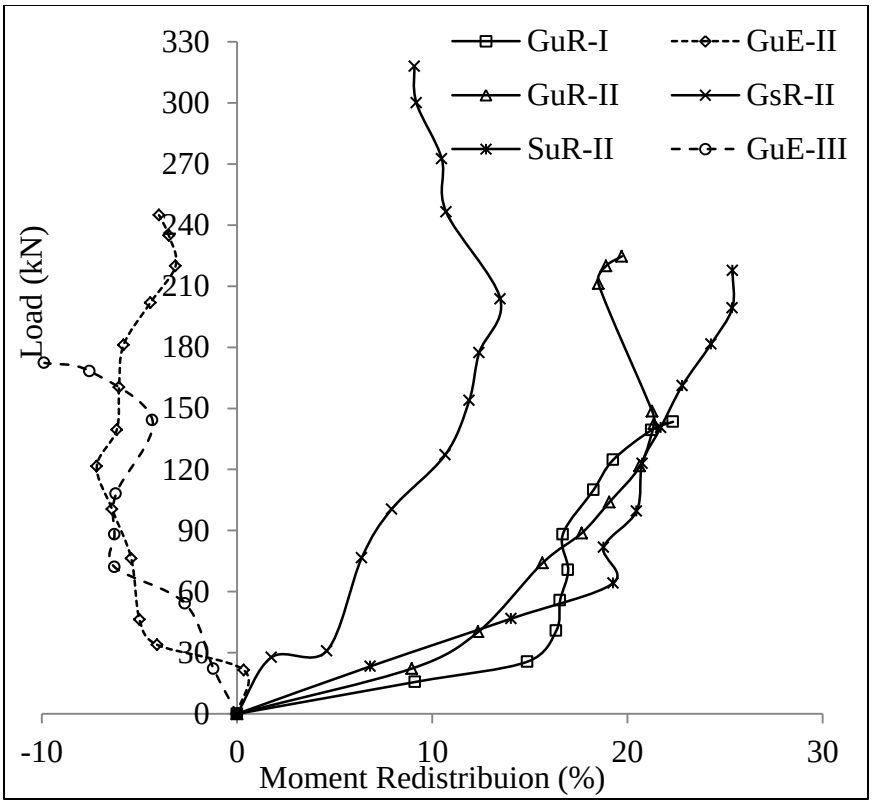

Figure 5.5: Moment redistribution versus the load on north span of the test beams

5.6 LOAD CARRYING CAPACITY

All GFRP-RC beams continued to carry loads even after the initiation of concrete crushing at the critical sections. In loading case I, beam GuR-I carried 13% more than the design load (*P*) of 125 kN. In loading case II, beams SuR-II, GuE-II, and GuR-II resisted additional 23, 30, and 18% load after exceeding the specified design load (*P*). In addition, the ultimate capacity of beam GsR-II was 47% high compared to that of its counterpart reinforced with steel bars, SuR-II. Lastly, beam GuE-III also was able to carry a load that is greater than the design load by 38%. Table 5.1 summarizes the experimental and predicted bending moments of the critical sections of all test beams. The predicted flexural capacities were calculated according to CSA/A23.3 (CSA 2014) for steel-RC beam or CSA S806-12 (CSA 2012) for GFRP-RC beams. The experimental-to-predicted moment ratio at all critical sections of steel-RC beam SuR-II was close to unity, as

shown in Table 5.1. This is because the beam failed in shear at the onset of yielding of the steel bars at all critical sections. On the other hand, the experimental moment in the sections where concrete crushing was observed was 6-43% higher than the predicted moment. This high reserve of the sectional capacity could be attributed to the improved confinement and subsequently, increased concrete strength by closely spaced stirrups.

Table 5.1 - Experimental and predicted moments of test beams at failure

Beams	Experimental moment (kN.m)			Predicted moment[a] (kN.m)			Experimental/Predicted			MR at failure (%)
	North mid-span section	Middle support section	South mid-span section	North mid-span section	Middle support section	South mid-span section	North mid-span section	Middle support section	South mid-span section	
GuR-I	70.0	59.6	70.0	68.4	56.3	68.4	1.02	1.06	1.02	22.3
SuR-II	116.9	71.2	64.6	109.5	71.7	63.2	1.07	0.99	1.02	25.4
GuE-II	116.8	105.4	60.8	93.4	85.7	58.6	1.25	1.22	1.04	-4.0
GuR-II	117.1	80.5	61.2	104.2	72.4	58.6	1.12	1.11	1.04	19.7
GsR-II	153.2	138.8	84	106.9	103.7	93.6	1.43	1.34	0.90	9.1
GuE-III	96.0	49.3	-	74.9	59.6	-	1.28	0.83	-	-9.9

[a] Calculated according to CSA/A23.3 (CSA 2014) or CSA/S806-12 (CSA 2012) as appropriate.

5.7 LOAD-DEFLECTION RESPONSE

The mid-span deflection versus the applied load at both north and south spans of all test beams is demonstrated in Fig. 5.6. For beam GuE-III, upward deflection of south mid-span is reported with the load applied on the north mid-span. Generally, in the pre-cracking stage, all beams showed linear response with small deflections; however, the development of the cracks in both hogging and sagging moment regions resulted in a significant reduction in the flexural stiffness and consequently higher deflections. Near failure, nonlinear behavior was also observed in all the GFRP-RC beams due to concrete softening. In beam GuR-I, similar deflections in both spans were noticed as the beam was subjected to symmetrical loading. In beams of loading case II, the north span of ULS based beams was highly over-reinforced with respect to the south span, which resulted in higher deflection in the south span. In addition, in beam GuE-III, the south span was deflecting upward with loading in contrast to the north span. Near failure, a sudden increase in the upward deflection showed up while concrete crushing was taking place in the north span.

Beam GuR-II showed higher deflections compared to its counterpart reinforced with steel, SuR-II, as expected. The measured deflection in beam GuR-II was approximately 2.5 and 4.9 times that in beam SuR-II at the north and south mid-span, respectively. This correlates well with the axial stiffness in both beams where the steel-to-GFRP axial stiffness ratio was 2.8 and 7.3 in the north and south spans, respectively. The effect of the assumed moment redistribution percentage on the deflection can be seen in beams GuE-II (MR = 0%) and GuR-II (MR = 20%). The measured deflection in the higher load span of beam GuR-II was approximately 15% less than that of beam GuE-II. This could be attributed to the high longitudinal reinforcement ratio in the north sagging moment region in beam GuR-II compared to that in beam GuE-II. Therefore,

considering moment redistribution in designing continuous beams has no adverse effect on the mid-span deflection. By comparing deflections of beams GsR-II and SuR-II in post-cracking stage, it can be seen that GsR-II exhibited deflection in both north and south spans that was approximately 60% higher than that in its counterpart beam reinforced with steel, SuR-II.

From the serviceability point of view, the allowable maximum deflection varies from 5.6 to 14.8 mm (span/480 to *span*/180) depending on the type and function of structural element, according to CSA/S806-12 (CSA 2012). At the service load, the measured deflection in beams SuR-II and GsR-II was 3.21 and 5.83 mm in north sagging moment region, respectively, whereas in the south sagging moment region, the deflection was 2.23 and 3.66 mm, respectively. This implies that only north span of GsR-II failed to satisfy the serviceability requirement for certain types of structural applications.

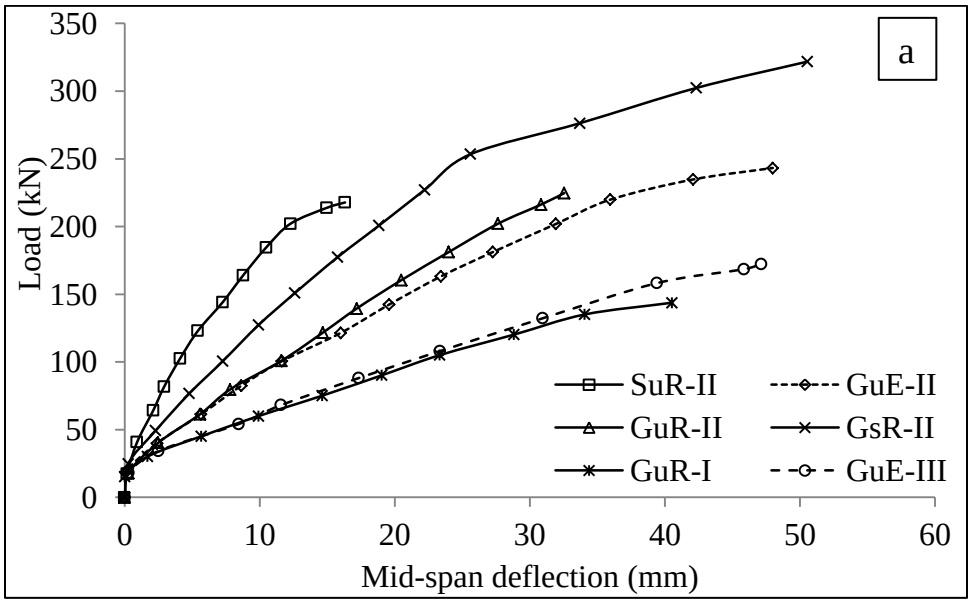

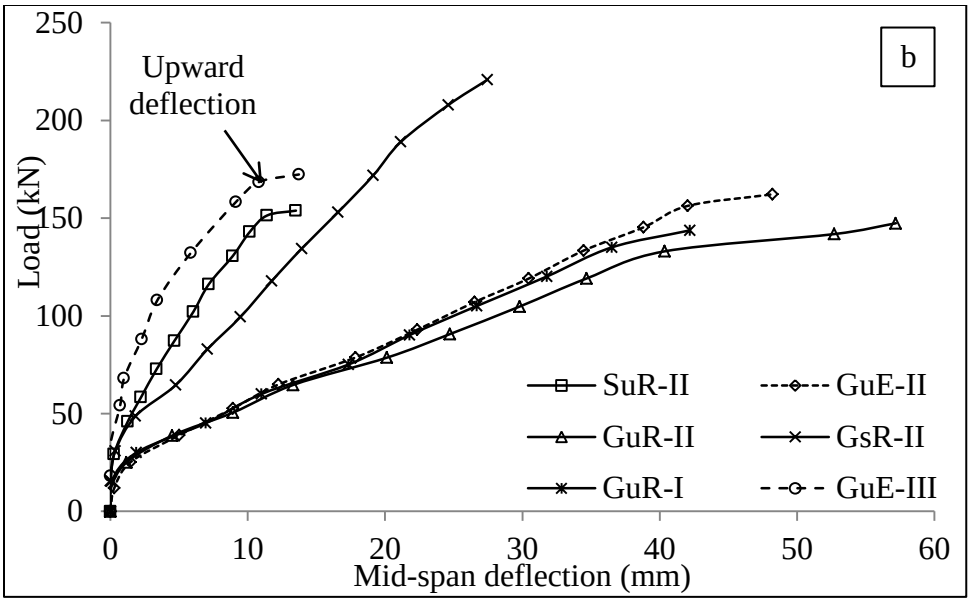

Figure 5.6: Load-deflection relationship at a) north span and b) south span of the test beams

5.8 PREDICTION OF LOAD-DEFLECTION RESPONSE

There are two different approaches for calculating the deflection; one is based on effective moment of inertia while the other one is based on moment-curvature integration. In this paper, only models based on the effective moment of inertia are considered. Models proposed by ISIS Canada (2007), Habeeb and Ashour (2008), and the ACI 440.1R-15 (ACI committee 440 2015) are used to predict the mid-span deflection of the test beams (Table 4). It should be noted that the CSA/S806-12 (CSA 2012) adopts the moment-curvature integration approach and thus it is not considered in this study. The predicted deflection is then compared to the experimental results. The first model, proposed by ISIS Canada (2007), assumes a uniform moment of inertia instead of actual variable moment of inertia along the beam span. The second model is basically a modified version of the widely acknowledged Branson's equation of effective moment inertia which was derived for steel-RC beams subjected to service loads. The expression was modified with factor (β_d) to take into consideration the less tension stiffening effect of FRP-RC beams and

reduction factor (γ_G) to the second term which represents the post-cracking phase. Moreover, ACI 440.1R-15 (ACI Committee 440 2015) model is suggesting an expression with γ factor which depends on load and boundary conditions and accounts for the uncracked regions and stiffness variation in the cracked regions. For continuous beams, an expression of effective moment of inertia, $I_e = 0.85I_{em} + 0.15I_{ec}$, was suggested to calculate the deflections where, I_{em} and I_{ec} is effective moment of inertia at mid-span and central support sections, respectively.

Table 5.2 – Models for deflection prediction of GFRP-RC beams

Models	Effective moment of inertia, I_e (mm^4)	Relevant formulas
ISIS Canada (2007)	$I_e = {I_t I_{cr}}/{(I_{cr} + (1 - 0.5(M_{cr}/M_a)^2)(I_t - I_{cr}))}$	$I_g = \frac{bh^3}{12}$
Habeeb and Ashour (2008)	$I_e = (M_{cr}/M_a)^3 \beta_d I_g + (1 - \left(\frac{M_{cr}}{M_a}\right)^3) I_{cr} \gamma_G \leq I_g$ Where $\beta_d = 0.2 * (\rho_f/\rho_{fb}) \leq 1$	$M_{cr} = \frac{0.62\lambda\sqrt{f_c'} I_g}{y_t}$ $k = \sqrt{2\rho_f n_f + (\rho_f n_f)^2}$- $\rho_f n_f$
ACI 440.1R-15 (ACI Committee 440 2015)	$I_e = {I_{cr}}/{(1 - \gamma(M_{cr}/M_a)^2(1 - I_{cr}/I_g))} \leq I_g$ Where $M_a \geq M_{cr}$ and $\gamma = 1.72 - 0.72 * (M_{cr}/M_a)$	$I_{cr} = \frac{bd^3}{3} k^3$ $+ n_f A_f d^2 (1 - k)^2$

Fig. 5.7 illustrates the experimental and the predicted deflection of the north sagging moment region of test beams for the three different loading conditions. In loading case I and II, models proposed by ISIS Canada (2007) and ACI 440.1R (2015) reasonably predicted the trend up to 40-65% of the failure load and afterwards, progressive underestimation of the deflection was observed. However, in loading case III, both models showed close predictions until failure. Similarly, the model proposed by Habeeb and Ashour (2008), in all loading cases, yielded good predictions of the deflection in the early loading stages (25-45% of the failure load) while it highly overestimated the deflections at high load levels.

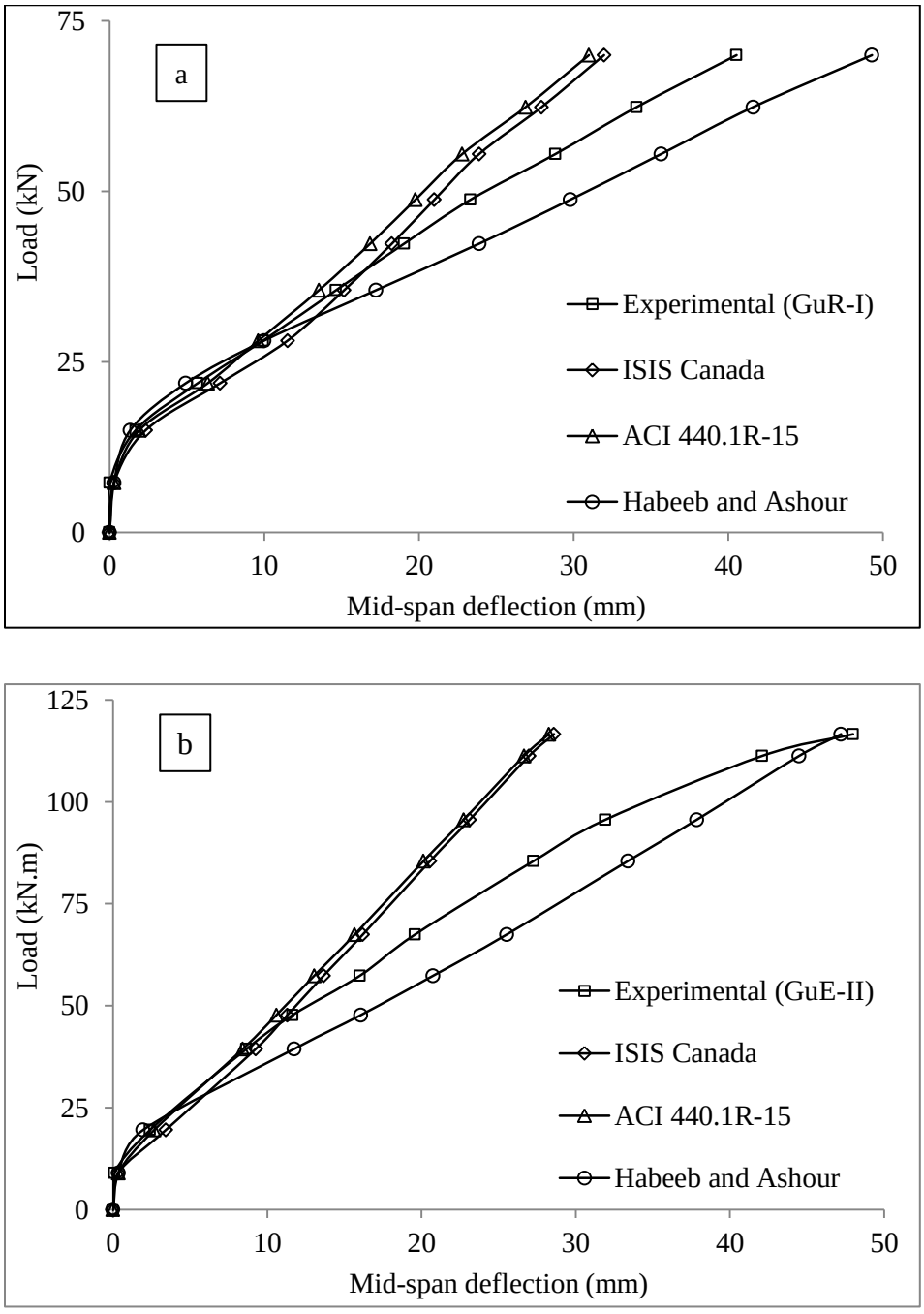

Figure 5.7: Experimental and predicted load-deflection response of test beam a) GuR-I, b) GuE-II, c) GsR-II and d) GuE-III (Continued)

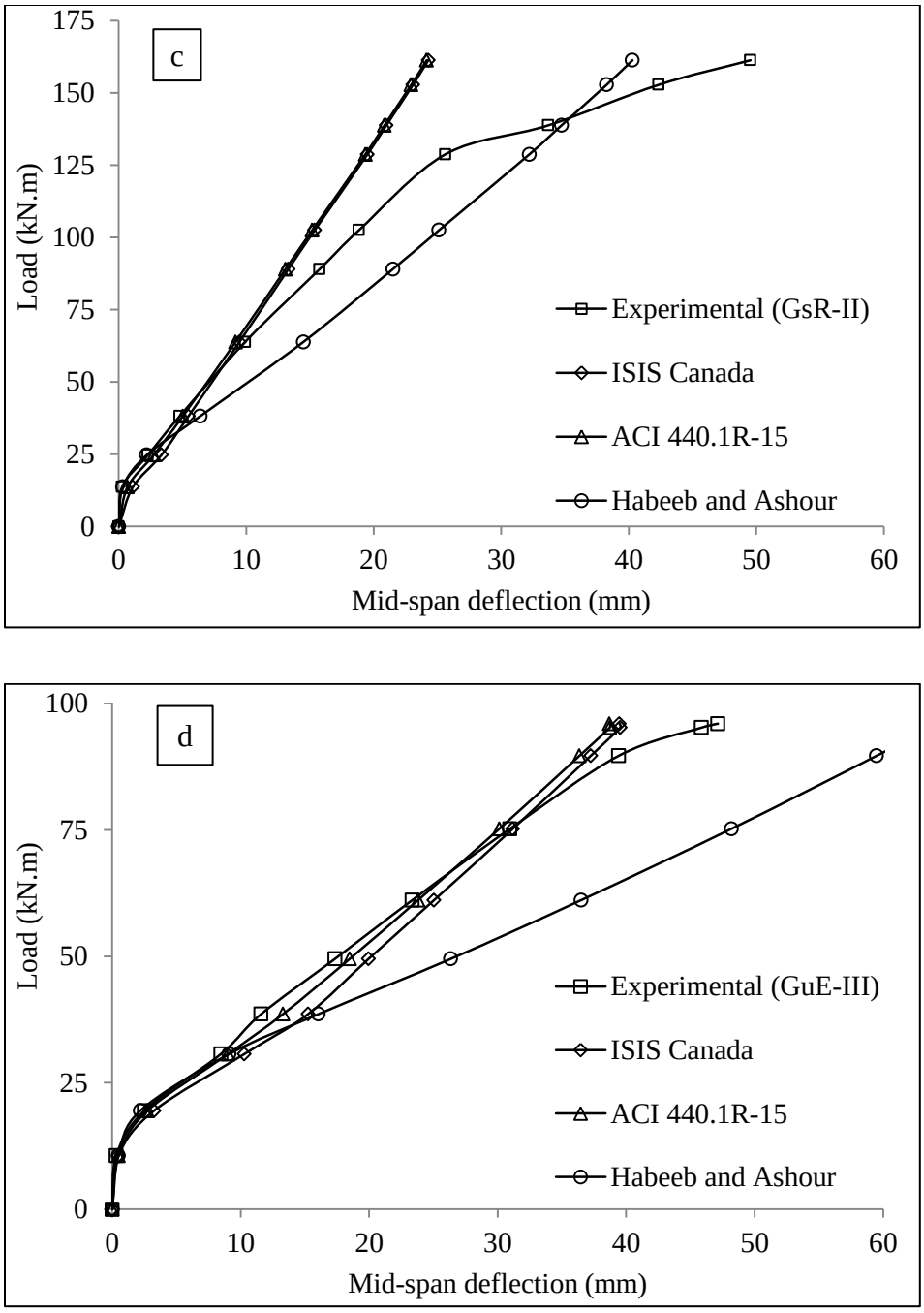

Figure 5.7: Experimental and predicted load-deflection response of test beam a) GuR-I, b) GuE-II, c) GsR-II and d) GuE-III.

Table 5.3 enlists the ratio of experimental-to-predicted deflection as well as the statistical evaluation of the predictions at the service and design load levels. At the service load level, the

model proposed by ACI 440.1R (2015) gave the best predictions where the mean value of the experimental-to-predicted deflection ratio was 0.99 with a coefficient of variation of 8.24%. However, the model proposed by ISIS Canada (2007) yielded the most conservative predictions where the mean value of the experimental-to-predicted deflection ratio was 0.79 with a coefficient of variation of 11.8%. At the design load level, both models proposed by ACI 440.1R (2015) and the ISIS Canada (2007) consistently underestimated the deflections by 25 and 22%, respectively. On the other hand, the model proposed by Habeeb and Ashour (2008) produced inconsistent predictions while it gave conservative prediction at the service load level and unconservative predictions at the design load level.

Table 5.3 – Experimental-to-predicted deflection ratio for GFRP-RC beams

Beam	ISIS Canada 3 (2007)		Habeeb and Ashour (2008)		ACI 440.1R (2015)	
	Service load	Design load	Service load	Design load	Service load	Design load
GuR-I	0.79	1.23	1.31	0.89	0.94	1.28
GuE-II	0.69	1.37	1.36	0.84	1.03	1.39
GuR-II	0.67	1.31	1.33	0.8	1.12	1.34
GsR-II	0.93	1.2[a]	0.72	0.74[a]	0.99	1.22[a]
GuE-III	0.76	0.98	1.05	0.64	0.87	1.02
Mean	0.77	1.22	1.16	0.78	0.99	1.25
Standard deviation	0.09	0.13	0.24	0.08	0.08	0.13
Coefficient of variation, %	11.8	10.9	21.0	10.9	8.2	10.4

[a] Deflection was calculated at design load of ULS based beams (P = 125 kN)

CHAPTER 6– CONCLUSIONS AND FUTURE WORK

6.1 SUMMARY

This section presents the findings from the current investigation and the recommendations for the future work. The current study investigated the behavior of continuous beams which were reinforced with GFRP bars and stirrups. The experimental scheme included two different series, namely, Series 1 dealing with testing of T-beams under symmetrical loading, and Series 2 dealing with behavior of rectangular beams under different loading conditions.

A total of twelve large-scale beams were constructed and tested in the experimental phase with six in each series. The test variables in Series 1 were material type (steel or GFRP), an assumed percentage of moment redistribution, spacing of stirrups, and spacing of transverse bars in the flange, and serviceability. On the other hand, in Series 2, the beams were tested under three different loading conditions: I) equal load P (symmetrical) on both spans, II) load P on one span and $1.5P$ on the other, and III) load P on one span only. Under the loading condition-III, the variables chosen were type of reinforcing material (steel or GFRP), an assumed moment redistribution percentage, and serviceability. After the analysis, some conclusions regarding both of series are made and given in the following sections.

6.2 CONCLUSIONS FROM RESULTS OF SERIES 1

Six large-scale GFRP-RC continuous T-beams were tested to failure to investigate the overall behavior and to determine their ability to redistribute bending moments between critical sections.

Based on the test results and discussion presented in this study, the following conclusions can be drawn:

1. The steel-RC beam experienced tension-controlled failure (yielding of steel) and ultimately crushing of concrete was observed in both hogging and sagging regions. In all GFRP-RC beams, crushing of concrete in the hogging moment region took place; then, the beams continued to resist more loads until failure occurred due to either crushing of concrete in the sagging moment region or diagonal shear cracks near the middle support.

2. All beams partially lost the composite action as a T-section in the sagging moment region due to the development of two longitudinal cracks at the overhanging flange-web interface; however, decreasing the spacing of the lateral bars in the flange prevented the formation of such cracks at these locations.

3. All GFRP-RC beams, achieved a reasonable deformability factor which was higher than the minimum factor of 6.0 specified by CHBDC code (CAN/CSA-S6-14) for T-beams. However, based on the energy ductility method proposed by Grace et al. (1998), the reference beam reinforced with steel exhibited ductile failure while the GFRP-RC beams exhibited semi-ductile or brittle failure. Decreasing the spacing of either stirrups or lateral reinforcement in the flange increased the energy ductility. The high deformability factor in GuR-18-4.5 was due to the enhanced concrete strength and rotation capability as a result of using the stirrups with small spacing.

4. All tested beams exhibited moment redistribution from the hogging to the sagging moment region. The GFRP-RC continuous concrete beams could successfully achieve the assumed percentage of moment redistribution (approximately 15%). Also, the beams with closer stirrup spacing or more lateral flange bars experienced more moment

redistribution compared to their counterparts with larger spacing of lateral bars or stirrups.

6.3 CONCLUSIONS FROM RESULTS OF SERIES 2

Six large-scale rectangular continuous beams were tested to failure under three different loading conditions to investigate the structural performance and to determine their ability to redistribute bending moments between critical sections. Moreover, the experimental results were compared to the available models to predict the mid-span deflections of the test beams. Based on the discussion presented earlier, the following conclusions can be drawn:

1. As expected, beam tested under symmetrical loading exhibited almost identical cracking, crack widths, strain and deflections in both spans. In beams tested under unsymmetrical loading case II, the higher load span showed less crack widths, strains and deflections compared to those in the less load span. This is due to the larger amount of longitudinal reinforcement ratio in the higher load span compared to that in the other span. Beam with one loaded span (case III), exhibited very similar crack width, strains and deflections in the loaded span to those in beams tested under symmetrical loading. Also, this behavior was observed at the hogging moment section of beam tested under symmetrical loading (case I) and beam with one loaded span (case III).

2. The steel-RC beam achieved a moment redistribution percentage higher than the assumed percentage of 20%. Also, normal moment redistribution ranging from 19.7 to 22.3% was observed in all GFRP-RC beams which were designed based on the ultimate limit state. However, the beam designed for the serviceability limit state exhibited low moment redistribution at failure (9.1%) as a result of the high reinforcement ratios at the critical

sections. In addition, the unsymmetrical loading conditions adversely affected the moment redistribution.

3. The GFRP-RC beams, tested under unsymmetrical loading and designed for elastic moment, exhibited reversed moment redistribution in the hogging region up to 9.9%. This can be attributed to the reduced flexural stiffness due to the formation of excessive cracks in the higher load region. This caused the sagging moment region to be weaker than the hogging moment region; therefore, the internal forces were redirected to the strong hogging moment region.

4. The arrangement of longitudinal reinforcement, considering moment redistribution, had a positive effect in reducing both crack width and deflection in the higher load span. Similarly, the steel-RC beam showed superior performance compared to its ULS based counterpart GFRP-RC beam under loading case II. Also, in all loading cases, deflection and crack width at the same moment level were inversely related to the amount of flexural reinforcement.

5. Beam GsR-II, designed for SLS, showed similar behavior to that of the steel-RC beam in terms of cracking behavior and strains; however, it experienced higher deflection compared to its counterpart reinforced with steel. Also, the beam was reasonably able to meet the serviceability requirements for most types of structural applications, according to CSA/S806-12 (CSA 2012).

6. Deflection prediction models proposed by the ACI 440.1R (2015) and ISIS Canada (2007) gave conservative predictions of the deflections at the service load level while they underestimated the deflection at high load levels. On the other hand, model proposed

by Habeeb and Ashour (2008) gave inconsistent predictions where it gave unconservative predictions at the service load level and very conservative predictions at high load levels.

6.4 RECOMMENDATIONS FOR FUTURE WORK

Within the scope of flexural behavior of continuous beams, the following recommendations can be made for future work:

1. The beams investigated in this study were continuous over two spans where each exterior end was discontinuous. Continuous beams with different exterior support conditions (fixed exterior end and continuous both end) can be studied. A substantially higher moment at the hogging moment section compared to that at the sagging moment section is expected to affect the redistribution of flexural stiffness after cracking takes place.
2. The beam spans of the current study were symmetrical. Moment redistribution can be studied with unsymmetrical span length and can also be extended to beams continuous over multi-spans. Due to the asymmetry in span length, the cracked stiffness of the adjacent spans is different; which can affect the moment redistribution.
3. The current study included the beams which were designed for different occupancy intensity on each span and accordingly, the load was applied. The beams designed for same intensity of occupancy on either span can be investigated under the unsymmetrical loading conditions. This represents a condition where one span is fully loaded by the occupants while the adjacent one is partially loaded at a certain time. As both spans are provided with the same reinforcement ratio, the partially loaded span is stiffer than the fully loaded span. Therefore, the moment redistribution is expected to be affected.

4. Testing of beams with T-section was carried out under symmetrical loading and span arrangements. Therefore, T-beams can also be tested under unsymmetrical loading and span conditions and can be compared with that of rectangular beams.
5. As the present study was carried out over the GFRP-RC beams, further experimental studies are required to investigate the behavior of such beams with different reinforcement type (CFRP, AFRP, and BFRP) under different circumstances recommended above.

REFERENCES.

Achillides, Z. and Pilakoutas, K. (2004). “Bond Behavior of Fiber Reinforced Polymer Bars under Direct Pullout Conditions.” ASCE, Journal of Composites for Construction, 8(2), 173-181.

ACI Committee 318. (2011). “Building Code Requirements for Reinforced Concrete.” ACI 318-11, American Concrete Institute, Farmington Hills, MI.

ACI Committee 440. (2015). “Guide for the Design and Construction of Structural Concrete Reinforced with Fiber-Reinforced Polymer (FRP) Bars.” ACI 440.1R-15, American Concrete Institute, Farmington Hills, MI.

Allen, R. and Edwards, S. (1987). “Repair of Concrete Structures.” Ed Blackie, London, U.K.

Apostolopoulos, C. A. and Papadakis, V. G. (2007). “Consequences of Steel Corrosion on the Ductility Properties of Reinforcement Bar.” Construction and Building Materials, 22(12): 2316-2324.

Baker, A. L. and Amarakone, A. M. (1965). “Inelastic Hyperstatic Frames Analysis.” Proceedings of the international symposium on Flexural Mechanics of Reinforced Concrete, ASCE/ACI SP-12: 85-136.

Benmokrane, B., Challal, O. and Mamoudi, R. (1996a). “Flexural Response of Concrete Beams Reinforced with FRP Reinforcing Bars.” ACI Structural Journal, 93(1): 46-55.

Benmokrane, B., Tighiouart, B. and Chaallal, O. (1996b). "Bond Strength and Load Distribution of Composite GFRP Reinforcing Bars in Concrete." AC1 Materials Journal, 93(3): 246-253.

Carmo, R. N. F. and Lopes, S. M. (2006). "Required Plastic Rotation of RC Beams." Proceedings of the institution of civil engineers, structures and buildings, 159(SB2): 77-86.

Carmo, N. F. C. and Lopes, S. M. R. (2008). "Available Plastic Rotation in Continuous High-Strength Concrete Beams." Canadian Journal of Civil Engineering, 35 (5): 1152-1162.

CSA (Canadian Standards Association). (2012). "Design and Construction of Building Structures with Fibre-Reinforced Polymers." CSA/S806-12, Toronto, Ontario.

CSA (Canadian Standards Association). (2014a). "Canadian Highway Bridge Design Code." CSA/S6-14, Toronto, Ontario.

CSA (Canadian Standards Association). (2014b). "Code for the Design of Concrete Structures for Buildings." CSA/A23.3-14, Toronto, Ontario.

CSA (Canadian Standard Association). (2014c). "Concrete Materials and Methods of Concrete Construction/Test Methods and Standard Practices for Concrete." *CSA/A23.1-14/A23.2-14*, Toronto, Ontario.

El-Mogy, M., El-Ragaby, A. and El-Salakawy, E. (2010). "Flexural Behavior of Continuous FRP-Reinforced Concrete Beams." ASCE, Journal of Composites for Construction, 14(6):669–680.

El-Mogy, M., El-Ragaby, A., and El-Salakawy, E. (2011). "Effect of transverse reinforcement on the flexural behavior of continuous concrete beams reinforced with FRP." ASCE, Journal of Composites for Construction, 15(4): 672-681.

Ernst, G. C. (1958). "Moment and Shear Redistribution in Two-Span Continuous Reinforced Concrete Beams." ACI Structural Journal, 30(5): 573–589.

Grace, N. F., Soliman, A. K., Abdel-Sayed, G. and Saleh, K. R. (1998). “Behavior and Ductility of Simple and Continuous FRP Reinforced Beams.” ASCE, Journal of Composites for Construction, 2(4), 186-194.

Habeeb, M. N. and Ashour, A. F. (2008). "Flexural Behavior of Continuous GFRP Reinforced Concrete Beams" ASCE, Journal of Composites for Construction, 12(2), 115-124.

Holland, R. (1997). “Appraisal and Repair of Reinforced Concrete.” ICE Publishing, Edition 1, Thomas Telford, London.

ISIS Canada. (2007). “Design Manual 3: Reinforcing concrete structures with fibre reinforced polymers (FRPs).” ISIS Canada Corporation, The Canadian Network of Centers of Excellence on Intelligent Sensing for Innovative Structures, Winnipeg, Manitoba, Canada.

Issa, M. S., Metwally, I. M. and Elzeiny, S. M. (2011). “Influence of Fibres on Flexural Behavior and Ductility of Concrete Beams with GFRP Rebars.” Engineering Structures, 33(5), 1754-1763.

Jaeger, L. G., Tadros, G. and Mufti, A. (1995). “Balanced Section, Ductility and Deformability in Concrete with FRP reinforcement.” Res. Rep. 2-1995, Industry’s Centre for Computer-Aided Engineering, CAS CAM, Tech. Univ. Of Nova Scotia, Halifax, Nova Scotia.

Kara, I. F. and Ashour, A. F. (2013). “Moment Redistribution in Continuous FRP Reinforced Concrete Beams.” Construction and Building Materials, 49, 939–948.

Kocaoz, S., Samaranayake, V. A. and Nanni, A. (2005). “Tensile Characterization of Glass FRP bars.” Composites: Part B 36, 127-134.

Lin, C. H. and Chien, Y. M. (2000). “Effect of Section Ductility on Moment Redistribution of Continuous Concrete Beams.” Journal of the Chinese Institute of Engineers, 23(2), 131-141.

Mahmoud, K., and El-Salakawy, E. (2014). “Shear Strength of GFRP-Reinforced Concrete Continuous Beams with Minimum Transverse Reinforcement.” ASCE, Journal of Composites for Construction, 18(1).

Mahmoud, K., and El-Salakawy, E. (2016). “Effect of Transverse Reinforcement Ratio on the Shear Strength of GFRP-RC Continuous Beams.” ASCE, Journal of Composites for Construction, 20(1).

Malvar, L. J. (1995), "Tensile and Bond Properties of GFRP Reinforcing Bars." AC1 Materials Journal, 92 (3), 276-285.

Matos, B., Correia, J. R., Castro, L. M. S. and Franca, P. (2011). “Structural Response of Hyperstatic Concrete Beams Reinforced with GFRP Bars; Effect of Increasing Concrete Confinement” Journal of Composite Structures, 94(3), 1200-1210.

Mattock, A. H. (1959). “Redistribution of Design Bending Moments in Reinforced Concrete Continuous Beams.” The Institution of Civil Engineers, 13(1), 35-46.

Mattock, A. H. (1965). “Rotational Capacity of Hinging Regions in Reinforced Concrete Beams.” Proceedings of the International Symposium on Flexural Mechanics of Reinforced Concrete, ASCE-ACI, Miami, 143-181.

Mosley, C. P., Tureyen, A. K. and Frosch, R. J. (2008). “Bond Strength of Non-metallic Reinforcing Bars.” ACI Structural Journal, 105(5), 634-642.

Mostofinejad, D. (1997). “Ductility and Moment Redistribution in Continuous FRP Reinforced Concrete Beams,” PhD thesis, Department of Civil and Environmental Engineering, Carleton University, Ottawa, Ontario, Canada.

Mota, C., Alminar, S. and Svecova, D. (2006). “Critical Review of Deflection Formulas for FRP Reinforced Concrete.” ASCE, Journal of Composites for Construction, 10(3), 183-194.

Mufti, A. A., Newhook, J. P. and Tadros, G. (1996). “Deformability versus Ductility in Concrete Beams with FRP Reinforcement.” Proceeding, 2nd International Conference on Advanced Composite Materials in Bridges and Structures. El-Badry. Ed., Canadian Society for Civil Engineering, Montreal, Canada, 189-199.

Nilson, A., Darwin, D., and Dolan, C. (2010). “Design of concrete structures.” 14th Edition, McGraw-Hill, New York.

Park, R. and Paulay, T. (1975). “Reinforced Concrete Structures.” John Wiley and Sons, New York, NY.

Rafi, MM. and Nadjai, A. (2009). “Evaluation of ACI Deflection Model for FRP Reinforced Concrete Beams and Suggested Modification.” ACI Structural Journal, 106(6), 762-771.

Razaqpur, A. G. and Kashef, A. (1993). “State-of-the-Art on Fibre Plastics for Buildings: Final Report.” Institute for Research in Construction (Canada).

Rodriguez, J. J., Bianchini, A. C., Viest, I. M. and Kesler, C. E. (1959). “Shear Strength of Two-Span Continuous Reinforced Concrete Beams.” ACI Structural Journal, 55(4), 1089-1130.

Santos, P., Laranja, G., Franca, P. M. and Correia. J. R. (2013). "Ductility and Moment Redistribution Capacity of Multi-Span T-Section Concrete Beams Reinforced With GFRP Bars," Construction and Building Materials, 49, 949–961.

Scholz, H. (1993). "Contribution to Redistribution of Moments in Continuous Reinforced Concrete Beams." ACI Structural Journal, 90(2), 150-155.

Scott, R. H. (1997). "Behavior of High Strength Concrete Beam," American Concrete Institute, SP 172-7, 119-133.

Vijay, P. V., Kumar, S. V. and GangaRao, H. V. S. (1996). "Shear and Ductility Behavior of Concrete Beams Reinforced with GFRP Rebars." Proceeding, 2nd International Conference Advanced Composite Materials in Bridges and Structures El-Badry. Ed., Canadian Society for Civil Engineering. Montreal, Canada, 217-226.

Vijay, P. V. and GangaRao, H. V. (2001). "Bending Behavior and Deformability of Glass Fiber-Reinforced Polymer Reinforced Concrete Members." ACI structural journal, 98(6), 834-842.

Wang, H. and Belarbi, A. (2011). "Ductility Characteristics of Fibre-Reinforced Concrete Beams Reinforced With FRP Rebars." Construction and Building Materials, 25(5), 2391-2401.

APPENDIX A

DESIGN OF TEST BEAMS OF SERIES 1

SERIES 1

Among the six beams, the design of two ULS based beams which are steel-RC SuR-60-4.5 and GFRP-RC GuE-30-4.5 and one SLS based beam GsR-24-4.5 is described here. The design of the middle support and mid-span section is given here.

Given that,

Concrete compressive strength, f_c'= 40 MPa

Yield strength of longitudinal reinforcement, f_y= 430 MPa

Yield strength of 8-mm diameter stirrups = 400 MPa

Height of the beam, *h*= 300 mm

Width of the beam, *b*= 200 mm

Design load on each span, P =155 kN

Span length, L= 2.8 m

Beam Designation: SuR-60-4.5

Design load on either span, P =155 kN

Span length, L= 2.8 m

Flexural design:

Elastic moment at the middle support section,

$$M_{dl} = 0.1875 * 155 * 2.8 = 81.4\ kN.m$$

Elastic moment at the mid-span section,

$$M_d = 0.15625 * 155 * 2.8 = 67.8\ kN.m$$

Considering 15% moment redistribution, redistributed moment at the middle support section,

$$M_{dl} = 0.85 * 81.4 = 69.2\ kN.m$$

To achieve the same load (P) under moment redistribution, the following equation was used.

$$2M_{dl} + 4M_d = PL$$

Redistributed moment at the mid-span section,

$$M_d = \frac{155 * 2.8 - 2 * 69.2}{4} = 73.9\ kN.m$$

Effective depth of the sections, $d = 253\ mm$,

$$\alpha_1 = 0.85 - 0.0015 * 40 \geq 0.67 = 0.79$$

$$\beta_1 = 0.97 - 0.0025 * 40 \geq 0.67 = 0.87$$

To ensure steel yielding, the neutral axis-to-depth ratio,

$$c/d \leq 700/(700 + 430) = 0.62$$

$$c \leq 156.9\ mm$$

From equilibrium conditions for middle support section assuming steel yielding,

$$A_s * 430 = 0.79 * 40 * 0.87 * c * 200 \ldots\ldots\ldots\ldots\ldots\ldots (1)$$

$$69.2 * 10^6 = A_s * 430 * \left(253 - 0.87 * \frac{c}{2}\right) \ldots\ldots\ldots\ldots (2)$$

Solving above equations,

$$c = 54.94\ mm < 156.9\ mm$$ So, steel yielded.

Required amount of steel, $A_s = 702\ mm^2$

Check minimum reinforcement for T-beams according to clause 10.5.1.2 (CSA A.23.3-14)

$A_{s,min} = \frac{0.2*\sqrt{f_c'}}{f_y} b_t h$, where b_t=2.5 b_w= width of the tension zone for T-section

$$= \frac{0.2 * \sqrt{40}}{430} * (2.5 * 200) * 300 = 441\ mm^2 < 702\ mm^2$$

Provide **2-15M+1-20M** bars at the middle support section.

Check, $A_{s,provided}$= 700 mm^2 $\approx$ 702 mm^2 (OK)

From equilibrium conditions for mid-span section assuming steel yielding,

$$A_s * 430 = 0.79 * 40 * 0.87 * c * 600 \ldots\ldots\ldots\ldots\ldots\ldots (3)$$

$$73.9 * 10^6 = A_s * 430 * \left(253 - 0.87 * \frac{c}{2}\right) \ldots\ldots\ldots\ldots (4)$$

Solving above equations, $c = 18.29\ mm < 156.9\ mm$

So, steel yielded.

Required amount of steel, $A_s = 701\ mm^2$

Check minimum reinforcement according to clause 10.5.1.2 (CSA A.23.3-14)

$A_{s,min} = \frac{0.2*\sqrt{f_c'}}{f_y} b_t h$, where b_t= b_w= width of the tension zone

$$= \frac{0.2 * \sqrt{40}}{430} * (200) * 300 = 177\ mm^2 < 701\ mm^2$$

Provide **2-15M+1-20M** bars at the mid-span section.

Check, $A_{s,provided}$= $700\ mm^2 \approx 701\ mm^2$ (OK)

Reinforcement in transverse direction of flange:

Provide 10M@ 450 mm c/c

(Clause 7.8.1, CSA A23.3-14 and Clause 8.12.5.2, ACI 318-11a)

Shear design:

Design shear force, $V_f = 155 - \frac{73.9}{1.4} = 102.2\ kN$

According to 11.3.3 (CSA A.23.3-14),

Shear resistance,, $V_r = V_c + V_s,\ and\ V_{r,max} \leq 0.25 \emptyset_c f_c' b_w d_v$

$$d_v = greater\ of \begin{cases} 0.9d = 227.7\ mm\ (governed) \\ 0.72h = 216\ mm \end{cases}$$

Maximum shear resistance of section,

$$V_{r,max} = \ 0.25\emptyset_c f_c' b_w d_v = 0.25 * 1 * 40 * 200 * 227.7 = 455\ kN$$

Also, since $0.125\emptyset_c f_c' b_w d_v = 0.125 * 1 * 40 * 200 * 227.7 = 228\ kN > 102.2\ kN$

Therefore, it's not necessary to divide the maximum spacing by 2.

Maximum spacing of stirrups,

$$s = smaller\ of\ \begin{cases} 0.7d_v = 160\ mm\ (governed) \\ 600\ \ mm \end{cases}$$

Taking spacing *s*= 160 mm c/c,

$$A_{v,min} = 0.06 * \sqrt{f_c'}\frac{b_w s}{f_y} = 0.06 * \sqrt{40} * 200 * \frac{160}{400} = 30.4\ mm^2$$

According to clause 11.3.6.4 (following general method),

Moment at a section d_v from the face of the middle support having width of 160 mm,

$$M_f = 46.83\ kN.m$$

$$\varepsilon_x = \frac{\frac{M_f}{d_v} + V_f}{2E_s A_s}$$

$$= \frac{\frac{46.83*10^6}{227.7} + 102200}{2 * 200000 * 700} = 0.0011$$

The angle of inclination, $\theta = 29^\circ + 7000\varepsilon_l = 36.7^\circ$

The value of $\beta = \frac{0.40}{(1+1500\varepsilon_x)} \times \frac{1300}{(1000+S_{ze})}$

$= \frac{0.40}{(1+1500*0.0011)} \times \frac{1300}{(1000+300)}$ =0.151

$(considering\ minimum\ transverse\ reinforcement)$

Now, $V_c = \emptyset_c \lambda \beta \sqrt{f_c'} b_w d_v = 1 * 1 * 0.151 * \sqrt{40} * 200 * 227.7 = 43.5\ kN$

Now, considering 8-mm steel bar (2-legged) and spacing of 150 mm,

$$V_s = \frac{A_v f_y d_v cot\theta}{s} = \frac{2 * 50.26 * 400 * 227.7 * cot36.7°}{150} = 81.9\ kN$$

Total shear resistance, $V_r = 43.5 + 81.9 = 125.4\ kN > V_f = 102.2\ kN$ (**OK**)

Provide 8-mm bar@150 mm c/c

Specimen Designation: GuE-30-4.5

Design load= $155\ kN$

According to clause 8.4.1.4 of CSA S806-12, the extreme compressive strain in concrete can be assumed to have reached 0.0035 only when

$$\frac{c}{d} \geq \frac{7}{(7 + 2000 * \varepsilon_{Fu})}$$

$$\frac{c}{d} \geq \frac{7}{(7 + 2000 * 0.023)} = 0.132$$

$(assuming\ GFRP\ bar\ No.16\ and\ using\ characteristic\ design\ strain)$

Again, according to clause 8.4.1.5, concrete stress of $\alpha_1 \emptyset_c f_c'$ can be assumed uniformly distributed over a compressive zone only after the above condition is satisfied.

$$\text{Now, } \alpha_1 = 0.85 - 0.0015 * 40 \geq 0.67 = 0.79$$

$$\beta_1 = 0.97 - 0.0025 * 40 \geq 0.67 = 0.87$$

Using GFRP bar no. 16,

Area=197.9 mm^2,

Characteristic design strength, $f_{frpu} = 1560\ MPa, E_{frp} = 65000\ MPa,$

Characteristic design strain, $\varepsilon_{frpu} = 2.3\%$

Effective depth, d =251 mm

Balanced reinforced ratio, $\rho_{frpb} = \alpha_1 \beta_1 \frac{\emptyset_c}{\emptyset_f} \frac{f_c'}{f_{frpu}} (\frac{\varepsilon_{cu}}{\varepsilon_{cu} + \varepsilon_{frpu}})$

$$\rho_{frpb} = 0.79 * 0.87 * \frac{1}{1} * \frac{40}{1560} * \left(\frac{0.0035}{0.0035 + 0.023}\right) = 0.00233$$

Design of the middle support section:

Design moment at middle support section= $0.1875 * 155 * 2.8 = 81.4\ kN.m$

Try using 3 No. 16 GFRP bar, $A_{frp} = 3 * 197.9 = 593.7$ mm^2

$$\rho_{frp} = \frac{A_{frp}}{bd} = \frac{593.7}{200 * 251} = 0.011827 > \rho_{frpb}$$

So, concrete crushing will control the failure mode.

For over-reinforced concrete section, stress in GFRP bar at failure can be calculated as follows (ISIS Canada 2007):

$$f_{frp} = 0.5E_{frp}\varepsilon_{cu}\left(\left(1 + \frac{4\alpha_1\beta_1\emptyset_c f_c'}{\rho_{frp}\emptyset_{frp}E_{frp}\varepsilon_{cu}}\right)^{0.5} - 1\right) \leq f_{frpu}$$

$$= 0.5 * 65000 * 0.0035\left(\left(1 + \frac{4 * 0.79 * 0.87 * 1 * 40}{0.011827 * 1 * 65000 * 0.0035}\right)^{0.5} - 1\right) = 622.3\ MPa$$

$$a = \frac{593.7 * 622.3}{0.79 * 40 * 200} = 58.5\ mm$$

$$c = \frac{58.5}{0.87} = 67.2\ mm$$

Now, $\frac{c}{d} = \frac{67.2}{251} = 0.268 > 0.132$ $(clause\ 8.4.1.4\ and\ 8.4.1.5\ are\ satisfied)$

Moment resistance,
$M_r = 593.7 * 622.3 * \left(251 - \frac{58.5}{2}\right) = 81.9\ kN.m > 81.4\ kN.m\ (OK)$

Check if minimum reinforcement is required:

Here, cracking moment, $M_{cr} = \frac{I_g}{y_t} f_r = \frac{I_g}{y_t} * 0.6\lambda\sqrt{f_c'}$

$$= \frac{723.33 * 10^6}{110} * 0.6 * 1 * \sqrt{40} = 24.95\ kN.m$$

$$(here, \lambda = 1\ for\ normal\ desnsity\ concrete)$$

Since, moment resistance of section $M_r = 81.4\ kN.m > 1.5M_{cr} = 37.4\ kN.m$

So, requirement for minimum reinforcement is satisfied according to clause 8.4.2.1 (CSA S806-12)

Provide 3 No. 16 at the middle-support section.

Design of the mid-span section:

Moment at mid-span=$0.15625 * 155 * 2.8 = 67.8\ kN.m$

Assuming rectangular beam first and using GFRP bar no. 16,

Try using 2 No. 16 GFRP bar, $A_{frp} = 2 * 197.9 = 395.8$ mm^2

$$\rho_{frp} = \frac{A_{frp}}{bd} = \frac{395.8}{600 * 251} = 0.0026 > \rho_{frpb} = 0.0023$$

So, concrete crushing will control the failure mode.

For over-reinforced concrete section, stress in GFRP bar at failure can be calculated as follows (ISIS Canada 2007):

$$f_{frp} = 0.5E_{frp}\varepsilon_{cu}\left(\left(1 + \frac{4\alpha_1\beta_1\emptyset_c f_c'}{\rho_{frp}\emptyset_{frp}E_{frp}\varepsilon_{cu}}\right)^{0.5} - 1\right) \leq f_{frpu}$$

$$= 0.5 * 65000 * 0.0035\left(\left(1 + \frac{4 * 0.79 * 0.87 * 1 * 40}{0.0026 * 1 * 65000 * 0.0035}\right)^{0.5} - 1\right) = 1441\ MPa$$

$$a = \frac{395.8 * 1441}{0.79 * 40 * 600} = 30.1\ mm$$

$$c = \frac{30.1}{0.87} = 34.6\ mm$$

Now, $\frac{c}{d} = \frac{34.6}{251} = 0.138 > 0.132$ $(clause\ 8.4.1.4\ and\ 8.4.1.5\ are\ satisfied\ )$

$$M_r = 395.8 * 1441 * \left(251 - \frac{30.1}{2}\right) = 134.6\ \ kN.m\ > 67.7\ kN.m\ (OK)$$

Check if minimum reinforcement is required:

Here, cracking moment, $M_{cr} = \frac{I_g}{y_t} f_r = \frac{I_g}{y_t} * 0.6\lambda\sqrt{f_c'}$

$$= \frac{723.33 * 10^6}{190} * 0.6 * 1 * \sqrt{40}$$

$$= 14.45\ kN.m$$

Since, moment resistance of section $M_r = 134.6\ kN.m > 1.5M_{cr} = 21.7\ kN.m$

So, requirement for minimum reinforcement is satisfied according to clause 8.4.2.1

Provide 2 No. 16 at mid-span section

Design for shear:

Design shear force at the middle support section V_f =155-67.8/1.4=106.6 kN

According to the provisions of CSA S806-12,

Total shear resistance, $V_r = V_c + V_{sF}$

$$V_c = 0.05\lambda\emptyset_c k_m k_r (f_c')^{1/3} b_w d_v$$

Where, $k_m = \sqrt{\frac{V_f d}{M_f}} \leq 1.0$ and $k_r = 1 + (E_F \rho_{Fw})^{1/3}$

$$d_v = greater\ of \begin{cases} 0.9d = 226\ mm\ (govern) \\ 0.72h = 216\ mm \end{cases}$$

M_f
$= moment\ at\ d_v\ from\ the\ face\ of\ the\ middle\ support\ having\ support\ width\ of 160\ mm$

$$= 48.8\ kN.m$$

$$k_m = \sqrt{\frac{106.6 * 0.251}{48.8}} = 0.741$$

$$k_r = 1 + (65000 * 0.011827)^{1/3} = 10.2$$

Now, $V_c = 0.05 * 1 * 1 * 0.741 * 10.2 * 40^{\frac{1}{3}} * 200 * 226 = 58.4\ kN$

Now check,

$$0.11\emptyset_c\sqrt{f_c'} b_w d_v \leq V_c \leq 0.22\emptyset_c\sqrt{f_c'} b_w d_v$$

$$31.5\ kN \leq V_c \leq 62.9\ kN \qquad (OK)$$

Shear resistance from stirrup, $V_{sF} = \frac{0.4\emptyset_F A_{Fv} f_{Fu} d_v}{s} cot\theta$

Where, $\varepsilon_l = \frac{\frac{M_f}{d_v} + V_f}{2E_F A_F}$

$$= \frac{\frac{48.8 * 10^6}{226} + 106600}{2 * 65000 * 593.7} = 0.00417$$

$$check, \qquad 30^\circ \leq \theta = 30^\circ + 7000\varepsilon_l = 59.2^\circ \leq 60^\circ$$

$$\theta = 59.2^\circ$$

Maximum spacing of stirrup (clause 8.4.6.1),

$$spacing\ of\ stirrup, s = smaller\ of \begin{cases} 0.6 d_v cot\theta = 80.8mm \approx 80\ mm \\ 400\ \ mm \end{cases}$$

Now try assuming 2-legged 13 mm stirrup @75 mm c/c,

$$V_{sF} = \frac{0.4 * 1 * 2 * 127 * 265 * 226}{75} cot 59.2^{\circ} = 48.4\ kN$$

$$here, f_{Fu} \leq 0.005 E_F = 265\ (clause\ 8.4.4.9)$$

$$V_r = 58.4 + 48.4 = \mathbf{106.8\ kN} \approx V_f = 106.6\ kN \quad (OK)$$

Check for maximum shear resistance of the section,

$$V_{r,max} = 0.22 \emptyset_c f_c' b_w d_v$$

$$= 0.22 * 1 * 40 * 200 * 226 = 398\ kN > 106.8\ kN\ (\ section\ is\ adequate)$$

So, use 2-legged No. 13 @ 75 mm c/c

Specimen Designation: GsR-24-4.5

The serviceability criteria of the middle support section govern the SLS based design for whole beam. As such, the calculations related to the middle support section are presented here.

Calculation for service moment of the middle support section in SuR-60-4.5:

$$\rho = \frac{700}{200 * 253} = 0.0138; \quad n = \frac{E_s}{E_c} = \frac{200000}{28460} = 7.03;$$

$$k = \sqrt{2 * \rho n + (\rho n)^2} - \rho n = 0.356$$

$$\text{Service moment, } M = A_s * \left(0.6 * f_y\right) * \left(d - \frac{kd}{3}\right)$$

$$= 700 * 258 * \left(253 - 0.356 * \frac{253}{3}\right)$$

$$= 39.8\ kN.m$$

All serviceability requirements are satisfied at the same service moment (39.8 kN.m) to design the GsR-24-4.5

The main design criteria include the following:

- Crack control parameter and deflection should not exceed the limits specified in codes.
- At service state, stress in the GFRP bar should be less than 25% of ultimate strength, CSA S806-12 (CSA 2012);

Try using 4 No. 22 bars in the middle support section,

For exterior exposure, crack control parameter, z = 38,000 N/mm;

k_b =1.2, d_c =56 mm, and Tension zone per bar, $A = \frac{2*600*56}{4} = 16{,}564$

And $\frac{E_s}{E_f} = \frac{200}{67} = 2.98$

Using equation of $z = k_b \frac{E_s}{E_f} f_F \sqrt[3]{(d_c A)}$

$$38{,}000 = 1.2 * 2.98 * f_F * \sqrt[3]{(56 * 16{,}200)}$$

$$f_F = 109.6\ MPa\ < 0.25\%\ of\ 1600 = 400\ MPa \quad (\boldsymbol{OK})$$

$$\rho_f = \frac{1552}{200 * 244} = 0.0315; \quad n_f = \frac{E_f}{E_c} = \frac{67000}{28460} = 2.35;$$

$$k = 0.356$$

$$\text{Service moment, } M_s = A_f * f_F * \left(d - \frac{kd}{3}\right)$$

$$= 1552 * 109.6 * \left(244 - \frac{0.356 * 244}{3}\right)$$

$$= 37.2\ kN.m \approx 39.8\ kN.m\ (OK)$$

Load corresponding to service moment = $\frac{37.2}{0.1875*2.8} = 70.9\ kN \approx 71\ kN$

Moment at the mid-span section corresponding to the service load,

$$M = 0.15625 * 71 * 2.8 = 31.1\ kN.m$$

Try with 3 No. 22 bars

$$\rho_f = \frac{1164}{600 * 244} = 0.0079; \quad n_f = \frac{E_f}{E_c} = \frac{67000}{28460} = 2.35;$$

$$k = 0.175$$

$$f_F = \frac{M_s}{A_{frp} * j * d} = \frac{31.1 * 10^6}{1164 * 0.942 * 244} = 115.3\ MPa < 0.25\%\ of\ 1600 = 400\ MPa \quad (\boldsymbol{OK})$$

$$k_b = 1.2;\ \frac{E_s}{E_{frp}} = 2.98;\ d_c = 56; A = 7467;\ f_F = 115.3\ MPa$$

$$z = 1.2 * 2.98 * 115.3 * \sqrt[3]{(56 * 7467)} = 30{,}832\frac{N}{mm}$$
$$< 38{,}000\frac{N}{mm}\ \ for\ exterior\ exposure\ \ (\boldsymbol{OK})$$

Providing 4 No. 22 in the middle support section and 3 No. 22 in the mid-span section,

Check deflection:

Following the equation suggested by ISIS 2007, Canada

$$I_e = \frac{I_t I_{cr}}{I_{cr} + \left(1 - 0.5 * (\frac{M_{cr}}{M_a})^2\right) * (I_t - I_{cr})}$$

$$I_e = 1.43 * 10^8 \text{mm}^4$$

$$\Delta = \frac{7}{768} * \frac{P * l^3}{E_c I_e}$$

$$= \frac{7}{768} * \frac{71 * 1000 * (2.8 * 1000)^3}{28460 * 1.43 * 10^8}$$

$$= 3.5\ mm$$

Allowable deflection = $\frac{L}{480} \sim \frac{L}{180} = 5.6\ mm \sim 14.8\ mm \quad (OK)$

Ultimate capacity of the middle support section:

Using 4 No. 22 GFRP bars of the middle support section,

Now, $\quad f_{frp} = 0.5 E_{frp} \varepsilon_{cu} \left(\left(1 + \frac{4\alpha_1 \beta_1 \emptyset_c f_c'}{\rho_{frp} \emptyset_{frp} E_{frp} \varepsilon_{cu}} \right)^{0.5} - 1 \right) \leq f_{frpu}$

$$= 0.5 * 67000 * 0.0035\left(\left(1 + \frac{4 * 0.79 * 0.87 * 1 * 40}{0.0315 * 1 * 67000 * 0.0035}\right)^{0.5} - 1\right) = 350.1\ MPa$$

$$a = \frac{1552 * 350.1}{0.79 * 40 * 200} = 85.9\ mm$$

$$c = 98.7\ mm$$

Now, $\frac{c}{d} \geq \frac{7}{(7+2000*0.023)} = 0.132$ ($clause$ 8.4.1.4 and 8.4.1.5 $are\ satisfied$)

$$\frac{c}{d} = \frac{98.7}{244} = 0.405 > 0.132$$

$$M_r = 1552 * 350.1 * \left(244 - \frac{85.9}{2}\right) = 109.2\ \ kN.m$$

So, the ultimate load, $P = \frac{109.2}{0.1875*2.8} = 208\ kN$

Shear design:

Design shear force at middle support section V_f =208-91/1.4=143 kN

$$V_r = V_c + V_{sF}$$

$$V_c = 0.05\lambda\emptyset_c k_m k_r (f_c')^{1/3} b_w d_v$$

Where, $k_m = \sqrt{\frac{V_f d}{M_f}} \leq 1.0$ and $k_r = 1 + (E_F \rho_{Fw})^{1/3}$

$$d_v = greater\ of\ \begin{cases} 0.9d = 219.6\ \approx 220\ mm\ (govern) \\ 0.72h = 216\ mm \end{cases}$$

$$M_f = moment\ of\ section\ at\ d_v\ from\ middle\ support = 66.6\ kN.m$$

$$k_m = \sqrt{\frac{143 * 0.244}{66.6}} = 0.724$$

$$k_r = 1 + (67000 * 0.0315)^{1/3} = 13.83$$

Now, $V_c = 0.05 * 1 * 1 * 0.724 * 13.83 * 40^{\frac{1}{3}} * 200 * 220 = 75.3\ kN$

Now check,

$$0.11\emptyset_c\sqrt{f_c'} b_w d_v \leq V_c \leq 0.22\emptyset_c\sqrt{f_c'} b_w d_v$$

$$30.6\ kN \leq V_c \leq 61.2\ kN$$

$$V_c = 61.2\ kN\ (OK)$$

Shear resistance from stirrup, $V_{sF} = \frac{0.4\emptyset_F A_{Fv} f_{Fu} d_v}{s} cot\theta$

Where,

$$\varepsilon_l = \frac{\frac{M_f}{d_v} + V_f}{2E_F A_F}$$

$$= \frac{\frac{66.6*10^6}{220} + 143{,}000}{2 * 67000 * 1552} = 0.0021$$

$$check, \qquad 30^\circ \leq \theta = 30^\circ + 7000\varepsilon_l = 45^\circ \leq 60^\circ$$

$$\theta = 45^\circ$$

Maximum spacing of stirrup (clause 8.4.6.1),

$$spacing\ of\ stirrup, s = smaller\ of \begin{cases} 0.6d_v cot\theta = 132\ mm \\ 400\ mm \end{cases}$$

Now assuming 2-legged 12 mm stirrup @60 mm c/c,

$$V_{sF} = \frac{0.4 * 1 * 2 * 126.7 * 265 * 220}{60} cot45^\circ = 98.5\ kN$$

$$here, f_{Fu} \leq 0.005E_F = 265\ (clause\ 8.4.4.9)$$

$$V_r = 61.2 + 98.5 = 159.7\ kN > V_f = 143\ kN \qquad (OK)$$

Check for maximum shear resistance of the section,

$$V_{r,max} = 0.22\emptyset_c f_c' b_w d_v$$

$$= 0.22 * 1 * 40 * 200 * 220 = 387.2\ kN > 143\ kN\ (\ section\ is\ adequate)$$

So, use 2-legged No. 13 @ 60 mm c/c

APPENDIX B

DESIGN OF TEST BEAMS OF SERIES 2

SERIES-2

Among the six beams, the design of two ULS based beams which are steel-RC SuR-II and GFRP-RC GuE-II and one SLS based beam GsR-II is described here. The design of the north mid-span section and the middle support section is given here.

Given that,

Concrete compressive strength, f_c'= 40 MPa

Yield strength of longitudinal reinforcement, f_y= 430 MPa

Yield strength of 8-mm diameter stirrups = 400 MPa

Height of the beam, *h*= 300 mm

Width of the beam, *b*= 200 mm

Design load on lightly loaded span, P =125 kN

Design load on heavily loaded span, 1.5P =187.5 kN

Span length, L= 2.8 m

Beam Designation: SuR-II

Flexural design:

Elastic moment at the middle support section,

$$M_{dl} = 0.2344 * 125 * 2.8 = 82.0\ kN.m$$

Elastic moment at the mid-span section of heavily loaded span,

$$M_{d} = 0.2579 * 125 * 2.8 = 90.3\ kN.m$$

Considering 20% moment redistribution,

Redistributed moment at the middle support section,

$$M_{dl} = 0.80 * 82.0 = 65.6\ kN.m$$

To achieve the same load (1.5P) on heavily loaded span under moment redistribution, the following equation was used.

$$2M_{dl} + 4M_d = PL$$

Redistributed moment at the mid-span section,

$$M_d = \frac{1.5 * 125 * 2.8 - 2 * 65.6}{4} = 98.5\ kN.m$$

Effective depth of the sections, $d = 253\ mm$,

$$\alpha_1 = 0.85 - 0.0015 * 40 \geq 0.67 = 0.79$$

$$\beta_1 = 0.97 - 0.0025 * 35 \geq 0.67 = 0.87$$

To ensure steel yielding, the neutral axis-to-depth ratio,

$$c/d \leq 700/(700 + 430) = 0.62$$

$$c \leq 156.9\ mm$$

From equilibrium conditions for middle support section assuming steel yielding,

$$A_s * 430 = 0.79 * 40 * 0.87 * c * 200 \ldots\ldots\ldots\ldots\ldots\ldots (1)$$

$$65.6 * 10^6 = A_s * 430 * \left(253 - 0.87 * \frac{c}{2}\right) \ldots\ldots\ldots\ldots (2)$$

Solving above equations,

$$c = 51.8\ mm < 156.9\ mm$$

So, steel yielded.

Required amount of steel, $A_s = 663\ mm^2$

Check minimum reinforcement according to clause 10.5.1.2 (CSA A.23.3-14)

$$A_{s,min} = \frac{0.2 * \sqrt{f_c'}}{f_y} b_t h, \quad \text{where } b_t = \text{width of the tension zone}$$

$$= \frac{0.2 * \sqrt{40}}{430} * (200) * 300 = 176.5\ mm^2 < 663\ mm^2$$

Provide **2-15M+1-20M** bars at the middle support section.

Check, $A_{s,provided}$= 700 mm^2 > 663mm^2 (OK)

From equilibrium conditions for heavily mid-span section assuming steel yielding,

$$A_s * 430 = 0.79 * 40 * 0.87 * c * 200 \dots\dots\dots\dots\dots\dots (3)$$

$$98.5 * 10^6 = A_s * 430 * \left(251 - 0.87 * \frac{c}{2}\right) \dots\dots\dots\dots (4)$$

Solving above equations, $c = 83.4\ mm < 156.9\ mm$; So, steel yielded.

Required amount of steel, $A_s = 1066.4\ mm^2$

Check minimum reinforcement according to clause 10.5.1.2 (CSA A.23.3-14)

$A_{s,min} = \frac{0.2*\sqrt{f_c'}}{f_y} b_t h$, where b_t= b_w= width of the tension zone of this section

$$= \frac{0.2 * \sqrt{40}}{430} * (200) * 300 = 177\ mm^2 < 1066.4\ mm^2$$

Provide **2-20M+1-25M** bars at the mid-span section.

Check, $A_{s,provided}$= 1100 mm^2 > 1066.4 mm^2 (OK)

Shear design of heavily loaded span:

Design shear force, $V_f = 187.5 - \frac{98.5}{1.4} = 117.1\ kN$

According to 11.3.3 (CSA A.23.3-14),

Shear resistance,, $V_r = V_c + V_s$, $and\ V_{r,max} \leq 0.25 \emptyset_c f_c' b_w d_v$

$$d_v = greater\ of \begin{cases} 0.9d = 225.9\ mm\ (governed) \\ 0.72h \quad = 216\ mm \end{cases}$$

Maximum shear resistance of section,

$$V_{r,max} = 0.25 \emptyset_c f_c' b_w d_v = 0.25 * 1 * 40 * 200 * 225.9 = 452\ kN$$

Also, since $0.125 \emptyset_c f_c' b_w d_v = 0.125 * 1 * 40 * 200 * 225.9 = 226\ kN > 117.1\ kN$

Therefore, it's not necessary to divide the maximum spacing by 2.

Maximum spacing of stirrups,

$$s = smaller\ of\ \begin{cases} 0.7d_v = 158\ mm\ (governed) \\ 600\ mm \end{cases}$$

Taking spacing, *s*= 158 mm c/c,

$$A_{v,min} = 0.06 * \sqrt{f_c'}\frac{b_w s}{f_y} = 0.06 * \sqrt{40} * 200 * \frac{158}{400} = 30\ mm^2$$

According to clause 11.3.6.4 (following general method),

Since moment is higher at mid-span section compared to that at the middle support section, shear design governs for the mid-span section.

Moment at a section d_v from the face of the loading plate having width of 100 mm,

$$M_f = 66.1\ kN.m$$

$$\varepsilon_x = \frac{\frac{M_f}{d_v} + V_f}{2E_s A_s}$$

$$= \frac{\frac{66.1*10^6}{225.9} + 117100}{2 * 200000 * 1100} = 0.00093$$

The angle of inclination, $\theta = 29^\circ + 7000\varepsilon_l = 35.5$

The value of $\beta = \frac{0.40}{(1+1500\varepsilon_x)} \times \frac{1300}{(1000+S_{ze})}$

$= \frac{0.40}{(1+1500*0.00093)} \times \frac{1300}{(1000+300)}$ =0.167

$(considering\ minimum\ transverse\ reinforcement)$

Now,

$$V_c = \emptyset_c \lambda \beta \sqrt{f_c'} b_w d_v = 1 * 1 * 0.167 * \sqrt{40} * 200 * 225.9 = 47.7\ kN$$

Now, considering 8-mm steel bar (2-legged) and spacing of 150 mm,

$$V_s = \frac{A_v f_y d_v cot\theta}{s} = \frac{2 * 50.26 * 400 * 225.9 * cot35.5°}{150} = 84.9\ kN$$

Total shear resistance, $V_r = 47.7 + 84.9 = 132.6\ kN > V_f = 117.1\ KN$ (**OK**)

Provide 8-mm bar@150 mm c/c

Beam Designation: GuE-II

Flexural design:

Design of the middle support section:

Elastic moment at the middle support section,

$$M_{dl} = 0.2344 * 125 * 2.8 = 82.0\ kN.m$$

According to clause 8.4.1.4 of CSA S806-12, the extreme compressive strain in concrete can be assumed to have reached 0.0035 only when

$$\frac{c}{d} \geq \frac{7}{(7 + 2000 * \varepsilon_{Fu})}$$

$$\frac{c}{d} \geq \frac{7}{(7 + 2000 * 0.022)} = 0.137$$

$$(assuming\ GFRP\ bar\ No.16\ and\ using\ characteristic\ design\ strain)$$

Again, according to clause 8.4.1.5, concrete stress of $\alpha_1 \emptyset_c f_c'$ can be assumed uniformly distributed over a compressive zone only after the above condition is satisfied.

Now,

$$\alpha_1 = 0.85 - 0.0015 * 40 \geq 0.67 = 0.79$$

$$\beta_1 = 0.97 - 0.0025 * 40 \geq 0.67 = 0.87$$

Using GFRP bar no. 16,

Area=197.9 mm^2,

Characteristic design strength, $f_{frpu} = 1530\ MPa, E_{frp} = 65000\ MPa,$

Characteristic design strain, $\varepsilon_{frpu} = 2.2\%$

Effective depth, d =251 mm

Balanced reinforced ratio, $\rho_{frpb} = \alpha_1\beta_1 \frac{\emptyset_c}{\emptyset_f}\frac{f_c'}{f_{frpu}}\left(\frac{\varepsilon_{cu}}{\varepsilon_{cu}+\varepsilon_{frpu}}\right)$

$$\rho_{frpb} = 0.79 * 0.87 * \frac{1}{1} * \frac{40}{1530} * \left(\frac{0.0035}{0.0035 + 0.022}\right) = 0.00247$$

Design moment at the middle support section$= 0.2344 * 125 * 2.8 = 82.0\ kN.m$

Try using 3 No. 16 GFRP bar, $A_{frp} = 3 * 197.9 = 593.7$ mm^2

$$\rho_{frp} = \frac{A_{frp}}{bd} = \frac{593.7}{200 * 251} = 0.01183 > \rho_{frpb}$$

So, concrete crushing will control the failure mode.

For over-reinforced concrete section, stress in GFRP bar at failure can be calculated as follows (ISIS Canada 2007):

$$f_{frp} = 0.5E_{frp}\varepsilon_{cu}\left(\left(1 + \frac{4\alpha_1\beta_1\emptyset_c f_c'}{\rho_{frp}\emptyset_{frp}E_{frp}\varepsilon_{cu}}\right)^{0.5} - 1\right) \leq f_{frpu}$$

$$= 0.5 * 65000 * 0.0035\left(\left(1 + \frac{4 * 0.79 * 0.87 * 1 * 40}{0.01183 * 1 * 65000 * 0.0035}\right)^{0.5} - 1\right) = 622.1\ MPa$$

$$a = \frac{593.7 * 622.1}{0.79 * 40 * 200} = 58.4\ mm$$

$$c = \frac{58.4}{0.87} = 67.1\ mm$$

Now,

$$\frac{c}{d} = \frac{67.1}{251} = 0.267 > 0.137 \quad (clause\ 8.4.1.4\ and\ 8.4.1.5\ are\ satisfied\ )$$

Moment resistance,
$M_r = 593.7 * 622.1 * \left(251 - \frac{58.4}{2}\right) = 81.9\ \ kN.m\ \approx 82.0\ kN.m\ (OK)$

Check if minimum reinforcement is required:

Here, cracking moment, $M_{cr} = \frac{I_g}{y_t}f_r = \frac{I_g}{y_t} * 0.6\lambda\sqrt{f_c'}$

$$= \frac{450.0 * 10^6}{150} * 0.6 * 1 * \sqrt{40}\ \ = 11.4\ kN.m$$

$$(here, \lambda = 1\ for\ normal\ desnsity\ concrete)$$

Since, moment resistance of section $M_r = 81.9\ kN.m > 1.5M_{cr} = 17.1\ kN.m$

So, requirement for minimum reinforcement is satisfied according to clause 8.4.2.1 (CSA S806-12)

Provide 3 No. 16 at the middle-support section

Design of the mid-span section:

Elastic moment at the mid-span section of heavily loaded span,

$$M_d = 0.2579 * 125 * 2.8 = 90.3\ kN.m$$

According to clause 8.4.1.4 of CSA S806-12, the extreme compressive strain in concrete can be assumed to have reached 0.0035 only when

$$\frac{c}{d} \geq \frac{7}{(7 + 2000 * \varepsilon_{Fu})}$$

$$\frac{c}{d} \geq \frac{7}{(7 + 2000 * 0.021)} = 0.132$$

$$(assuming\ GFRP\ bar\ No.22\ and\ using\ characteristic\ design\ strain)$$

Again, according to clause 8.4.1.5, concrete stress of $\alpha_1 \emptyset_c f_c'$ can be assumed uniformly distributed over a compressive zone only after the above condition is satisfied.

Now,

$$\alpha_1 = 0.85 - 0.0015 * 40 \geq 0.67 = 0.79$$

$$\beta_1 = 0.97 - 0.0025 * 40 \geq 0.67 = 0.87$$

Using GFRP bar no. 22,

Area= 388 mm^2,

Characteristic design strength, $f_{frpu} = 1375\ MPa, E_{frp} = 68000\ MPa,$

Characteristic design strain, $\varepsilon_{frpu} = 2.1\%$

Effective depth, d =246 mm

Balanced reinforced ratio, $\rho_{frpb} = \alpha_1 \beta_1 \frac{\emptyset_c}{\emptyset_f} \frac{f_c'}{f_{frpu}} (\frac{\varepsilon_{cu}}{\varepsilon_{cu} + \varepsilon_{frpu}})$

$$\rho_{frpb} = 0.79 * 0.87 * \frac{1}{1} * \frac{40}{1375} * \left(\frac{0.0035}{0.0035 + 0.021}\right) = 0.00286$$

Moment at mid-span=$0.2579 * 125 * 2.8 = 90.3\ kN.m$

Using GFRP bar no. 22,

Try using 2 No. 22 GFRP bar, $A_{frp} = 2 * 388 = 776$ mm^2

$$\rho_{frp} = \frac{A_{frp}}{bd} = \frac{776}{200 * 246} = 0.0158 > \rho_{frpb} = 0.00286$$

So, concrete crushing will control the failure mode.

For over-reinforced concrete section, stress in GFRP bar at failure can be calculated as follows (ISIS Canada 2007):

$$f_{frp} = 0.5E_{frp}\varepsilon_{cu}\left(\left(1 + \frac{4\alpha_1\beta_1\emptyset_c f_c'}{\rho_{frp}\emptyset_{frp}E_{frp}\varepsilon_{cu}}\right)^{0.5} - 1\right) \leq f_{frpu}$$

$$= 0.5 * 68000 * 0.0035\left(\left(1 + \frac{4 * 0.79 * 0.87 * 1 * 40}{0.0158 * 1 * 68000 * 0.0035}\right)^{0.5} - 1\right) = 536\ MPa$$

$$a = \frac{776 * 536}{0.79 * 40 * 200} = 65.8\ mm$$

$$c = \frac{65.8}{0.87} = 75.6\ mm$$

Now,

$$\frac{c}{d} = \frac{75.6}{246} = 0.307 > 0.132 \quad (clause\ 8.4.1.4\ and\ 8.4.1.5\ are\ satisfied\ )$$

$$M_r = 776 * 536 * \left(246 - \frac{65.8}{2}\right) = 88.6\ \ kN.m\ \approx 90.3\ kN.m\ (OK)$$

Check if minimum reinforcement is required:

Here, cracking moment, $M_{cr} = \frac{I_g}{y_t} f_r = \frac{I_g}{y_t} * 0.6\lambda\sqrt{f_c'}$

$$= \frac{450 * 10^6}{150} * 0.6 * 1 * \sqrt{40}$$

$$= 11.4\ kN.m$$

Since, moment resistance of section $M_r = 88.6\ kN.m > 1.5M_{cr} = 17.1\ kN.m$

So, requirement for minimum reinforcement is satisfied according to clause 8.4.2.1

Provide 2 No. 22 at mid-span section

Design for shear:

Design shear force at (1.5*P) heavily loaded side of the middle support section V_f =187.5-90.2/1.4=123.1 kN

$$V_r = V_c + V_{sF}$$

$$V_c = 0.05\lambda\emptyset_c k_m k_r (f_c')^{1/3} b_w d_v$$

Where, $k_m = \sqrt{\frac{V_f d}{M_f}} \leq 1.0$ and $k_r = 1 + (E_F \rho_{Fw})^{1/3}$

$$d_v = greater\ of \begin{cases} 0.9d = 226\ mm\ (govern) \\ 0.72h = 216\ mm \end{cases}$$

$$M_f = moment\ at\ section\ d_v\ from\ the\ midde\ support\ section = \mathbf{48.8}\ kN.m$$

(Considering supporting plate with width of 160 mm)

$$k_m = \sqrt{\frac{123.1 * 0.251}{48.8}} = 0.796$$

$$k_r = 1 + (65000 * 0.01183)^{1/3} = 10.2$$

Now, $V_c = 0.05 * 1 * 1 * 0.796 * 10.2 * 40^{\frac{1}{3}} * 200 * 226 = \mathbf{62.7\ kN}$

Now check,

$$0.11\emptyset_c\sqrt{f_c'} b_w d_v \leq V_c \leq 0.22\emptyset_c\sqrt{f_c'} b_w d_v$$

$$31.5\ kN \leq V_c \leq \mathbf{62.9}\ kN \qquad (OK)$$

Shear resistance from stirrup, $V_{sF} = \frac{0.4\emptyset_F A_{Fv} f_{Fu} d_v}{s} cot\theta$

Where,

$$\varepsilon_l = \frac{\frac{M_f}{d_v} + V_f}{2E_F A_F}$$

$$= \frac{\frac{48.8*10^6}{226} + 123100}{2 * 65000 * 593.7} = 0.0044$$

$$check, \qquad 30^\circ \leq \theta = 30^\circ + 7000\varepsilon_l = 60.7^\circ \leq 60^\circ$$

$$\theta = 60^\circ$$

Maximum spacing of stirrup (clause 8.4.6.1),

$$spacing\ of\ stirrup, s = smaller\ of \begin{cases} 0.6 d_v cot\theta = 79.2\ mm \approx 80\ mm \\ 400\ mm \end{cases}$$

Now assuming 3-legged No. 13 mm stirrup @80 mm c/c,

$$V_{sF} = \frac{0.4 * 1 * 3 * 127 * 267 * 226}{80} cot60^{\circ} = \mathbf{66.4}\ kN$$

$$here, f_{Fu} \leq 0.005 E_F = 265\ (clause\ 8.4.4.9)$$

$$V_r = 62.9 + 66.4 = 129.3\ kN > V_f = 123.1\ kN \quad (\boldsymbol{OK})$$

Check for maximum shear resistance of the section,

$$V_{r,max} = 0.22 \emptyset_c f_c' b_w d_v$$

$$= 0.22 * 1 * 40 * 200 * 226 = 398\ kN > 123.1\ kN\ (\ section\ is\ adequate)$$

So, use 3-legged No. 13 @ 80 mm c/c

Specimen Designation: GsR-II

The serviceability criteria of the middle support section govern the SLS based design for whole beam. As such, the calculations related to the middle support section are presented here.

Calculation for service moment of the middle support section in SuR-II:

$$\rho = \frac{700}{200 * 253} = 0.0138; \quad n = \frac{E_s}{E_c} = \frac{200000}{28460} = 7.03;$$

$$k = \sqrt{2 * \rho n + (\rho n)^2} - \rho n = 0.356$$

$$\text{Service moment, } M = A_s * \left(0.6 * f_y\right) * \left(d - \frac{kd}{3}\right)$$

$$= 700 * 258 * \left(253 - 0.356 * \frac{253}{3}\right)$$

$$= 39.8\ kN.m$$

All serviceability requirements are satisfied at the same service moment (39.8 kN.m) to design the GsR-II.

The main design criteria include the following:

- Crack control parameter and deflection should not exceed the limits specified in codes.
- At service state, stress in the GFRP bar should be less than 25% of ultimate strength, CSA S806-12 (CSA 2012);

Try using 2 No. 25 and 1 No. 22 bars in the middle support section.

For exterior exposure, crack control parameter, z = 38,000 N/mm;

k_b =1.2, d_c =63 mm, and Tension zone per bar, $A = \frac{2*200*63}{2.8} = 9000$

And $\frac{E_s}{E_f} = \frac{200}{68} = 2.94$

Using equation of $z = k_b \frac{E_s}{E_f} f_F \sqrt[3]{(d_c A)}$

$$38{,}000 = 1.2 * 2.94 * f_F * \sqrt[3]{(63 * 9{,}000)}$$

$$f_F = 130\ MPa\ < 0.25\%\ of\ 1400 = 350\ MPa \quad (\boldsymbol{OK})$$

$$\rho_f = \frac{1402}{200 * 237} = 0.0295; \quad n_f = \frac{E_f}{E_c} = \frac{68000}{28460} = 2.39;$$

$$k = 0.312$$

$$\text{Service moment, } M_s = A_f * f_F * \left(d - \frac{kd}{3}\right)$$

$$= 1402 * 130 * \left(237 - \frac{0.312 * 237}{3}\right)$$

$$= 38.7\ kN.m \approx 39.8\ kN.m\ (OK)$$

Load corresponding to service moment = $\frac{38.7}{0.65625} = 58.9\ kN \approx 58\ kN$

Moment at the north mid-span section corresponding to the service load,

$$M = 0.722 * 58 = 41.9\ kN.m$$

Try with 3 No. 25 bars

$$\rho_f = \frac{1521}{200 * 237} = 0.0321; \quad n_f = \frac{E_f}{E_c} = \frac{68000}{28460} = 2.39;$$

$$k = 0.323$$

$$f_F = \frac{M_s}{A_{frp} * j * d} = \frac{41.9 * 10^6}{1521 * 0.892 * 237} = 130.3\ MPa < 0.25\%\ of\ 1400 = 350\ MPa \quad (\boldsymbol{OK})$$

$$k_b = 1.2;\ \frac{E_s}{E_{frp}} = 2.94;\ d_c = 63; A = 8{,}400;\ f_F = 130.3\ MPa$$

$$z = 1.2 * 2.94 * 130.3 * \sqrt[3]{(63 * 8{,}400)} = 37{,}183 \frac{N}{mm}$$
$$< 38{,}000 \frac{N}{mm}\ \ for\ exterior\ exposure\ \ (\boldsymbol{OK})$$

Provide 2 No. 25 and 1No. 22 in the middle support section and 3 No. 25 in the north mid-span section,

Check deflection:

Following the equation suggested by ISIS 2007, Canada

$$I_e = \frac{I_t I_{cr}}{I_{cr} + \left(1 - 0.5 * (\frac{M_{cr}}{M_a})^2\right) * (I_t - I_{cr})}$$

$$I_e = 1.26 * 10^8 \text{mm}^4$$

Using moment-area theorem, deflection $\Delta = 5.57\ mm$

Allowable deflection = $\frac{L}{480} \sim \frac{L}{180} = 5.6\ mm \sim 14.8\ mm \quad (OK)$

Ultimate capacity of the middle support section:

Using 2 No. 25 + 1 No. 22 GFRP bars of the middle support section,

Now, $$f_{frp} = 0.5 E_{frp} \varepsilon_{cu} \left(\left(1 + \frac{4\alpha_1 \beta_1 \emptyset_c f_c'}{\rho_{frp} \emptyset_{frp} E_{frp} \varepsilon_{cu}} \right)^{0.5} - 1 \right) \leq f_{frpu}$$

$$= 0.5 * 68000 * 0.0035 \left(\left(1 + \frac{4 * 0.79 * 0.87 * 1 * 40}{0.0296 * 1 * 68000 * 0.0035} \right)^{0.5} - 1 \right) = 365.2\ MPa$$

$$a = \frac{1402 * 365.2}{0.79 * 40 * 200} = 81\ mm$$

$$c = 93.1\ mm$$

Now, $\frac{c}{d} \geq \frac{7}{(7+2000*0.021)} = 0.143$ $(clause\ 8.4.1.4\ and\ 8.4.1.5\ are\ satisfied\ )$

$$\frac{c}{d} = \frac{93.1}{237} = 0.392 > 0.143$$

$$M_r = 1402 * 365.2 * \left(237 - \frac{81}{2}\right) = 100.6\ kN.m$$

So, the ultimate load, $P = \frac{100.6}{0.65625} = 153\ kN$

Therefore, $1.5P = 1.5 * 153 = 229\ kN$

Shear design:

Design shear force at middle support section V_f =229-111/1.4=149 kN

$$V_r = V_c + V_{sF}$$

$$V_c = 0.05\lambda\emptyset_c k_m k_r (f_c')^{1/3} b_w d_v$$

Where, $k_m = \sqrt{\frac{V_f d}{M_f}} \leq 1.0$ and $k_r = 1 + (E_F \rho_{Fw})^{1/3}$

$$d_v = greater\ of \begin{cases} 0.9d = 213.3\ \approx 215\ mm \\ 0.72h = 216\ mm\ (govern) \end{cases}$$

$$M_f = moment\ of\ section\ at\ d_v\ from\ middle\ support = 56.2\ kN.m$$

$$k_m = \sqrt{\frac{152 * 0.237}{56.2}} = 0.801$$

$$k_r = 1 + (68000 * 0.0296)^{1/3} = 13.63$$

Now, $V_c = 0.05 * 1 * 1 * 0.801 * 13.63 * 40^{\frac{1}{3}} * 200 * 216 = 80.6\ kN$

Now check,

$$0.11\emptyset_c\sqrt{f_c'} b_w d_v \leq V_c \leq 0.22\emptyset_c\sqrt{f_c'} b_w d_v$$

$$30.1\ kN \leq V_c \leq 60.1\ kN$$

$$\text{Chose, } V_c = 61.1\ kN\ (OK)$$

Shear resistance from stirrup, $V_{sF} = \frac{0.4\emptyset_F A_{Fv} f_{Fu} d_v}{s} cot\theta$

Where,

$$\varepsilon_l = \frac{\frac{M_f}{d_v} + V_f}{2E_F A_F}$$

$$= \frac{\frac{56.2*10^6}{216} + 152{,}000}{2 * 68000 * 1402} = 0.00216$$

$$check, \qquad 30^\circ \le \theta = 30^\circ + 7000\varepsilon_l = 45^\circ \le 60^\circ$$

$$\theta = 45^\circ$$

Maximum spacing of stirrup (clause 8.4.6.1),

$$spacing\ of\ stirrup, s = smaller\ of \begin{cases} 0.6d_v cot\theta = 130\ mm \\ 400\ mm \end{cases}$$

Now assuming 2-legged 12 mm stirrup @60 mm c/c,

$$V_{sF} = \frac{0.4 * 1 * 2 * 127 * 265 * 216}{70} cot45^\circ = 83.1\ kN$$

$$here, f_{Fu} \le 0.005E_F = 265\ (clause\ 8.4.4.9)$$

$$V_r = 61.1 + 83.1 = 144.2\ kN \approx V_f = 149\ kN \qquad (OK)$$

Check for maximum shear resistance of the section,

$$V_{r,max} = 0.22\emptyset_c f_c' b_w d_v$$

$$= 0.22 * 1 * 40 * 200 * 216 = 380\ kN > 149\ kN\ (\ section\ is\ adequate)$$

So, use 2-legged No. 13 @ 70 mm c/c